Doctoral Thesis

Development of a Versatile Three-arm Aerial Manipulator System

March 2021

Doctoral Program in Advanced Mechanical Engineering and Robotics
Graduate School of Science and Engineering
Ritsumeikan University

Hannibal Paul

Doctoral Thesis Reviewed

by Ritsumeikan University

Development of a Versatile Three-arm Aerial Manipulator System

(多用途 3 アーム空中マニピュレータシステムの開発)

March 2021

2021 年 3 月

Doctoral Program in Advanced Mechanical Engineering and Robotics

Graduate School of Science and Engineering

Ritsumeikan University

立命館大学大学院理工学研究科

機械システム専攻博士課程後期課程

Hannibal Paul

ハンニバル　ポール

Supervisor：Professor SHIMONOMURA Kazuhiro

研究指導教員：下ノ村 和弘　教授

Acknowledgment

In this auspicious moment of my life, I stand here with a long list of people to express my gratitude and indebtedness for their precious efforts put in for the successful completion of this dissertation.

I am indebted to my adviser: Prof. Kazuhiro Shimonomura, for letting me join his laboratory and for giving me the freedom to pursue every idea that I felt was worthy of investigating. I would also like to express my sincere gratitude to my other adviser: Prof. Shinichi Hirai for accepting me as a Ph.D. student and always supporting me with advice. It will always be an honor for me to work under both of them as a Ph.D. student.

I would like to thank Prof. Robert Ladig for his suggestion and comments throughout the completion of this research. I also wish to show my gratitude to other professors of the Ritsumeikan university's robotics department for their valuable comments during the development of this research.

I am also grateful for the financial supports provided by the Ritsumeikan University Special Encouragement Scholarship, Monbukagakusho Honors Scholarship for Privately Financed International Students (JASSO) and the KDDI Foundation International Students Scholarship. Their generosity not only gave me financial support but also gave me great encouragement to complete my study.

I wish to extend my appreciation to Mr. Ryo Miyazaki and Mr. Takamasa Kominami for their timely support in the successful completion of this project.

Finally, I wish to express special thanks to my family for their motivation, support, and for all of the sacrifices that they have made on my behalf. I wish to thank all the people whose assistance was a milestone in the completion of this dissertation.

Abstract

The applications of multirotor unmanned aerial vehicles (UAVs) is expanding. The current applications are mainly aerial photography and transportation, but in addition, "aerial manipulation" is expected as a next-generation application, in which a robotic manipulator is mounted on the airframe to perform work while flying. It is hoped that such a working flying robot will perform various tasks on behalf of humans in places that are not easily accessible to humans. For example, in locations where the situation cannot always be predicted, such as a disaster site, it is desirable to have the versatility to perform various tasks according to the situation, rather than being limited to a single function. However, due to payload constraints, it is not practical to have a large number of different hardware for each task in a UAV.

In this research, we develop a UAV equipped with three robotic manipulators and propose to use it to perform multiple tasks. As some example tasks, we consider landing on rough terrain, grasping objects, and avoiding collisions and propose manipulator system design, architecture, and task-specific sensing methods and implementations to realize these functions. Distance sensors and a stereo vision camera is used to obtain the three-dimensional shape of the landing site and the object to be grasped, and based on that, the attitude and movements of the three attached manipulators are controlled. In order to avoid collisions while navigating, the appropriate manipulator's attitude is adjusted based on the two-dimensional distance measurements provided by a Light Detection and Ranging (LIDAR) unit mounted on top of the UAV. Through actual indoor and outdoor experiments, it was confirmed that these three types of tasks can be performed by the proposed aerial manipulator system.

Contents

List of Figures

List of Tables

Chapter 1

Introduction

Rescue robotics has become one of the new field of interest for researchers recently. The academic community, as well as the stakeholders of emergency response are taking keen interest in this emerging field [1]. Both in industry as well as on fields, robots are assisting human operators to perform the task without any difficulty or risk to the human life. Robots can perform tasks like remote probing using on-board sensors and collecting data from hard to access or dangerous locations for humans. Some of the major situations where the rescue robots can be deployed include disaster response, industrial accidents, explosions or hostage situations [2]. Deploying robots instead of human personal will result in reduced manpower, reduced fatigue and efficient access and task performing in extremely hard to access locations.

The prominence of UAVs in recent years is noted by contrasting the limitations of land and marine robots in [3]. Its popularity is increasing rapidly due to the availability and production of light weight sensors and imaging products.

The potential of UAVs to traverse obstacles in the air makes them ideal for transporting supplies to victims quickly. The use of drones to distribute diagnostic samples between remote health centers and hospitals was pioneered by Médecins Sans Frontières in Papua, New Guinea, 2014 [4]. A drone delivery service in Rwanda has recently been introduced by the US medical product delivery company Zipline to supply blood, drugs and vaccines nationwide [5].

Other than transportation, as UAVs can travel at high altitudes, they can have a

view of the area from the bird's eye. This can be helpful for event surveying, security and surveillance. They are also necessary to help with emergency operations requiring protection and security. Multirotor type UAVs have the ability to hover in a fixed position in air. In addition to that they can perform vertical take-off and landing (VTOL) that makes them suitable for many tasks [6]. UAVs are being used to date in applications such as mapping [7], search and rescue [8], agriculture and forestry [9], bridge inspection [10], and enclosed industrial inspection [11].

Manipulation may be done at extremely high altitudes or hard to reach areas by adding manipulators to the UAV. This kind of manipulation is called as aerial manipulation. Various types of aerial manipulators are being researched recently based on their size, type and placements. Some recent literature studies in [12, 13, 14] provides the comparison on the types of aerial manipulators for small sized UAVs. Over the years, UAVs with different kinds of manipulator arrangements are developed like single gripper [15, 16], single robotic manipulator [17, 18] and dual robotic manipulator [19, 20].

The efficiency of the UAV's propulsion system is affected when in close proximity to the environment as noted in [12], which affects the UAV's stability. Furthermore movements of the manipulators also has a direct impact on the stability of the airframe [18]. Additionally, unlike terrestrial robots, one of the biggest challenge of UAVs is the severely limited payload, making it challenging to carry off-the-shelf robotic manipulators.

1.1 Motivation

Robots have been developed and used instead of humans in both industries and fields in the last five decades. Such robots are designed to perform a particular task at a very high accuracy. There has also been some developments in disaster response robots.

The use of unmanned aerial systems for civilian search and rescue activities or emergency response is not new when it comes to UAVs. In the aftermath of hurricane

Katrina in the United States, military drones were used. Also, rotary wing robots fitted with radiation monitors, infrared thermometers and cameras were used in Japan after the earthquake at the Fukushima nuclear plant.

Additionally, when deployed in disaster sites the robot may have to tackle some unexpected situations, like quickly avoiding moving or falling obstacles. Researches on obstacle avoidance using path planning can be often seen in literature [21, 22], but researches on physical contact based navigation is currently limited. Physical interaction with the environment typically results in a crash and immediate loss of the mission if the robot is unable to handle these unforeseen situations reasonably well. For example, when performing manipulation, the robot may need to escape a dropping structure, or a UAV may suddenly need to land on a cluttered site temporarily. Some studies such as [23] with the development of a four-leg UAV platform for adaptive landing using force sensor feedback displays the cases where this has been already applied. A UAV with a passive spherical shell was designed by [24] to touch and inspect structures while preventing collisions. However only either of these functions can be done by any of these UAVs. Researches including [25] and [26] explore the implementation of more than one function to adaptive robotics. [25] describes a hexapod robot prototype with legs that can be converted into object-grabbing limbs.

A start-up firm called Ross Robotics has recently attempted to develop adaptable unmanned ground vehicles (UGVs) that can easily respond to diverse roles to replace humans in dangerous environments [27]. Such robots can be trained and updated easily, as stated by their founder and CEO, to be able to work in harsh areas. They are designed primarily to help mitigate threats and save lives. Robots like this are more fitting and can easily be modified in dangerous conditions to undertake any variety of activities to replace humans in places where work is too hazardous.

1.2 Contributions

The goal of this thesis is to design and develop a three robotic arm on-board manipulator system for a multirotor UAV. The device is designed in such a manner that it

Figure 1.1: Various functions that can be realized with a UAV using a system of three on-board manipulators. From left to right: adaptive landing, transporting large item by means of manipulators, transporting objects by means of grippers, avoiding the UAV body from hitting a vertical surface when flying.

can be used for multipurpose operations and can also be ideal for use in emergency scenarios requiring complex on-site activities. For the developed system, some typical tasks such as aerial grasping, adaptive landing and physical contact based obstacle avoidance are discussed in this manuscript, as seen in Figure 1.1. In the following chapters of this manuscript, the explanations for using the three-arm device and its architecture are discussed.

This work's focus is outlined as follows:

- Proposal of a new general purpose manipulator system to circumvent a UAV's payload limitation to carry the hardware needed to execute a multitude of tasks.
- Emphasis on a three manipulator system. The minimum number of manipulators, after careful analysis of the task specifications.
- Performance and analysis of several trials in which irregular surface landing tests, grasping and physical touch based obstacle avoidance are used.
- Development of an autonomous vision and sensor-based algorithm for the tasks pointed above.

1.3 Outline

A brief introduction to multirotor UAV is summarized in Chapter 2 along with a short history and industrial utilization. Chapter 3 describes the concepts of several important tasks and the reason for choosing the proposed manipulator system. Structure of the manipulators along with the sensors and actuators used are detailed in Chapter 4. In Chapter 5, the kinematics analysis of the manipulator system for the intended tasks are identified. Chapter 6 details the autonomous vision based algorithms developed for autonomous landing, grasping and obstacle avoidance around the UAV as well. Some experiments to realize and verify the tasks are shown in Chapter 7. In Chapter 8 further step for future development is discussed. A brief conclusion in provided in Chapter 9, discussing the experiment result and limitations.

Chapter 2

Multirotor UAVs

2.1 Introduction

UAVs can be identified as flying robots operated remotely as they do not need human personal on-board for their operation. That makes them suitable for a wide range of applications in hazardous locations or in inaccessible locations. Based on its use, wing type (fixed wing and revolving wing), landing trajectory (vertical take-off and landing and horizontal take-off and landing), payload and so on, UAVs are divided into different categories [28]. Multirotor type UAV is a type of rotary wing UAV that has VTOL capacity, thereby reducing the need for a runway and can take off or land on any flat surface. For many applications such as monitoring, inspection, transportation and photography [29], the potential of the multirotor UAV to hover at a fixed space makes them suitable.

A multirotor UAV has six degrees of freedom (DoF). It is assumed to have a rigid and symmetrical body and the motors and their propeller blades are the only moving components. The dynamics of the multirotor UAV therefore depends solely on the angular velocities of its rotors. The opposing rotors, are designed to spin in opposite directions which are clock-wise and counter-clock-wise. This is required t o keep the UAV balanced. The multirotor body starts rotating if all the rotors spin in the same direction. The rotors and propellers are so built that the air is pushed downwards. The multirotor altitude can be controlled by adjusting the speed of all the rotors.

Multirotors are designed and constructed on the basis of their size, payload and power consumption [30], depending on the requirement. The most common type of multirotors used are quadrotors (with 4 rotors). The larger the number of rotors, the greater the capacity of the payload, but at the risk of increased overall power consumption, thereby reducing the flight time.

2.1.1 Modeling of Multirotor UAV

Based on the inputs, the mathematical model of a multirotor determines how the outputs are controlled. By using this it is possible to determine how the direction and orientation of the multirotor varies depending on the rotors' angular velocities.

In order to derive the dynamics of the multi-rotor, two frames are required in which it is regulated. They are inertial frames and body frames, both denoted by the Cartesian right-hand coordinate system. Let $\{A\}$ denote inertial frame with unit vectors $\{\vec{a_1}, \vec{a_2}, \vec{a_3}\}$ defined on the surface of the earth with the z axis upward from the surface of the ground, where $\vec{a_1} = \vec{x}$, $\vec{a_2} = \vec{y}$, $\vec{a_3} = \vec{z}$. The position of the center of mass of the UAV will be $r = (x, y, z) \in \{A\}$. Let $\{B\}$ be the body frame fixed on the multirotor frame with unit vectors $\left\{\vec{b_1}, \vec{b_2}, \vec{b_3}\right\}$ and is determined by its orientation, where the rotors point towards the z axis and the frame forms the $x-y$ plane, centered at the center of gravity (CoG) of the multirotor. A rotation matrix R can be written such that $\vec{b_1} = R\vec{x}$, $\vec{b_2} = R\vec{y}$, $\vec{b_3} = R\vec{z}$.

Using $Z - X - Y$ Euler angles, to get from $\{A\}$ to $\{B\}$, we first rotate about a_3 by ψ (yaw angle), followed by rotation about the x axis by θ (roll angle) in the rotated frame, followed by rotation of ϕ (pitch angle) in the new y axis resulting in,

$$R = \begin{bmatrix} c_\psi c_\phi - s_\theta s_\psi s_\phi & -c_\theta s_\psi & c_\psi s_\phi + c_\phi s_\theta s_\psi \\ c_\phi s_\psi + c_\psi s_\theta s_\phi & c_\theta c_\psi & s_\psi s_\phi - c_\psi c_\phi s_\theta \\ -c_\theta s_\phi & s_\theta & c_\theta c_\phi \end{bmatrix} \tag{2.1}$$

where c and s are cosine and sine terms respectively.

If $v \in \{A\}$ donates the linear velocity of $\{B\}$ with respect to $\{A\}$ and $\Omega \in \{B\}$ the angular velocity of $\{B\}$ with respect to $\{A\}$. Let m be the mass of the multirotor

and $I \in \mathbb{R}^{3\times3}$ the constant inertia matrix, the rigid body equations of a multirotor are,

$$\dot{\xi} = v \tag{2.2a}$$

$$m\dot{v} = mg\vec{a_3} + RF \tag{2.2b}$$

$$\dot{R} = R\Omega_\times \tag{2.2c}$$

$$I\dot{\Omega} = -\Omega \times I\Omega + \tau \tag{2.2d}$$

The vectors $F, \tau \in \{B\}$ combine the principal nonconservative forces and moments applied to the quadrotor airframe by the aerodynamics of the rotors. And $\Omega_\times$ denotes the skew-symmetric matrix, such that $\Omega_\times v = \Omega \times v$ for the vector cross product $\times$ and any vector $v \in \mathbb{R}^3$.

2.1.2 Multirotor Aerodynamics

A basic level of aerodynamic modeling is required to understand or build a multirotor UAV. According to the simplified model provided by [32], the steady state thrust generated by a hovering rotor is modeled as,

$$T_i := C_T \rho A_{r_i} r_i^2 \omega_i^2 \tag{2.3}$$

where for a rotor i, the thrust coefficient C_T depends on rotor geometry and profile, ρ is the density of air, A_{r_i} is the rotor disk area, r_i is the radius and ω_i is the angular velocity. It can be simplified using c_T which can be determined from static thrust tests,

$$T_i = c_T \omega_i^2 \tag{2.4}$$

And the reaction torque acting on the airframe generated by a hovering rotor in free air,

$$Q_i := c_Q \omega_i^2 \tag{2.5}$$

where the coefficient c_Q can be determined by static thrust tests. Assuming that each rotor thrust is directed in the z axis of the vehicle, the sum of the thrusts from each individual rotor is the overall hover thrust applied to the airframe. For a multirotor with N rotors the total thrust is,

$$T = \sum_{i=1}^{N} |T_i| = c_T \sum_{i=1}^{N} w_i^2 \tag{2.6}$$

The hover thrust is the primary component of the exogenous force,

$$F = T_{\sum} \vec{z} + \Delta \tag{2.7}$$

where Δ contains secondary aerodynamic forces that are caused when the assumption of rotor in hovering is violated.

The net moment $\tau = \{\tau_1, \tau_2, \tau_3\}$ arising from the aerodynamics is the combination of rotor forces and air resistances,

$$\begin{aligned} \tau_1 &= c_T \sum_{i=1}^{N} d_i \sin(\Phi_i) \omega_i^2, \\ \tau_2 &= -c_T \sum_{i=1}^{N} d_i \cos(\Phi_i) \omega_i^2, \\ \tau_3 &= c_Q \sum_{i=1}^{N} \sigma_i \omega_i^2 \end{aligned} \tag{2.8}$$

where d_i is the distance from the central axis of the UAV. In addition, $\sigma_i \in \{-1, +1\}$ denotes the direction of rotation of the ith rotor. $+1$ corresponds to clockwise and -1 to anticlockwise. And ω_i is the angle between airframe support arm and the airframe's x axis. For a quadrotor, this matrix can be written in the form,

$$\begin{bmatrix} T_{\sum} \\ \tau_1 \\ \tau_2 \\ \tau_3 \end{bmatrix} = \begin{bmatrix} c_T & c_T & c_T & c_T \\ 0 & dc_T & 0 & -dc_T \\ -dc_T & 0 & dc_T & 0 \\ -c_Q & c_Q & -c_Q & c_Q \end{bmatrix} \begin{bmatrix} \omega_1^2 \\ \omega_2^2 \\ \omega_3^2 \\ \omega_4^2 \end{bmatrix} \tag{2.9}$$

The constant matrix Γ can be represented as,

$$\Gamma = \begin{bmatrix} c_T & c_T & c_T & c_T \\ 0 & dc_T & 0 & -dc_T \\ -dc_T & 0 & dc_T & 0 \\ -c_Q & c_Q & -c_Q & c_Q \end{bmatrix} \tag{2.10}$$

In order for the multirotor to hover, suitable ω_i must be chosen by inverting Γ such that $\tau = 0$ and $T_{\sum} = mg$.

2.2 Short History of UAVs

UAVs, also referred to as drones, are a device first developed to destroy, but now used to enhance humankind. The article in [33] states that it is a basic technology of war that can now be used to execute activities that can not be performed on the ground easily. The UAV word for "drones" was taken from male honeybees. For many decades, drone technology has been around. While it may surprise the present generation, they have been used primarily in military uses, such as aerial bombardment, in the past.

The earliest use of this technology dates back to the Austrian-Venice War of August 1849. Pilotless hot air balloons were used by the Austrians to hold and drop bombs on the streets of Venice[34]. While they are not known as drones, this was the beginning of the UAV notion.

During World War 1, the first use of remote control aircraft documented in history was in 1918 [33]. To aid soldiers by bringing bombs, the United States created an unmanned aircraft named Kettering Bug [35]. However they were not actually used for that purpose. Following this incident, UAVs were used by numerous countries throughout history in many conflicts, including Israel's war against Lebanon, in the U.S. Vietnam War, and so on.

The most famous drones seen nowadays are the Quadrotor UAVs, and they have come a long way. The first experimental quadroter called Bréguet-Richet Gyroplane [36] was introduced by French inventor brothers Jacques and Louis Bréguet in 1907. It flew just two feet off the ground during its first flight and weighed about 578kg.

Since the beginning of the last century, UAVs have grown steadily, and since the last decade, development has been extreme. Instead of being used for military purposes, they are commercially used by various firms to distribute packages and medicines. They are being used for the welfare of humanity through the application of modern hardware and emerging technologies.

2.3 Features - Reason for its Popularity

UAVs have recently become popular and are being made accessible to the public. Quadrotor style UAVs are the most of the widely used UAVs that can be seen. Pricing is the key factor for its growth. The UAV's low inexpensive cost encourages researchers, businesses and hobbyists to use them in numerous ways. They are used in diverse applications, from 3D mapping of an area to rapid deliveries, by using their ability to quickly access the most remote regions. It's hard to believe that taking aerial photographs using a manned helicopter will be very costly without UAVs.

There is rapid progress in the production and deployment of UAVs with the increasing development of micro-electro-mechanical system (MEMS) [37], sensors and smaller-power-efficient embedded processors [38]. As a consequence, multirotor UAVs are common due to their following features:

- Easy Deployment: It is simple to set up a UAV using off-the-shelf components with fewer hardware on-board. The drones are made partially to fully autonomous with advanced technologies, making them easy to deploy even for an inexperienced person. Drones are becoming available to a wide variety of users, because of comparatively low cost for most variants.

- High maneuverability: Multirotor UAVs are lightweight and small. And it can also travel very close to the ground and can also quickly navigate to locations that are traditionally difficult to reach. Due to multiple rotors, UAVs often have a rapid and greater range of motions. Because of these qualities, they are often used for racing.

- Autonomous flight: Since UAVs use global positioning system (GPS), it is possible to configure and precisely maneuver in the set flight paths to specific location. In a variety of cases, this is extremely beneficial. To spray fertilizers on individual crops, for example, or to send packages to the right home. The accuracy of UAVs saves users both expense and time.

- High quality photography: UAVs are good for taking high-quality aerial video and photos and collect other sensor data. These high-resolution photographs can be used to construct maps that can be helpful for surveying or rescue operations. For inspections, UAVs can now carry video cameras, thermal image sensors, chemical sensors etc, with the production of various kinds of sensors.

- Security: UAVs have the benefit of providing security since they can cover a large region quickly. They can be used by private corporations for surveillance and monitoring. During and after natural disasters, they can also collect useful data to help in safety and rescue operations.

2.4 UAV Utilization in Various Industries

UAVs are capable of doing amazing tasks, whether it is movie production or emergency response. After 2016, industrial uses of UAV technology have expanded following the legalization of commercial UAV use for industries by the Federal Aviation Administration (FAA). According to [39], in the first month after the FAA registration system went live, around 300,000 users had registered their small UAVs.

Following the release of the Part 107 law for operating UAVs, there was a major barrier reduction after 2016. Before this regulation was introduced, any person attempting to fly a UAV needed to receive special approval from the FAA, which was costly and time-consuming. The relaxing of this law has helped UAV users without requiring special approval to fly drones. And these laws apply, of course, only to small UAVs that weigh less than 25kg. The flight beyond the line of sight at a maximum altitude of 400 feet [40] is restricted by certain additional limitations.

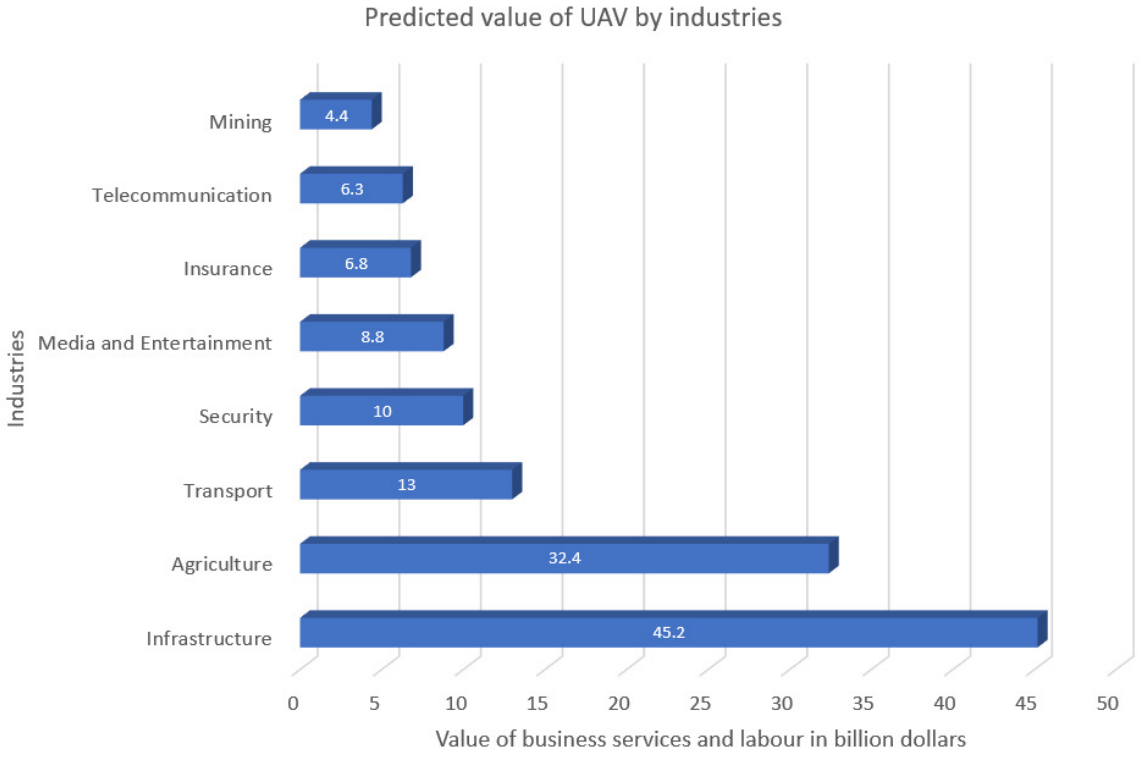

Figure 2.1: Predicted value of UAV by industries according to Business Insider Intelligence (BII).

Business Insider Intelligence (BII) forecasts drone revenues to exceed $12 billion by 2021 [41], rising 7.6% from $8.5 billion in 2016's compound annual growth rate (CAGR).

UAVs are most often thought to be used for aerial video and photography. UAVs are used as a multipurpose tools from agriculture to the Internet. According to Business Insider Intelligence [41], the graph in Figure 2.1 indicates the prediction of UAV values by industries. According to the information, with $45.2 billion, the infrastructure industry has major business services for UAVs, followed by agriculture with $32.4 billion, transport with $13 billion and security with $10 billion.

Some of the major use of UAVs in industrial sector are listed as follows:

2.4.1 Infrastructure

The land needs to be mapped before a civil engineering project starts, and sufficient site information and data needs to be gathered. With the advent of drones, it is possible to perform these time-consuming tasks even more easily. [42] records a decline in survey field hours by almost 30 times in construction and a strong ratio in survey grade data collection in mineral exploration is noted. The data can be transmitted by drones in 20-30 minutes, which can take several days for a manned team of surveyors.

A general overview of the use of UAVs in the civil engineering sector is given in another analysis in [43]. It is often claimed that, relative to other sectors, the use of drones in the construction industry is new. They can be used as an effective bridge inspection tool [44] since the drones can fly really high. Whereas [45] uses infrared sensors on UAVs to survey the thermography of buildings.

2.4.2 Agriculture

UAVs can be used in several different ways in the farming industry. UAVs can help detect failed crops, according to an article in [46], and provide inventory of the crops, which can save farmers a lot of money. They also state that, relative to the traditional time consuming procedure, the UAVs can perform the task faster. Through comparing UAV to a school bus, they quote that the significance lies in the sensors and software that helps to expand the potential UAV applications. UAVs may also be fitted to spray fertilizers, pesticides or water tanks, in addition. By easily recording their health conditions and numbers, UAVs will also assist in animal surveillance. It is therefore possible to support farmers in several different ways.

Biocarbon Engineering [47], a start-up venture, uses UAVs to plant trees within Australia's abandoned mines. They are now spreading to other countries where they work for a non-profit base, like in Myanmar. They are working on planting trees to tackle climate change. They use UAVs to gather a land's topographical data by flying over it. The best places to plant the seeds are determined on the basis of the

landscape and soil conditions. Planting is carried out by firing germinated seeds from the UAVs inside bio-degradable pods.

2.4.3 Transport

Drone-based delivery services are one of the most noticeable UAV solutions. Amazon Prime Air is one of the most well-known delivery systems focused on drones. These are very useful for distribution in remote areas or places where it is hard to navigate by road. Direct distribution to doors will become more real with further development in drone technology, according to [48].

Moreover, drones are now seen by corporations such as Google and Facebook as a feasible means to transport their services to the most distant and inaccessible regions. In order to see their viability in remote areas for providing internet access, Facebook is testing the solar powered UAVs [49]. The Facebook project HAPS (High Altitude Pseudo Satellite) promises the development of solar-powered drones which can fly for months at a time.

2.4.4 Media

Aerial photography is another of the most popular UAV applications. When photographing, they may have broader coverage. Therefore, costly equipment for large angles is not required. Even small media organizations can now afford to obtain aerial imagery relative to a pricey helicopter, years ago. Moreover by reaching remote areas and flying through confined spaces or closer to the ground, they can have better shots.

For video recording, drones are increasingly popular with production companies in the entertainment industry who require action sequences, literal birds-eye views, stunning panoramas or 360-degree views of subjects. For instance, companies such as Dronitech are specialized in the development of UAVs, as well as aerial photography [50], for groundbreaking drone technologies. For the aerial photography shoot of a wedding in India, they are considered to have adopted a commercial UAV.

2.4.5 Disaster Response

While UAVs are used in different applications, they are not seen used for emergency responses. They can be very beneficial, considering their advantage of flight in 3-dimensional area and fast movements. The work in [51] tests certain interactions based on UAV and discusses certain disaster relief projects. The use of UAVs to provide medical support will expand emergency response aid possibilities. It may provide emergency response doctors with an upper hand in critical circumstances by providing medical equipment or having a view of the emergency situation.

By sending warnings at the early stages to prevent fatal collisions, UAVs may be used to minimize hazards such as volcanic eruptions, forest fires, etc. Disasters can include chemical plant accidents, tankers transporting toxic chemicals that cause smoke and can be detected in the air. Besides avoidance, they also come in handy during disasters. UAVs can provide bird's eye view of an area, which can be useful for real-time tracking to provide useful emergency control information.

2.5 Aerial Manipulation

The intention of aerial manipulation is to combine the versatility and mobility of certain aerial platforms with the robotic arm's manipulation capabilities. Several review papers like [12], [14] and [52] can be found providing the collective study of results reached by various researches based on aerial manipulation. The letter in [53] discusses numerous approaches and requirements for evaluating and comparing the efficiency of aerial manipulators. In terms of accuracy, execution time, manipulation capability, or impact response, a range of benchmarks are established to assess the performance of the aerial manipulator.

Not only can the traditional UAV and manipulator combination realize aerial manipulation, but it can also be realized with a tailored UAV prototype. A review of snake-like aerial manipulators is found in [54]. They include the topics like dynamics, autonomy, sensors, controls methods, and so on.

There is also a new and increasing interest in the collaborative aerial manipulation

using multi-UAV system. The survey in [55] addresses and systematically analyzes multiple techniques for this collective aerial manipulation.

2.5.1 Manipulator Types

In early aerial manipulation, industrial robotic manipulators are found to be mounted to aerial platforms. Since these manipulators are heavy, the aerial platforms used are often very large, like a helicopter. For example, Huber et al. in [56] defines an aerial manipulator system consisting of a helicopter platform and a fully actuated 7 DoF redundant industrial robotic arm. In the same way, the study in [57] focuses on the efficiency optimization of an aerial manipulation device consisting of a Flettner-helicopter and 7 DoF manipulator.

In addition the research in [58], in order to avoid the problem of collision between rotor blades and obstacles in a complex environment during aerial manipulation, a robotic manipulator is installed on an active platform which is fixed on the aerial platform by means of a cable. Instead of being attached straight to the aerial platform.

Unlike the aerial manipulation using industrial manipulators, a new multi-link arm connected to the UAV for aerial assembly tasks is introduced through the paper in [59]. Considering the motion of the arm, the procedures for controlling the UAV are also illustrated. A low weight compliant arm for aerial manipulation is presented by the authors in [60], which also allows for calculating payload mass, as well as detecting collisions against forearm obstacles. In addition, the paper in [61] introduces the concept and development of a 4 DoF aerial manipulator for bridge inspection , where the arm is mounted at the top of the multirotor frame. The manipulator joints are fitted with a compliant mechanism that allows for environmental interaction to reduce the effect on the stability of the airframe.

To pick up and deliver objects using an multirotor UAV, [62] develops a novel combination of an electro-permanent magnetic gripper with a passively compliant structure to grasp stationary and moving objects. Whereas, in [63], an aerial manipulator for perching a multirotor UAV on a smooth vertical surfaces based on passive vacuum cup technology and the absorption of aerial impacts is presented.

In addition, a model for a manipulator that is suitable for a UAV with two passive rotating hemispherical shells is presented in the [64]. And the authors in [65], propose a new mechanical specification for the tentacle device for aerial manipulation . Using cable-driven system with servos and 3D printed components, the tentacle arm is made simpler and effective.

2.5.2 Aerial Tasks

When designing aerial manipulator systems, many aerial manipulation tasks have been considered by various researchers. Lee et al. in [66], to thoroughly investigate the idea of aerial manipulation, presents contact with moving structures using a multirotor-based aerial manipulator opening a hinged door. Similarly, Kim et. al. in [67] demonstrates how an unknown drawer is opened and closed using an aerial manipulator. The research in [23], as mentioned in Chapter 1, explores a multicopter landing on uneven surfaces using an adaptive landing gear with four compliant robotic legs.

A hybrid control model for the combined micro aerial vehicle-arm system is formulated in [68], which incorporates interaction forces acting on the end effector to perform aerial-writing tasks on a whiteboard. The paper for semi-autonomous canopy sampling in [69] presents a physical interaction between an aerial manipulator and a tree. Whereas, Suarez et al. in [70], a contact-based inspection of long arrays of tube structures in hard-to-reach locations is considered, using a hybrid rolling-aerial platform capable of landing and moving along the tubes during the inspection without wasting energy in the propellers.

The work presented in [71] from our laboratory describes an implementation of high-altitude torsional work using a UAV equipped with an upward directed hand on top of a hexarotor frame to successfully unscrew a light bulb. And [72] proposes airborne docking using two multi-rotor aerial robots transport, one multirotor UAV using another using a winch mechanism to minimize the effect of downwash.The work in [73] describes the efforts to develop an aerial robotic platform with the ability to use a top mounted omni-wheel drive system and an AR-marker system to traverse a ceiling

with high stability and accuracy. In an infrastructure inspection work environment, it is suitable for setting painted ink-markers used as direction for drilling, measuring or maintenance tasks on the ceiling.

2.5.3 Manipulator Placements on a UAV

Manipulators are attached on the UAV frame to perform aerial manipulation. Manipulators are placed on the UAV depending on the task. The most common type of manipulator attachment is under the UAV similar to the human sized manipulator in [20] and grasping mimicking manipulator in [74]. Since the UAV can fly high or hover over a place, the downward mounter manipulators come in handy to perform manipulation tasks in these places.

The manipulators are seen attached on the top of the UAV frame for contact based structure inspection from its underside [75] and in the case of [76], for docking the UAV using the gripper onto a pipe like structure.

In addition, side-ward manipulation is also required sometimes for force application tasks [77], wall contact based inspection [10], and bridge inspection by hammering [78].

2.5.4 Altered UAV Frames

A UAV's mobility in its standard configuration is limited, as all propeller force vectors are parallel and only 4-DoF actuation is achieved. The study in [79], without the need for any additional hardware, considers a different hexarotor architecture where propellers are tilted. In this way, the hexarotor acquires a 6 DoF motion that allows it to independently achieve free space positions and orientations and to be able to exert forces to avoid any wrench for aerial manipulation tasks.

Similar works can be seen in [80], suggesting a tiltrotor architecture for a UAV for improved locomotion and manipulation in unstructured surroundings. Also in [81], showing path-hindering obstacle that is forcibly eliminated by a tiltrotor UAV via pushing manipulation.

In the work of Bodie et al. in [82], they use a completely actuated tilt-rotor aerial system fitted with a rigidly mounted end-effector for contact with unstructured environments through force application. They call it an omnidirectional aerial manipulation platform. A new omni-directional multi-rotor aerial platform is also proposed by Park et al. in [83], which is entirely powered by six opportunistically spaced rotors, each operated for bi-directional thrust generation.

2.5.5 In-flight Transformable UAVs

Though aerial manipulation is carried out using the attached manipulator, some studies concentrate on the realization of aerial manipulation using the UAV body itself. Zhao et al. in [84], for instance, introduces aerial manipulation by using a transformable aerial robot's entire body. They illustrate the use of two-dimensional multilinks through experiments that allow secure aerial transformation and can be used as a gripper. The study in [85] also focuses on aerial grasping through adaptive shape transformation to the form of the target.

In addition, for a vertical take off and landing UAV, the work in [86] presents shape-shifting transformation. They demonstrate an effective multi-rotor, tail-sitter, and fixed-wing function with in-air transformation.

Similarly, Falanga et al. suggests a morphing configuration for quadrotors in [87] consisting of a structure of four individually rotating arms folding around the robot body. In various functions, such as navigating narrow spaces, close inspection of vertical surfaces, and object grasping and transportation, they illustrate the flexibility of the proposed adaptive morphology.

2.5.6 Cooperative Manipulation

Research in [88] demonstrates the planning and control of three quadrotors handling and transporting payloads in three dimensions through cables. Nguyen et al., however, proposes a novel robotic platform for aerial manipulation through rigid frame and passive spherical joints by spherically linked multi-quadrotor platform in [89].

They serve as distributed rotating thrust generators to mutually drive the frame by changing its attitude and thrust power.

In addition, the study in [90] introduces a new model for aerial payload transport and object manipulation by the UAV team. This latest model, called cooperative payload lifting and handling, implements a continuous deformation agent approach for transporting and handling objects individually with collision protection.

Researches such as [91] and [92] demonstrate a heterogeneous cooperative robotic system. The former suggests the scenario of a ground robot and an aerial robot working together to shut a valve in a disaster-ridden industrial setting. Whereas the latter consists of a ground manipulator and a team of aerial robots armed with a basic grip to control the same entity. This kinds of heterogeneous robotic systems incorporate the benefits of physical power from ground platform along with a large workspace of aerial platform.

Chapter 3

Design Concepts of a Multipurpose Manipulator System

UAVs with manipulators to execute different sorts of operations can be recently seen in the literature. In [76], we used a UAV attached with a gripper on its top for docking on objects and executing manipulation using another manipulator attached at the bottom of the UAV, during a research on aerial manipulation. After conducting manual stray object removal tests, we observed that it is very difficult to work and control using a single manipulator. For dynamic tasks, two or more manipulators will be optimal. We have noticed that having a considerably large manipulator attached to the UAV makes it very difficult to take-off and land the UAV. Therefore an idea was developed to create a manipulator system to act both as a landing gear and to perform other tasks. That culminated in the design of a UAV with three-manipulator design.

There aren't many studies with three manipulators on a multirotor UAV. Therefore the potential tasks that can be performed are not generally discussed in literature. The definition of three essential fundamental tasks that can be carried out using a UAV with manipulators is explored in this chapter. The tasks are landing, aerial grasping and sideways physical contact with the environment. For almost every multirotor UAV to be deployed in an unknown area, these three tasks are important.

3.1 Landing

Multirotor type UAVs have the potential to hover in a fixed position relative to fixed wing type UAVs. This capability of a multirotor UAV makes it acceptable to be used for applications such as aerial photography. In addition, using some position feedback, it is possible to maneuver the UAVs autonomously, making them more desirable for aerial manipulation. In autonomous navigation, the UAV is able to travel by itself at the desired speed to the destination, provided the target position. This form of autonomous control is used by some studies to land the UAV on landing pads [93] or markers [94] autonomously. Attempts were also made to autonomously land the UAV, as in [95], on a moving platform relying on vision feedback.

Work on autonomous landing has recently advanced into the development of adaptive landing gears. A research [96] released in 2015 sponsored by the United States Defense Advanced Research Projects Agency (DARPA) to enhance four-leg helicopter landing gears by using force-sensitive touch sensors on its feet. And recently, in their work published in 2018, Russian researchers developed dynamic landing gears using torque sensors for a multirotor UAV. We have also published a report [97] on adaptive UAV landing using the proposed three manipulator system using depth camera feedback during the development of our research.

When contemplating land interaction for a robot, such as standing or walking, the surface forms must be recognized. The capability of multirotor UAVs to take-off and land vertically does not need a lot of take-off or landing space. But for landing, the surface has to be flat. For a legged robot, the terrains are classified in the work of Schue et al. [98] as (a) plain, (b) with a deep pit whose bottom cannot be reached by the robot's legs, (c) with elevations, (d) elevations and pits, and (e) normal rugged terrain.

The stability of the UAV is critical for safe landing. The axes of the rotors are kept perpendicular to the ground for ascending or descending in the case of a typical multirotor UAV. Therefore to safely land, the orientation of the UAV legs should be so that the body of the UAV is parallel to the horizon of the earth. The legs must allow

the UAV body to remain mechanically stable even after landing, without the need for any external force to stabilize the robot after landing. This is important when touching the ground or taking off from the ground to keep the UAV from rolling. Rooftops, tree branches or rocky mountains are the most common sites for landing during UAV deployments during disasters. These surfaces are not smooth, and ending up in a rolling crash is very much possible for a UAV. Two types of rollover accidents are discussed in the research paper in [23]. They are accidents that are static and dynamic. There occurs a static rollover accident when the UAV is stationary with the propellers shut-off on the ground, and the UAV topples. They can occur because of the surface shift that results in the UAV body being elevated. The by-product of the centre of gravity of the UAV is (CoG). When the UAV is about to land on a surface or is about to take-off from the ground, dynamic rollovers may occur. Dynamic rollover can occur either if the field is stagnant with elevation or if the surface is cluttered, and the UAV takes-off or lands on it.

In [99], McGhee et al. explains that a sufficient condition for point feet robot's static stability is that the robot always has at least three of its legs on the ground. And the projection of the robot's CoG lies inside the support polygon formed on the ground by the legs of the robot. The stability margin is defined as the shortest distance to the boundary of the support polygon from the vertical projection of the CoG (Cg marked in Figure 3.1) of the robot onto earth's horizontal plane. If the CoG is inside the support polygon it is defined as positive and otherwise negative.

In order to measure the Stability Margin (SM), the support polygon formed by the three manipulators (or legs) of the UAV landed on the ground can be decomposed into three sub-triangular regions. The sub-triangles are shaped on the basis of the CoG projection of the UAV frame on the ground surface as seen in Figure 3.1, labeled areas as S_1, S_2 and S_3.

The vertical projection of C_g is still inside the stability polygon in the case of landing a UAV on a flat surface with fixed landing gears, so it is statically stable. In the case of landing on an inclined ground, if the slope angle is too angled, the vertical projection of Cg shifts onto the polygon boundary and eventually beyond.

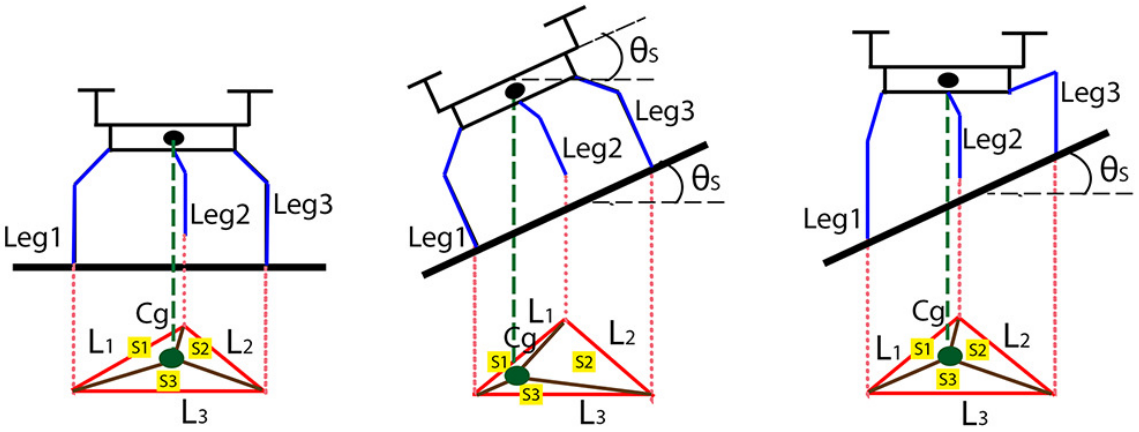

Figure 3.1: Illustration demonstrating the mandatory conditions for safe landing of UAV with robotic manipulators attached. For static stability, the center of gravity (C_g) should be inside the support polygon produced on the ground by the manipulator tips. [97]©2019 IEEE.

However, stabilization can be accomplished on an inclined surface by changing the posture of the legs to keep the body of the UAV parallel to the horizon of the earth. In other words, the robot can be statically stable if the manipulator tips are outside the vertical projection of the body on the ground. The manipulator's minimum and maximum height postures can be used to determine the maximum slope at which a successful landing can be carried out. The manipulators should be strategically positioned in the case of dynamic terrain with varying elevations so that the UAV body can not hit any surface to prevent collision.

Given the lack of friction on the ground floor, there are risks of skidding while landing if the manipulator tips make non-perpendicular contact on the surface. Moreover more torque is required to sustain the manipulator postures on the joints θ_2 and θ_3 combined. Whereas, the orthogonal distance from the ground touch point to the force is zero at θ_3 in the event of perpendicular contact. The overall torque needed is then decreased. The manipulator tips are thus assumed to be maintained perpendicular to the ground for stabilization while landing, as seen in Figure 3.1.

3.2 Grasping

In applications such as rescue operations, mobile robot deployments also require manipulation capability, such as door opening or debris removal. Numerous algorithms were developed for robots to detect entity shapes [100, 101] and identifying suitable grasps [102, 103]. Schnaubelt et al. in [104], for instance, offers a solution that allows arbitrary rigid objects to be grasped by extracting the scene based on geometric segmentation to allow a ground robot to grasp different objects in a cluttered environment. Whereas, a 3D form detection approach for extracting stacked rubbles is used in [105] by independently recognizing their characteristics such as shapes, masses, center of gravity locations, and so on.

To effectively grasp an entity, grasp planning is necessary. The grasp planning consists of deciding the hand positions capable of maintaining the distorted object from external disruptions. In other words, it is known to be in a force-closure grasp [106] if the position of the fingers guarantees object immobility against any external force or moment applied to the object.

As shown in Figure 3.2, various potential grasping techniques can be used in a three manipulator configuration with grippers:

- Two finger grasp - using the manipulator's gripper
- Two sets of opposite fingers - using two of the manipulator's grippers aligned to grasp a long object
- Three finger grasp - using three manipulators together to grasp an object

In the figure, (a) and (b) actuators of the gripper are used to grasp objects. In (c) three manipulator tips without gripper actuation are used.

The choice of a secure grasp is one of the main components of grasp planning. Secure grasp, as indicated in [107], is defined as a force closure grasp on the object. Nguyen et al. tackled the issue of synthesizing planar grasps in [106] by considering force-closure as a necessary condition. Provided a grasp in a plane, if all the forces applied lie in the plane of the object, then the form of the object is the only input

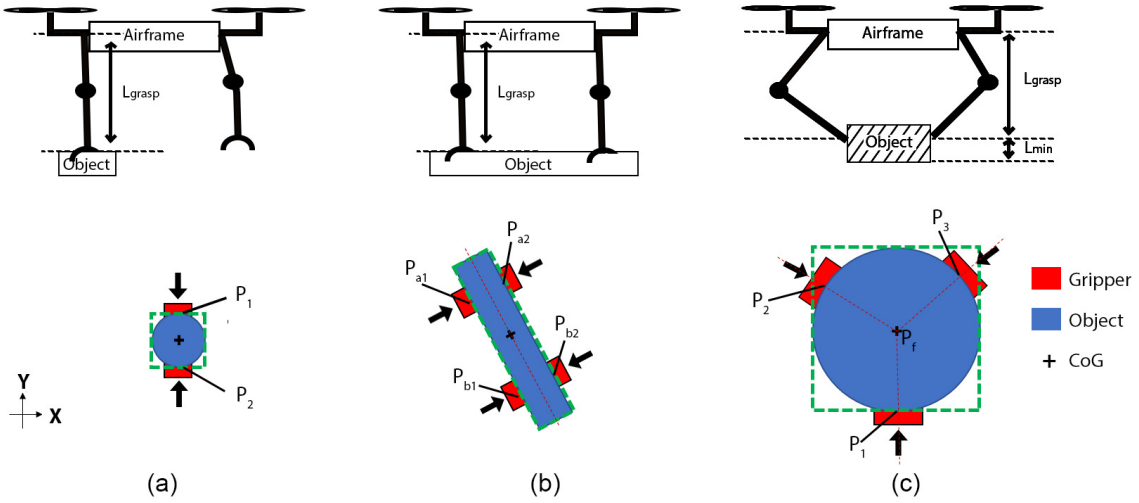

Figure 3.2: Using a three manipulator mechanism with grippers, different grasping strategies can be realized. (a) Single manipulator. (b) Two manipulators. (c) Three manipulators. The direction of force applied during grasp is indicated by arrows.

into the system. Any contact between the fingertips with the target may be depicted as a convex total of three primitive contacts.

The conditions for forming a two and three point planar force-closure grasp are defined as follows, as specified in [106] and summarized in [107]:

- Two finger grasp: A two-point grasp is in force-closure through opposite fingers, P_1 and P_2 with friction if and only if $\overline{P_1P_2}$ points out and into P_1 and P_2 respectively at their friction cones.

- Three finger grasp: If a point P_f (power focus point) exists, a three-point grasp at contacts, P_1, P_2 and P_3 with friction is in force closure, so that for each point P_i, $\overline{P_fP_i}$ points out the i^{th} friction cone. Let k_i be an edge-pointing unit vector of $\overline{P_fP_i}$, a strictly positive combination of the three directions being zero: $\sum_{i=1}^{3} \alpha_i k_i = 0$

The altitude of the UAV can be controlled and the force-closure plane for the object can also be modified. Depending on the object size and surroundings, an acceptable distance for grasping will therefore be adjusted. As seen in Figure 3.2,

to prevent unwanted interaction with the surface, L_{grasp} is the grasping distance and L_{min} is the minimum distance the UAV must sustain from the object. However it is usually best to grasp the object from as far as possible.

Moreover the farther the object is from the UAV, the less the down-wash of the propeller blades affects it. However, the transport of an object far from the UAV's vertical center increases the average vertical height of the entire robot and results in aerodynamic drag. It is also therefore important to hold the object as close as possible to the body of the UAV. One way to solve this issue is to grasp the object from afar, and shift the manipulators to get it closer to the UAV's body.

3.3 Obstacle Avoidance

When navigating outdoors, GPS is the most common method used by UAVs to monitor their location. Indoor flights, however, have a variety of difficulties. GPS signal may not be available, contact may be challenging, obstacles need to be located and avoided, traversing may be difficult or impossible, or dark and smoke-filled conditions may result in low visibility. In addition to operating in open spaces, UAVs may be worked beneficently in enclosed regions such as partly collapsing structures, trenches, caves or underwater mines, as discussed in [3]. For the secure operation of UAVs, the potential to prevent collisions with fixed and shifting objects is crucial. Even a slight drift from its desired location can lead to a crash. Work such as [108] implements UAV collision avoidance path planning by applying UAV sampling-based path planning strategies to eliminate moving obstacle collisions.

The performance of the UAV propulsion system varies in close proximity to walls or ground [109] in addition to the positioning error, which makes it very difficult to maneuver in a very tight space [12], like tunnel or hallway. Research such as [24] has built a passive spherical shell to prevent collisions, which may reduce the UAV system's manipulation capability.

We go for a hardware-based technique in this study, to prevent crashing by touching physically and stopping the UAV with the manipulators near a barrier. The same

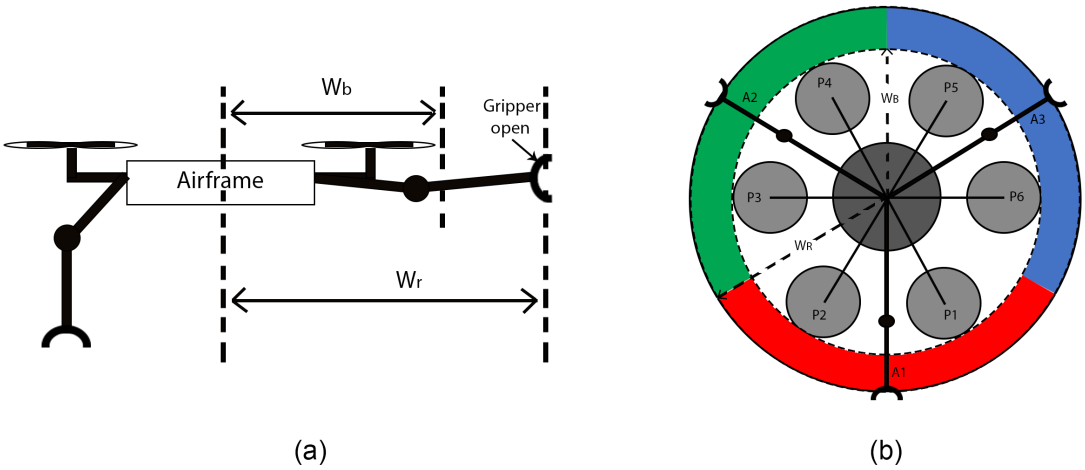

Figure 3.3: Illustration of the criteria for preventing UAV collision when interacting with vertical structure. (a) The length of the manipulator should be longer than the UAV frame to prevent the UAV body from reaching any vertical surface. (b) UAV circumference, split into three regions for each of the manipulators.

set of manipulators placed on the UAV can establish physical interaction. The push and pull tasks discussed in [81, 110] or door opening tasks as defined in [111] are also suitable for this sort of approach. UAVs with three or more manipulators, similar to the method mentioned in [112], can also help in crossing narrow tunnels by touching the walls to navigate.

The manipulators should be longer than the outer radius of the UAV, including the propellers, if the UAV manipulators are to be used for physical contact-based obstacle avoidance. And they should be able to stop obstacles farther away from the UAV diameter. Figure 3.3(a) shows the manipulator length criterion with respect to the radius of the UAV. The overall circumference around the UAV can be split among the manipulators for a multiple manipulator system attached around the UAV to avoid just the obstacles in their area. For a three manipulator system, each of the regions is separated by 120 degrees, with a manipulator each located at the middle of their respective regions. Adding more manipulators will decrease the working area of each manipulator and can simultaneously cover a larger UAV circumference. Nevertheless

the UAV's nominal payload limit reduces the amount of manipulators placed on its frame.

For a three or more limbed robot, Shapiro et al. in [112] proposes an algorithm based on the foothold position. Through raising one leg, they recognize motion, while the other two brace the robot against the walls of a tunnel. A UAV would be able to maneuver through a very narrow tunnel (with a width greater than the diameter of the airframe) if it could brace from outside the propeller area on both sides, to prevent its body from swinging or to prevent the propeller from touching the tunnel walls. Therefore, for a UAV with three manipulator system at least one manipulator on each side can be used to protect the airframe from hitting the tunnel walls, and one can be used in the direction of navigation. Taking this into account, it is feasible to use a three manipulator system for object avoidance and narrow indoor traversal. As seen in Figure 3.3(b), the manipulator area along the circumference of the UAV can be split for a three manipulator system. To have a wider impact area on the wall, the grippers should be left open. The opening of the grippers also covers a wider vertical surface of the UAV at the end-points of the desired manipulator.

3.4 Reasons for the Choice of a System with Three Manipulators

The greater the number of manipulators, the better the system can be used to execute several functions. But the weight of hardware that can be borne by a UAV is often reduced due to payload restrictions. By accurately listing some of the most significant functions, it is possible to draw an inference about the minimum possible number of manipulators to be placed on a UAV. The need of atleast three point contact for landing safely, the various forms of grasping ability and the ability to grasp large object using three manipulators, and the ability to avoid obstacles or tunnel navigation by bracing the tunnel walls, all points to a three manipulator system, as described in this chapter. It is therefore considered in this study to build a manipulator device with three robotic arms to accomplish the tasks described above.

Chapter 4

Hardware Design and Peripherals

A robot prototype is developed to realize the tasks discussed in Chapter 3. The robot's hardware configuration consists of an off-the-shelf hexarotor airframe and a 300E propulsion system comprising DJI's brushless motors and ESCs (electronic speed controllers). For high level navigation control, a DJI N3 flight controller system is installed. The flight controller facilitates serial communication with an external computer, providing autonomous navigation feedback and controls.

NVIDIA Jetson TX2 [113] is placed on the top of the airframe to control the manipulator and to connect with the flight controller in order to perform autonomous navigation control. The Jetson TX2 is power-efficient on-board computing system with dual core NVIDIA Denver2 and quad-core ARM Cortex-A57 processors is an integrated system-on-module (SoM). It comes integrated with an 8GB 128-bit LPDDR4 RAM and a 256-core Pascal GPU. The device supports Linux operating system and according to the vendors, can offer computational output of more than 1 teraFLOPS of FP16 (half precision floating point arithmetic) with less than 7.5 watts of power. To store the operating system and data, it has an inbuilt 32GB eMMC. A development board with a wide range of peripherals comes with the processor. In our UAV system, however, some of the peripherals are not required. We therefore use Connect Tech Inc.'s ASG003 Orbitty carrier board [114] along with the Jetson TX2 processor, making the device lightweight and portable. Along with the peripheral support, the characteristics of the Orbitty carrier board are as seen in the Table 4.1.

Features	Specifications
Dimensions	87mm × 50mm
Display	1× HDMI
USB	1× USB 3.0
Ethernet	1× Gigabit Ethernet (10/100/1000)
Audio	1× HDMI Integrated Audio
SD Card	1× microSD
Serial	2× 3.3V UART
Misc	4× GPIO, I2C
Power Requirements	+9V to +14V DC Nominal (+19V Peak)
Weight	Orbitty Carrier: 41 grams Jetson TX2: 144g (with heatsink)
Operating Temperature	-40°C to +85°C (-40°F to +185°F)

Table 4.1: Specifications of ASG003 Orbitty carrier board.

At similar spacing, three equivalent robotic manipulators are constructed and attached around the UAV. The manipulators are mounted in such a manner that the manipulator will provide a wide workspace and the tips will reach the UAV's top, side and bottom. To make it as small as possible, the material, actuators and sensors used in the manipulators are specifically chosen to address the restricted payload of the UAV.

The manipulators are of an original design and made of materials such as aluminum pipes, ABS and PLA 3D printed parts. Serial servo actuators are connected to each manipulator to support three DoF in the yaw and 2 rotational axes. In addition to these joints, the tip of each manipulators are provided with a gripper. The inclusion of the gripper makes a large possibility for tasks to be carried out. The subsequent sections detail the different peripherals used in the manipulator's architecture.

4.1 Motors with Angle, Joint Torques and Other feedback

Serial servo motors from Robotis, i.e. Dynamixel AX-12A [115], are used to actuate the joints for the manipulators. These servo motors are operated using serial communication connections, unlike traditional servo motors, which can only accept pulse width modulation (PWM) signal input and provide output angle control. They are equipped with sensors in addition to output position control to provide other feedback functionality. For communicating with the controller, these servo motors use serial lines, thereby eliminating separate wiring for both power and input. Feedback signals such as its RPM, temperature, shaft location, voltage, and load can be given by the servo motors. With a unique address ranging from 0 to 254, each of the servo motors can be programmed. If a control signal with a particular address is to be sent to a servo, it is first transmitted to the serial contact link. Each of the servos tests the address and the control signal and is acknowledged by only the servo with the correct address. Therefore it is possible to monitor the shaft location of individual servos simultaneously. The servo's built-in micro-controller performs all of the sensor management and position control.

A control table with several data fields is used by the servo's built-in micro-controller to read and control the servo. Users can access a field in the control table by using a particular address. Write instructions are used to operate the servos, and to receive input, read instructions are used. The speed of contact depends on the baud rate fixed in the read only memory (ROM) of the servo. AX-12A serial servo motor specifications are specified in the Table 4.2. In the table, the maximum instantaneous and static torque is stall torque. The manufacturer recommends that the load should be equal to or less than 1/5 of the rated stall torque for steady motion. The load applied to the servo shaft may be captured, including the position of the load, by reading the correct register in the servo's random access memory (RAM). The amount of the load applied, however is measured by the percentage of the full load and is not so exact. It may only be used to confirm whether or not there is a

Features	**Specifications**
Baud Rate	7843 bps ∼1 Mbps
Resolution	0.29 [°]
Running Degree	0 [°] ∼300 [°] Endless Turn
Weight	53.5g(AX-12, AX-12+), 54.6g(AX-12A)
Dimensions (W x H x D)	32mm × 50mm × 40mm
Gear Ratio	254 : 1
Stall Torque	1.5 Nm (at 12V, 1.5A)
No Load Speed	59rpm (at 12V)
Operating Temperature	-5 [°C] ∼+70 [°C]
Input Voltage	9.0 ∼12.0V (Recommended : 11.1V)
Command Signal	Digital Packet
Protocol Type	Half Duplex Asynchronous Serial Communication (8bit, 1stop, No Parity)
Physical Connection	TTL Level Multi Drop Bus
ID	0 ∼253
Feedback	Position, Temperature, Load, Input Voltage, etc
Material	Engineering Plastic

Table 4.2: Specifications of serial servo motor AX-12A.

load, useful in applications such as deciding whether or not the gripper has an object grasped.

To prevent breakdowns during the service due to faults such as over voltage, overload, etc the servo has built-in safety mechanism. To stop short circuits or breaking down, the servo shuts itself down. After restarting, it would return to a normal state.

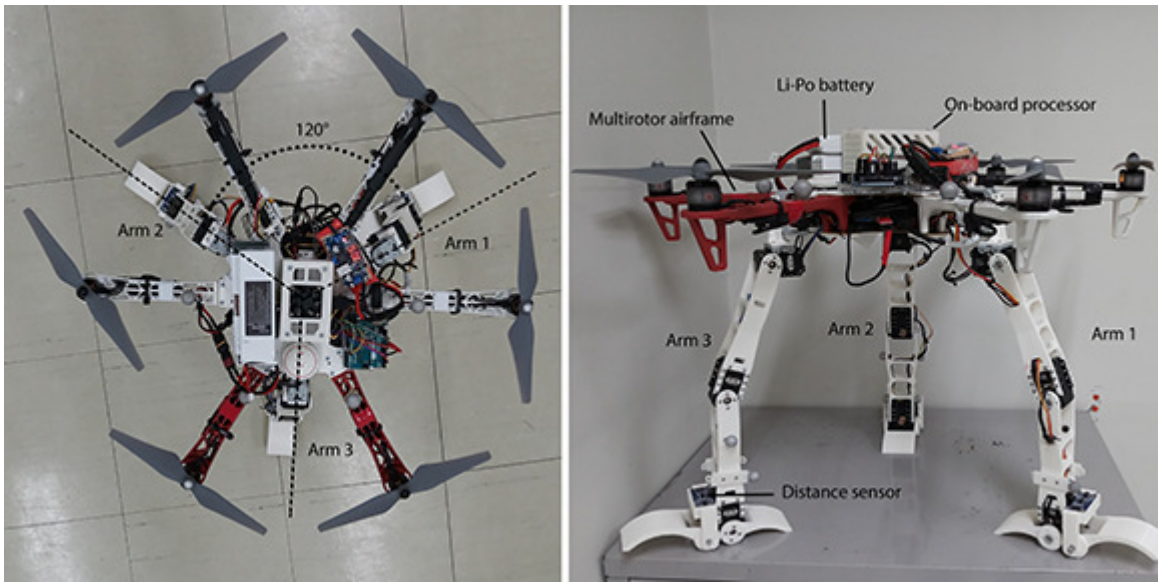

Figure 4.1: Hardware configuration of Prototype 1. (a) Top view showing the mounting of the manipulator with regard to the UAV core. (b) Side view showing the manipulators and distance sensors.

4.2 Prototype 1 with Distance Sensors

Manipulators made entirely of 3D printed ABS plastic were mounted in the first prototype of the proposed system. The servo motors were connected between the bracket structure in the links of the manipulators. The configuration and attachment of the manipulator to the UAV frame is as shown in Figure 4.1.

Low-cost, non-contact ultrasonic distance sensors (HC-SR04) are attached near the tips of each manipulator in addition to the actuators. The sensor specifications are specified in the Table 4.3. A transmitter, a receiver and a control circuit make up the sensor. The transmitter emits sound waves of a high frequency that bounce on a surface and return to the receiver, which is then interpreted by the control circuit. For the measurement of the distance to the object, the time interval between the transmission and the echo is used. For processing and calculating the distance from all three sensors, an Arduino is used and transmitted to the on-board processor for control.

Features	Specifications
Power Supply	+5V DC
Ultrasonic Frequency	40kHz
Working current	15mA
Effectual Angle	<15°
Ranging Distance	2400cm
Resolution	0.3cm
Measuring Angle	30°
Trigger Input Pulse width	10us
Dimension	43mm × 20mm × 15mm
Weight	10g (approx)

Table 4.3: Specifications of HC-SR04 ultrasonic distance sensor.

During landing, the purpose of the distance sensors is to sense the distance to an irregular surface. The reason for preferring ultrasonic distance sensors over infrared sensors is that the measurement is not based on the environment and can thus be used in bright areas as well. Links have been produced sufficiently thick as detailed in Table 4.4 so that it does not crack due to impact during landing and to totally hold the weight of the UAV.

4.3 Joint Actuator Motor Torques

To choose a proper actuating motor, assumptions are made to simplify the calculations. All of the legs are identical to each other. The angles are taken between the horizon and the link and it is assumed that all three manipulators are configured the same. In order to find the torque acting at each joint, a free body diagram is drawn as shown in Figure 4.2. Only two of the manipulators are shown in the figure for simplicity.

In Figure 4.2, L_1, L_2, L_3 are the link lengths, W_1, W_2, W_3 are the weights of each actuators. $N1$, $N2$, $N3$ are the reaction force acting on each manipulator tips. T_1,

Part	Specification	Dimension
Whole robot	Width	590mm
	Height (max)	470mm
	Weight	3200g
	Rotors	6
	Manipulators	3
Manipulator (each)	Degrees of Freedom	3 DoF + 1 gripper
	Link lengths (L1, L2, L3)	45mm, 155mm, 155mm
	Width × Thickness	5mm × 3mm
	Weight	360g

Table 4.4: Specifications of the Prototype 1.

T_2 are the torques acting at each joints. When determining the torque T_1, the rest of the body is considered rigid. Similarly, when finding T_2, the rest of the structure (including the torque T_1) is considered rigid. W_{body} is the weight acting at the center of mass and is the sum of various components of the system and can be written as in equation 4.1.

$$W_{body} = W_{frame} + W_{electronics} + W_{battery} + 3W_{manipulators} \tag{4.1}$$

The weight of the UAV is assumed to be evenly distributed on all the manipulators, so the reaction forces, N_1, N_2 and N_3 can be considered equal. The sum of the torque for an object not in motion is zero, therefore using conventional notation we can find the torque about the joint T_1 as given in equation 4.2.

$$\begin{aligned} T_1 = {} & N_1 L_1 \cos\theta_1 + W_2 L_2 \cos\theta_2 + W_3 L_2 \cos\theta_2 \\ & + W_{body}(L_2 \cos\theta_2 + L_3) + 2W_3(L_2 \cos\theta_2 + 2L_3) + 2W_2(L_2 \cos\theta_2 + 2L_3) \\ & + 2W_1(2L_2 \cos\theta_2 + 2L_3) - 2N_1(2L_2 \cos\theta_2 + 2L_3 + L_1 \cos\theta_1) \end{aligned} \tag{4.2}$$

Similarly, torque about the joint T_2 can be written as in equation 4.3.

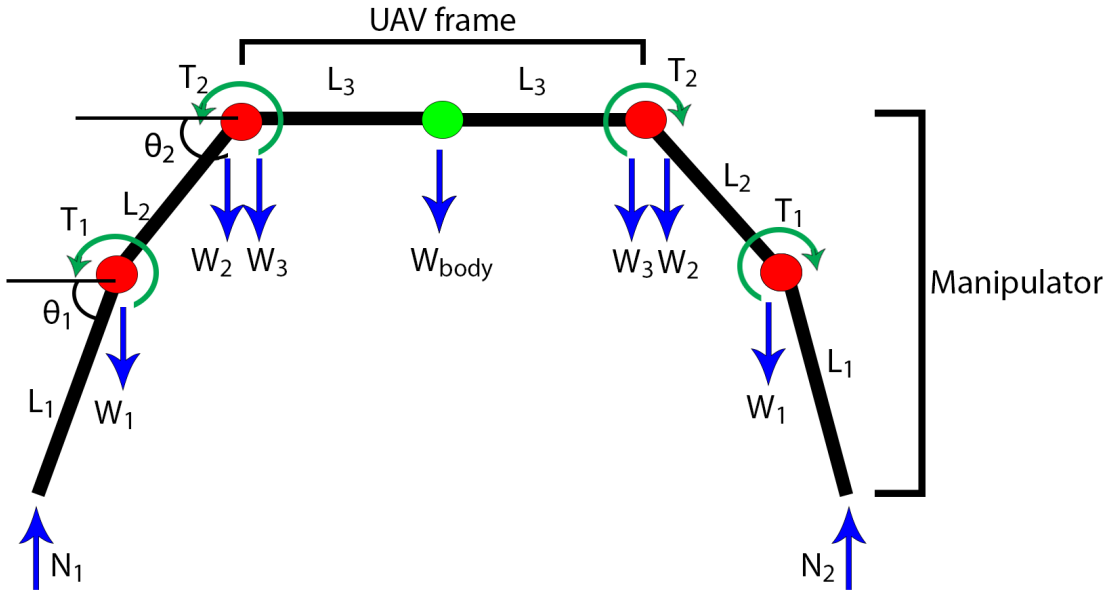

Figure 4.2: Free body diagram of the system to calculate the torques at each joints of a manipulator.

$$T_2 = N_1(L_1\cos\theta_1 + L_2\cos\theta_2) - W_1(L_2\cos\theta_2) + W_{body}L_3 + 2W_2L_3 + 2W_3L_3 + 2W_1(2L_3 - L_2\cos\theta_2) - 2N_1(2L_3 + L_2\cos\theta_2 + L_1\cos\theta_1) \quad (4.3)$$

The required joint torques were calculated early during the start of this work, when the system was much lighter. The same set of motors are used throughout the development because of lightweight and cost. The same set of motors were tested and verified if they can handle the increase in the weight before they were adapted in the design modifications.

4.4 Prototype 2 with Depth Camera

Prototype 2 was designed to use the same set of manipulators to perform autonomous landing and grasping activities. It is basically a modified design of Prototype 1. It is important to have a proper map of the surface or object under the UAV to perform

autonomous landing and grasping. Therefore a compact and lightweight RGB based depth camera (ZED mini) is mounted on the bottom side (facing downward) of the UAV frame in addition to the ultrasonic distance sensors at the manipulator tips. This camera can perceive objects in the range of 0.1m to 15m, which is suitable for various purposes, according to its parameters. Detailed camera information can be found in the Table 4.5. The camera also features a gyroscope and accelerometer for visual-inertial motion tracking, which can be helpful in understanding the location of the UAV while performing autonomous navigation.

Prototype 1's manipulator links are modified and lightweight aluminum pipes are used for strength and weight minimization along with 3D printed PLA components. By using aluminum pipes of 15mm thickness, the links are made thinner so that they can shift and pass between two propeller blades to reach the top of the UAV frame when flying. The attachment of the manipulator and the attachment of the depth camera in Prototype 2 can be seen in Figure 4.3. The link lengths of the manipulators were carefully selected in conjunction with the UAV frame size as defined in Table 4.6 during the design of Prototype 2.

4.5 Compliant Mechanism

Landing is one of the most significant activities considered during the construction of the manipulator system. Ultrasonic distance sensors are used at the tip of the manipulators in both Prototype 1 and Prototype 2 to estimate the distance to the ground during landing. The tip should be perpendicular and should always point downward in order to accurately estimate the distance. Additionally, making the last link perpendicular to horizon would provide the UAV with a safe landing position.

However because the link L_3 is to be maintained perpendicular to the horizon during landing, it will be difficult to land on steep slopes. Also if the manipulator tips are positioned according to the slope's surface height, the UAV would not be able to maintain stable position after touchdown. The design of the lower joint of the L_3 link therefore consists of a mechanical compliance realized using springs. On either

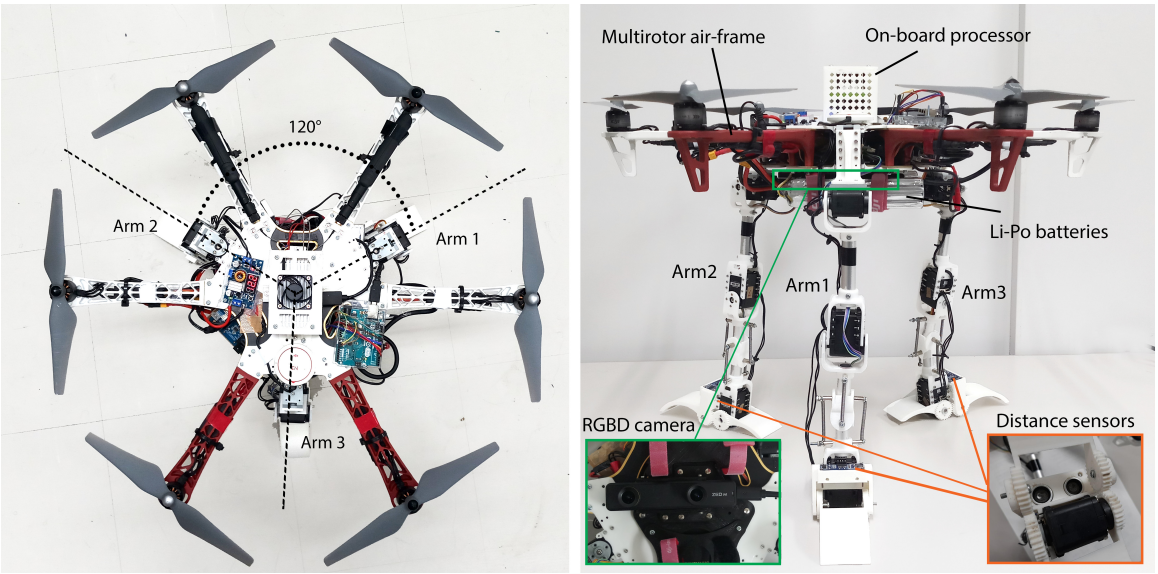

Figure 4.3: Hardware structure of Prototype 2. (a) Top view showing the manipulator mounting with respect to the UAV center. (b) Side view showing the sensors and other peripherals. [97]©2019 IEEE.

side of the joint, extension springs with a spring constant of 0.951N/mm were used, producing a torque of 242.82N-mm at the joint, which is sufficient to hold them in place when the UAV is not landed on a sloped surface.

In both the roll and the pitch axis of the gripper, passive mechanical compliance is implemented. Using this mechanism, after touch down, the manipulators are able to passively modify the gripper angle according to the ground surface slope. When landing on a slope, the weight of the robot adds adequate force to these passive joints to ensure compliance. Figure 4.4 depicts the mechanical compliance used in the system which is mechanically restricted to slopes up to an angle of 40° and is passively adjusted. The compliance retracts the manipulator tip back to its initial position as the UAV takes-off from the ground.

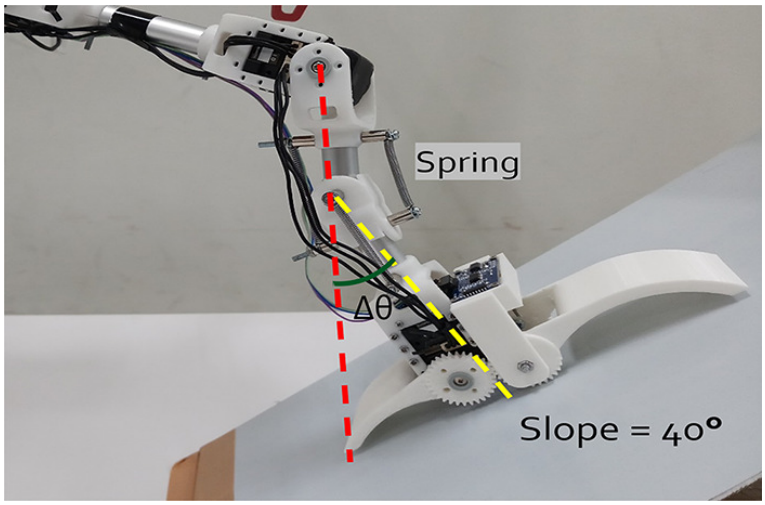

Figure 4.4: Compliant mechanism introduced near the tip of the manipulators. [97]©2019 IEEE.

Features	Specifications	
Video	**Video mode**	**Frames per second**
	2.2K	15
	1080p	30
	720p	60
	WVGA	100
Depth	**Depth range**	0.1 - 15m
	FPS	Up to 100Hz
	Depth FOV	90° (H) × 60° (V) × 100° (D) max.
	Depth technology	Stereo Depth Sensing
Motion	**Motion sensors**	Accelerometer, Gyroscope, Data Rate: 800Hz
	Pose update rate	Up to 100Hz
	Technology	6-DoF visual-inertial stereo SLAM with sensor fusion
	Pose drift	Translation: 1.0%, Rotation: 0.013°/m (without loop correction)
Image sensors	**Sensor Resolution**	Dual 4M pixels sensors with large 2-micron pixels
	Sensor Format	Native 16:9
Connectivity	**Connector**	USB 3.0 Type-C port
	Power	Power via USB 5V / 380mA
	Operating temperature	0°C to +45°C

Table 4.5: Specifications of Zed-mini camera.

Part	Specification	Dimension
Whole robot	Width	590mm
	Height (max)	480mm
	Weight	3500g
	Rotors	6
	Manipulators	3
Manipulator (each)	Degrees of Freedom	3 DoF + 1 gripper
	Link lengths (L1, L2, L3)	45mm, 155mm, 170mm
	Width × Thickness	5mm × 3mm
	Weight	350g

Table 4.6: Specifications of Prototype 2. [97]©2019 IEEE.

Chapter 5

Manipulator System Kinematic Design and Analysis

5.1 Manipulator Kinematics

There are three identical robotic arms mounted to the UAV frame in the manipulator system developed in this research. Each of the manipulators is built with three DoFs and grippers at their tip, in addition to that. As marked in Figure 5.1, the active joints are given in the yaw axis and two in the pitch axis of the manipulator. Two rotational joints in the pitch axis are given since the manipulator movement in vertical direction involves much of the essential tasks mentioned in the previous chapters. For improved torque, feedback and to minimize the wiring, the joints are actuated using AX-12A serial servo motors.

The manipulator's kinematics are derived according to the markings in Figure 5.1(b). Using the equation 5.1, the relationship between the joint angles θ_1, θ_2 and θ_3 and the end effector position with respect to the manipulator reference frame is obtained. Where s_i is $\sin\theta_i$ and c_i is $\cos\theta_i$ for ith joint.

$$\begin{bmatrix} x \\ y \\ z \end{bmatrix} = \begin{bmatrix} L_1c_1 + L_2c_1c_2 - L_3s_2s_3c_1 + L_3c_1c_2c_3 \\ L_1s_1 + L_2s_1c_2 - L_3s_1s_2s_3 + L_3s_1c_2c_3 \\ L_2s_2 + L_3s_2c_3 + L_3s_3c_2 - L_0 \end{bmatrix} \tag{5.1}$$

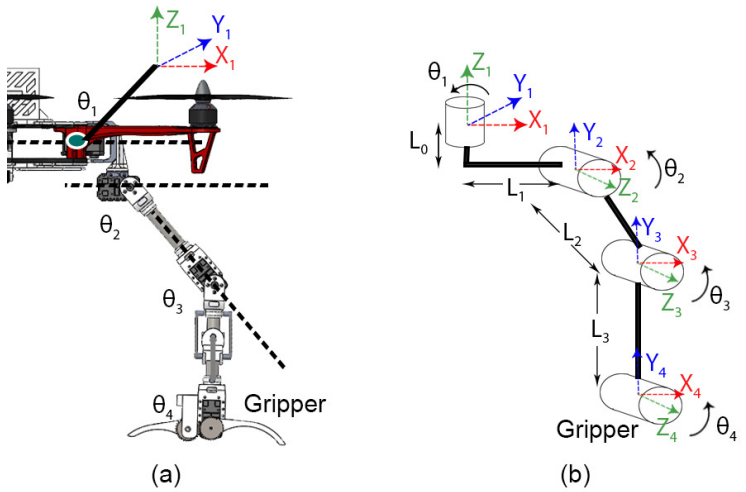

Figure 5.1: Design of the UAV platform attached with manipulators used in the experiments. According to this modeling scheme, all the three manipulators are designed identically. (a) A model of one of the manipulator attached to the UAV. (b) Simplified link model with corresponding axis marked for each joint.

The Jacobian is used to apply inverse kinematics to control the end-effectors depending on the inputs in a Cartesian coordinate. The Jacobian matrix is given in equation 5.2.

$$J_v = \begin{bmatrix} -(L_1 + L_2c_2 + L_3c_{23})s_1 & (L_1 + L_2c_2 + L_3c_{23})c_1 & 0 \\ -(L_2s_2 + L_3s_{23})c_1 & -(L_2s_2 + L_3s_{23})s_1 & L_2c_2 + L_3c_{23} \\ -L_3s_{23}c_1 & -L_3s_1s_{23} & L_3c_{23} \\ 0 & 0 & 1 \\ 1 & 0 & 0 \\ 1 & 0 & 0 \end{bmatrix} \tag{5.2}$$

If Δe is a manipulator tip position error, the joint angle error $\Delta\theta$ is determined using the equation 5.3a. By using J_v^T, the transpose of the Jacobian matrix of equation 5.2, the target angle θ_{target} is obtained by using equation 5.3a and equation 5.3b. The expression α here is the step size and should be reasonable small.

$$\Delta\theta = J_v^T \Delta e \tag{5.3a}$$

$$\theta_{target} = \theta_{target} + \alpha\Delta\theta \tag{5.3b}$$

The above equations are the kinematics of individual manipulators. The manipulator kinematic base transformation is used to achieve kinematics in relation to the UAV coordinate, using the translation matrix (mount radius) and the rotation matrix (each manipulators with 120 degrees spacing between them). To obtain the manipulator tip position with respect to UAV coordinate, first the distance from the manipulator base to UAV base is added to the manipulator base, and then the rotation in z axis is applied using the rotation matrix of equation 5.4. To transform from UAV coordinate to manipulator coordinate, the rotation is applied first in reverse direction and then the manipulator mount distance is subtracted.

$$R_z(\theta) = \begin{bmatrix} \cos\theta & -\sin\theta & 0 \\ \sin\theta & \cos\theta & 0 \\ 0 & 0 & 1 \end{bmatrix} \tag{5.4}$$

5.2 Conditions for Landing

UAV deployment in an unfamiliar area means that it is not assured that a suitable flat landing surface is accessible. The ground is likely to be sloped or covered with debris. In these surfaces, conventional landing gears can not be used. In such cases, dynamic landing gears with adjustable legs are helpful. For dynamic landing gears alone the issue of landing on a rough surface is not solved. The legs have to be adjusted according to the surface. More importantly, it is important to ensure that the dynamic landing gears are able to resolve the variation of the given landing surface. Before descending to the surface to prevent collisions or losing flight time, it would be best to estimate the possibility to land on the given surface when still in air. One of the solutions to solving this problem is surface elevation sensing using a depth camera. The dynamic landing gears can be adjusted for safe landing according to the terrain after receiving the surface variations before descending.

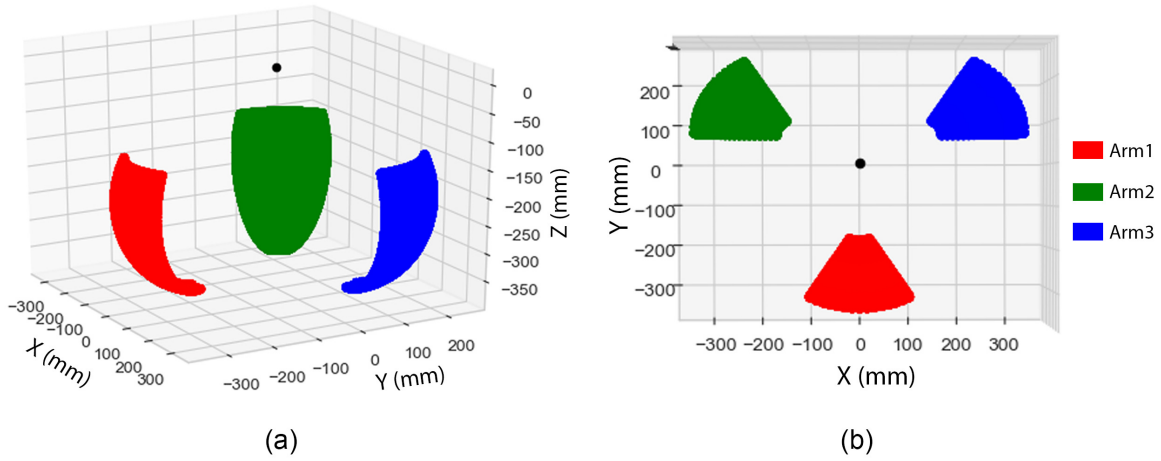

Figure 5.2: Workspace of the system used during landing. The coordinate system is in respect to the UAV frame. Each of the manipulator's region are shown in different colors for better understanding. (a) Perspective view. (b) Top view. Axes are marked according to the distance from the UAV center.

It takes a lot of computation to process the data from the depth camera and often can be delayed. Therefore in addition to the data from the depth camera, the distance sensors mounted to the manipulator tips can also be used for surface distance measurement and monitoring. The distance sensors are directional and must thus be facing downward vertically. To accomplish this, ensuring the last link of the manipulators is perpendicular to the ground is essential. Furthermore, this also leads to a stable posture with decreased torque on the joints after landing. During the descending phase of UAV before touch-down, the distance sensor feedback is continuously tracked by the system.

The manipulator's workspace with its constraints is used as given in the equation 5.5 to determine the manipulator pose. In the form of a 3D plot in Figure 5.2, the workspace area obtained from this equation is shown. The manipulator pose is automatically measured according to the terrain under the UAV by projecting the workspace area onto the point cloud data collected by the depth camera.For manipulator pose estimation, a diagram showing the workspace projection onto the surface

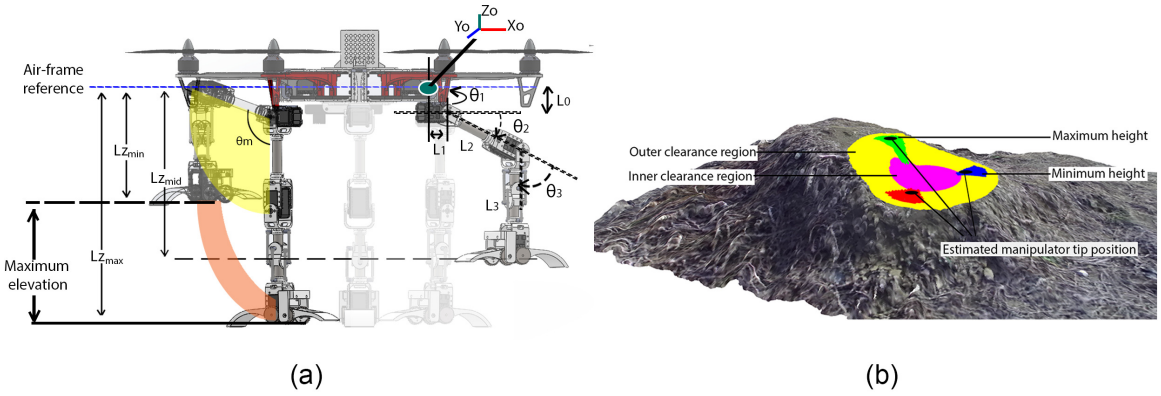

Figure 5.3: Manipulator constraints for stability during adaptive landing. (a) Manipulator pose during landing operation. (b) Point cloud processing and land pose estimation. [97]©2019 IEEE.

point cloud is in Figure 5.3. For enhanced static stability, the yaw angle θ_1 is better held as close to zero as possible during manipulator pose estimation.

$$\begin{aligned} -30^\circ \leq \theta_1 \leq 30^\circ \\ -90^\circ \leq \theta_2 \leq 30^\circ \\ -90^\circ \leq \theta_3 \leq 30^\circ \end{aligned} \tag{5.5}$$

The maximum height of the manipulator in the equation 5.5 is constrained by restricting the maximum angle of θ_2 to 30° to keep the manipulator links from hitting the propellers during the flight. The sum of the angles θ_2 and θ_3 must be maintained at 90° in order to preserve the perpendicular posture of the last link of the manipulators while landing. The inverse kinematics equation can be generalized and rewritten because of this posture of the manipulator, as in equation 5.6.

$$\begin{bmatrix} \theta_1 \\ \theta_2 \\ \theta_3 \end{bmatrix} = \begin{bmatrix} atan2(y,x) \\ \sin^{-1}(\frac{z}{L2}) \\ 90 - \sin^{-1}(\frac{z}{L2}) \end{bmatrix} \tag{5.6}$$

5.3 Conditions for Grasping

One of the most regular tasks used for UAVs fitted with manipulators is aerial grasping [15]. Since the robot is capable of traveling through the air, objects can also be easily moved from and to locations that are normally difficult to reach. Although this study focuses on grasping any particular object with the gripper of the manipulators, we often suggest using the manipulators in tandem to grasp larger objects. Providing such grasping strategies will be helpful to grasp a wide range of objects with varying dimensions.

In this chapter, we identify the three different grasping techniques applied using the suggested manipulator system with the example of a large object, a long thin object and a small object.

5.3.1 Manipulators in Unison

It is necessary to use the three manipulators together to grasp a large object almost the size of the base of the manipulator mount. Together the manipulators are controlled to behave like a broad three-fingered gripper. The workspace for grasping objects is shown in Figure 5.4, based on the manipulator scale and mount distance on the UAV frame. As defined in the equation 5.7, the manipulator joint angles are constrained. The object should overlap with all three manipulator regions in order to get a firm grasp, and the object's center of mass should be near to the intersecting point of each manipulator area. The base orientation of each manipulator (yaw angle) is set such that it points outward from the middle of the UAV, creating a triangular grasp to create force closure, equivalent to a three finger gripper spaced equidistantly.

$$\begin{aligned} \theta_1 &= 0^\circ \\ -120^\circ \leq \theta_2 &\leq 0^\circ \\ -120^\circ \leq \theta_3 &\leq 0^\circ \end{aligned} \tag{5.7}$$

In addition, the joint angles should also satisfy the condition $\theta_1 + \theta_2 < -90^\circ$ in order to be according to the joint ranges, such that the object does not drop easily

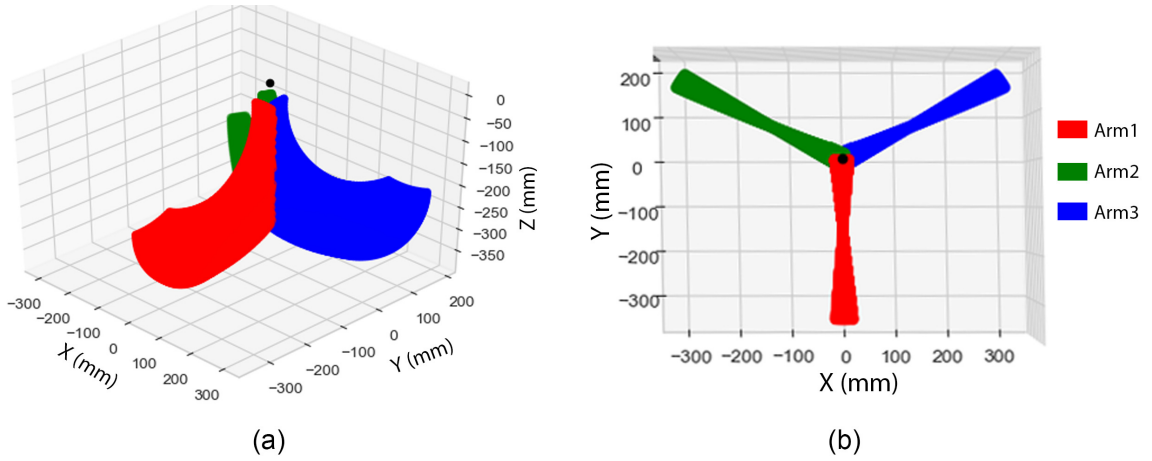

Figure 5.4: Workspace of the system used during grasping. The coordinate system is in respect to the UAV frame. (a) Perspective view. (b) Top view. Axes are marked according to the distance from the UAV center.

after grasping, even when there is a slight force change. This state, along with the mounting distance of the manipulator, is used to assess the maximum object size that can be grasped. From the workspace in Figure 5.4(b), it can be found that an object with a maximum radius of about 340 mm can be grasped. Without considering the gripper, the above grasping posture determines the location of the manipulator tip. However, depending on the combined angle of θ_1 and θ_2, the gripper may be configured to maintained either to be open or close, as seen in Figure 5.5. To grasp smaller objects that are closer to the UAV frame, an open gripper configuration is appropriate. Using the passive compliance joint, a closed gripper configuration adjusts to the rough surface of the objects, in which case a greater force is applied to the object by pulling the tip further towards the object. The distance sensors at the manipulator tip and the directional load input from the actuators of the manipulator are used during the autonomous grasping process to determine whether the object is grasped.

Figure 5.5: Two approaches of grasping a large object using all three manipulators in unison. The gripper is kept open or closed based on the relative distance between the UAV and the object while grasping.

5.3.2 Single and Dual Manipulators

Specific manipulator grippers may be used to grasp objects smaller than 50mm wide. While it is possible to grasp with grippers pointing sideways when the UAV is hovering over them, it is typically easier to grasp an object with the gripper pointing downwards. In comparison, objects with a diameter of less than 50mm and a length of more than 250mm can be grasped using the same technique using two of the manipulators' grippers in the object's length span for stability. $\theta_2 + \theta_3 = 90°$ is the condition for setting the gripper to aim downwards. When using a single manipulator to grasp, the manipulator's reach is within the manipulator's whole workspace.

The grasping workspace, using two grippers of the manipulator, is as seen in Figure 5.6. As an active workspace, only the points of both grippers pointed downward are considered. The workspace is created under the same conditions for the θ_2 and θ_3 joints as the landing conditions from the equation 5.5. Depending on the location of the object, the constraint for the joint θ_1 to grasp a long object is set to $\theta_1 = -60°$ or $\theta_1 = 60°$. The object is necessary to be somewhere within the complete workspace region of manipulators in order to grasp using a single manipulator. The UAV has to be aligned to grasp using two manipulators in such a way that the long object to be grasped intersects in perpendicularly with any two of the regions of the manipulator

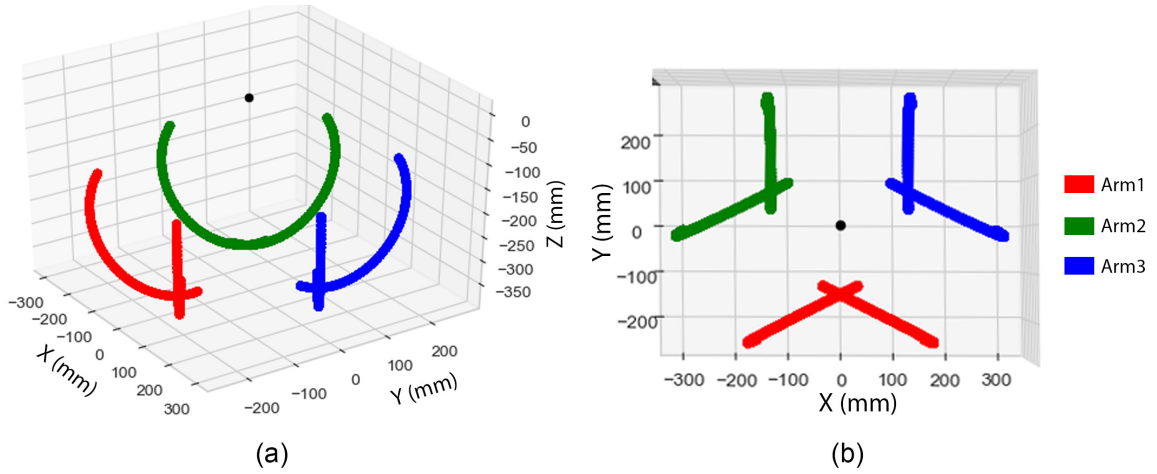

Figure 5.6: Workspace of the system used during grasping using grippers of two manipulators. The coordinate system is in respect to the UAV frame. (a) Perspective view. (b) Top view. Axes are marked according to the distance from the UAV center.

as in Figure 5.6 .

In addition, according to [116] due to the downwash they produce, the proximity operations of a UAV face a special problem. Flight disruptions may be caused by the vertical flow disturbance created by the downward wind. This disturbance also extends to the objects under the UAV when grasping. Figure 5.7 shows the downwash profile of the UAV used in this work along with the manipulators system. The wind profile is recorded at different heights under the UAV when the UAV is hovering at 125cm above the ground. From the profile it can be observed that the wind velocities are very high directly under the rotors compared to the center and either sides of the UAV. In comparison, the disruption in the middle immediately under the UAV frame is very small. These less disturbing areas will form suitable places for aligning the UAV during object grasping.

5.4 Conditions for Obstacle Avoidance

The manipulators should be used in the near horizontal vicinity of the UAV for interaction with the surface of an obstacle. It would be helpful to constantly look for

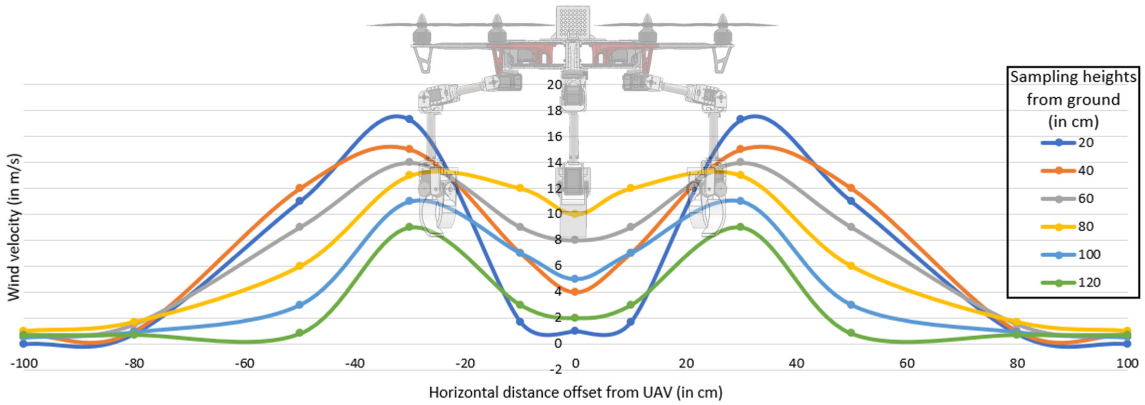

Figure 5.7: Downwash profile when hovering the UAV at about 125cm from the ground with 3 manipulators attached.

contact between the manipulator and the obstacles to avoid crash during traversal, which can often not be completely prevented by UAV navigation control alone. This positional configuration can also be used in the environment for tasks that include moving or pulling an object. The manipulator joints are operated such that the end-effectors point outward and are beyond the radius of the UAV frame. Figure 5.8 shows the resulting workspace regions obtained using the conditions in the equation 5.8. The workspace reveals that the manipulators' outer boundary stretches across the UAV. The condition $W_r > W_b$ (in Figure 3.3) is also satisfied by these ranges.

The manipulator's horizontal interaction with the environment can be effective in carrying out the following tasks:

- The manipulators can be used while traveling at high speeds to force the UAV body away from any vertical barriers by retracting and spreading the manipulator in the direction of the obstacle.

- As assistance for navigation in very narrow tunnels (just large enough for the UAV). In both sides, the manipulators can be stretched to touch the walls when directing the UAV. The third manipulator will at the same time, be used to move any object or guard the front of the UAV.

- In a narrow tunnel, the manipulators alone can be used to maneuver the hov-

ering UAV by doing proper gaiting, as in [112], similar to the above example. Where minor motions are needed or to reinforce the location of the UAV against external disturbances such as strong wind, this method is useful.

- Push-pull manipulation. The pushing or pulling actions can be performed by making contact with the object's surface with the manipulator tip and guiding the UAV in the right direction. The positioning of the manipulator ensures the UAV does not strike the exterior surface during operation.

$$\begin{aligned} -80^\circ \leq \theta_1 \leq 80^\circ \\ -5^\circ \leq \theta_2 \leq 0^\circ \\ -5^\circ \leq \theta_3 \leq 0^\circ \end{aligned} \tag{5.8}$$

It is possible to set a threshold area around the UAV and the necessary manipulators are actuated with respect to the UAV based on the orientation of the object. From Figure 5.8(b), the relationship between the angle of each manipulator with respect to its origin and the angle around the circumference of the UAV is obtained and plotted in Figure 5.9. The relationship is obtained by measuring the angle for each point produced by the tip of the manipulator around the UAV to the origin. The zero point of the UAV is in the front direction (the x axis' zero line in Figure 5.8). By preserving the mutual angle relationship $\theta_2 + \theta_3 = 0^\circ$, manipulators are actuated on the horizontal plane of the UAV for collision avoidance. In addition to the horizontal direction, it is also possible to transfer the end-effectors to the top of the UAV frame in order to apply force upwards.

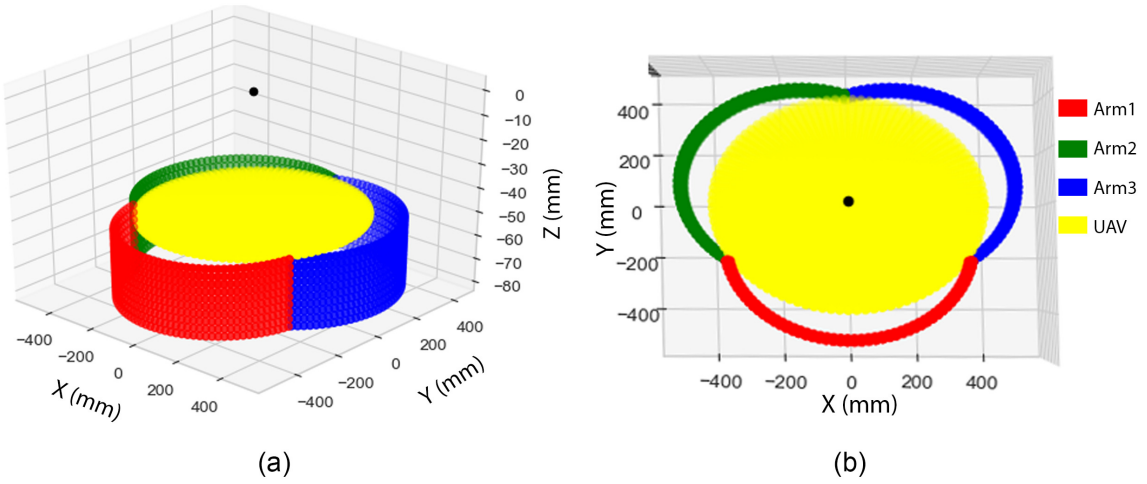

Figure 5.8: Workspace of the system used during contact based navigation. The coordinate system is in respect to the UAV frame. (a) Perspective view. (b) Top view. Axes are marked according to the distance from the UAV center.

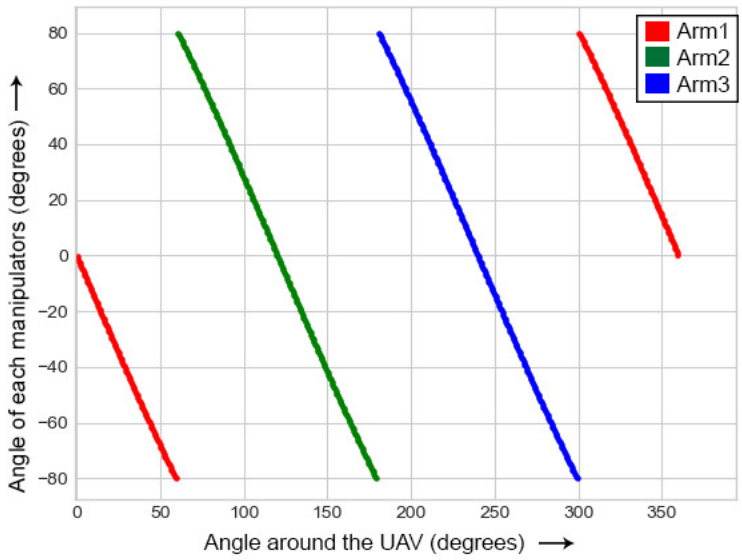

Figure 5.9: Relationship between the angle around the UAV and the angle of each manipulator in respect to their mounting position on the UAV.

Chapter 6

Perception System

6.1 System Overview

The sensing and control systems are divided into individual processes and the interaction between the processes is provided using the Robot Operating System (ROS) communication bridge as seen in Figure 6.4. The sensor input is often made available to be received by multiple processes concurrently over the ROS communication channel. Interface access is given to control the manipulators on the basis of joint angles and the Cartesian coordinate positions as well if necessary. While the navigation system for the flight controller is attached to the on-board computer to act as a fully autonomous system, we used a semi-autonomous control to carry out the tests, i.e. the UAV position is controlled remotely by a teleoperator.

For an autonomous system to understand a physical world or object, a vision system is required. In the event of a landing, it is important to acquire the ground surface details before landing on it. A significant aspect is sensing the slope of the ground, as landing on steep terrain with high elevations will result in a crash. Another significant aspect that should be addressed before landing is adequate clearance under the airframe and propeller blades. The vision system also plays an important role during object grasping or manipulation, in addition to terrain mapping during landing. The location of an object in a 3D world, along with its dimensions, are necessary to grasp it.

Using some distance sensors under the airframe is one of the easiest ways used for landing. Ultrasonic distance sensors mounted next to the tip of the three manipulators are used in one of the first designs of this work (see Prototype 1 in section 4.2). The distance to the surface pointed by the manipulator tip can be obtained, as these sensors are directional. Another version (see Prototype 2 in section 4.4) was designed with a depth camera mounted facing downwards below the airframe. Such an attachment enables the device during landing to accurately perceive the ground and during grasping to locate objects under the UAV. The following sections describe the algorithms for both Prototype 1 and Prototype 2.

6.2 Prototype 1: Autonomous Landing System with Distance Sensors

In Prototype 1, an autonomous landing system was developed using only distance sensor feedback. During the landing process, the control of the position of each manipulator is based on each manipulator's current configuration. The data consists of the current location of each manipulator and the distance from each tip of the manipulator to the surface. The system's block diagram is as seen in the Figure 6.1. With Python, interaction between the various components of the system is implemented using ROS running on the on-board computer.

The distance to the ground is obtained from the ultrasonic distance sensors, and from the current angle feedback by the servo motors, the new manipulator configuration with respect to the UAV frame is determined. The distance data is combined to measure the distance from each of the manipulator attachment points in the airframe to the surface. To position all the manipulator tips to ensure an equal distance to the ground, a corresponding control signal is produced. The manipulator tips should correspond to the surface underneath it for secure landing when the surface is rough.

In the case of landing, however the perpendicular position of the manipulator tip must be held all the time in order to sense the distance as well as to land. Furthermore, for each manipulator, the yaw axis joints are fixed such that 120° is spaced apart for

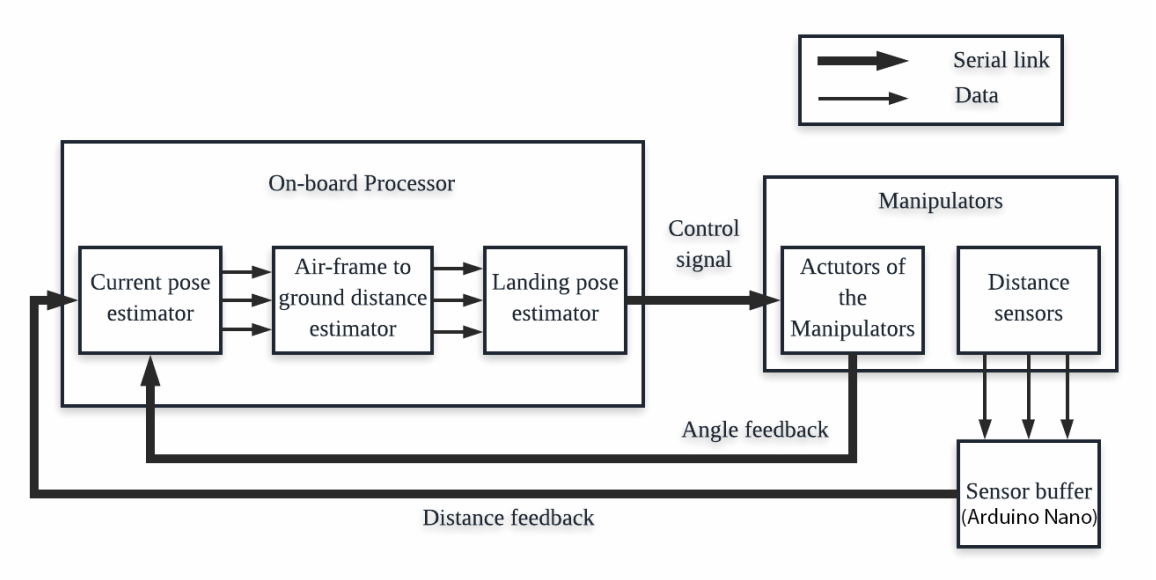

Figure 6.1: Block diagram of the landing system used in Prototype 1.

stability after landing. The Figure 6.2 shows one of the manipulators' workplaces. The red region is the shoulder link movement area with a length of L_2 and the yellow region is the corresponding elbow link workspace with a length of L_3 when keeping a perpendicular position immediately below the surface.

The manipulator's current position in 3D space is determined using the forward kinematics equation in 5.1 from the feedback angles. The distance h to the surface from the point of the manipulator base attachment in the airframe is needed to change the manipulator, as seen in Figure 6.3. This parameter can be measured by adding the distance sensor reading d_s and the height of the manipulator, d_m, which is the z portion of the manipulator's forward kinematic equation. Or it can actually be obtained in this case by adding d_2 and L_3, where d_2 is obtained by equation 6.1.

$$d_2 = L_2 \sin \theta_2 \tag{6.1}$$

The manipulator with the largest ground distance is controlled to extend the maximum i.e. E_{max} in Figure 6.2 which is proportional to the relation lengths $L_2 + L_3$ after the distance to surface from the airframe at each manipulators are measured. The z component of the other 2 manipulators is determined by subtracting their respective

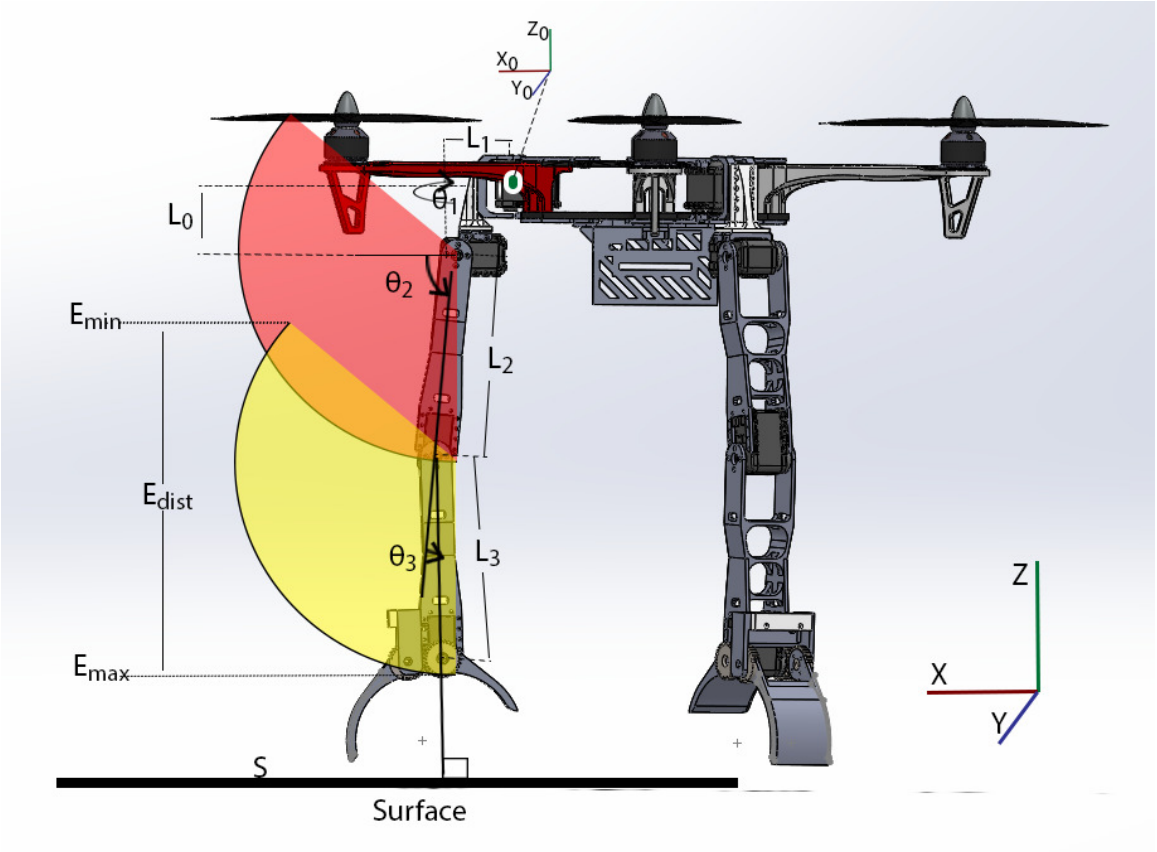

Figure 6.2: Illustration showing the relationship of link movements maintaining the manipulator tip perpendicular to the surface.

h from the d_s component of the first manipulator to hold the same distance from the ground for all the end-effectors. The angles in degrees θ_2 and θ_3 are determined using the equations 6.2, 6.3 and 6.4 if Z_{pos} is the desired z axis location of the end-effector.

$$d_2 = Z_{pos} - L_3 \tag{6.2}$$

$$\theta_2 = \left(\frac{180}{\pi}\right) \sin^{-1}\left(\frac{d_2}{L_2}\right) \tag{6.3}$$

$$\theta_3 = 90 - \theta_2 \tag{6.4}$$

The offsets of the terrain exactly under manipulators are their resulting end-

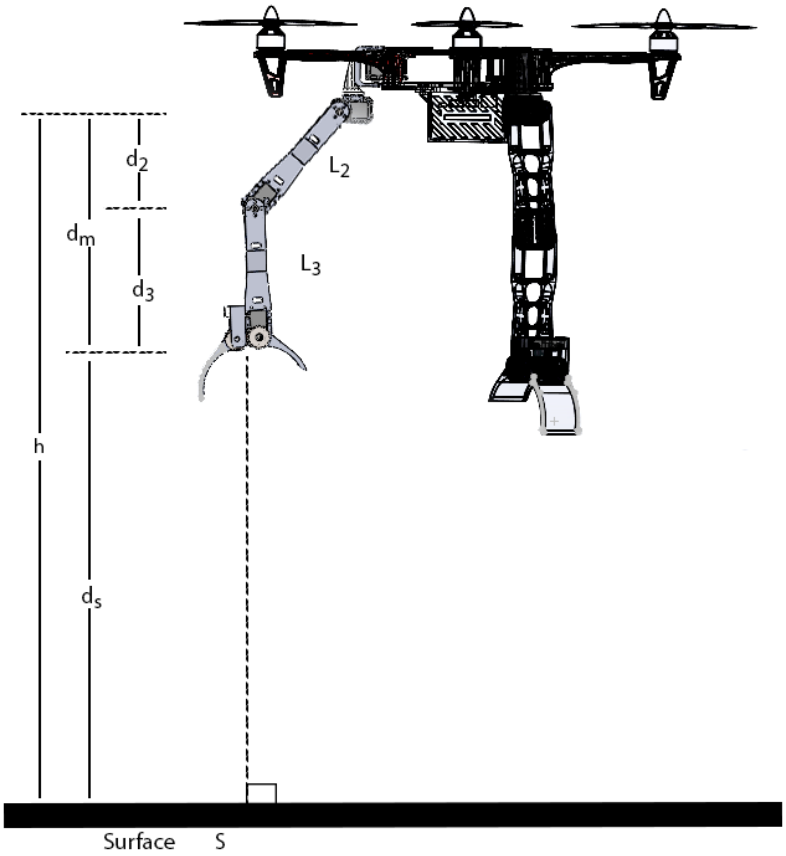

Figure 6.3: Estimation of distance between the surface and the airframe by combining distance sensor and manipulator position feedback.

effector locations. As seen in Figure 6.2, the minimum(E_{min}) and maximum(E_{max}) end-effector location depends on the length of the manipulator, where E_{dist} is the maximum surface elevation that can be covered by the landing mechanism. The highest surface elevation gap that the robot can overcome and yet securely land on is 270mm in the design of Prototype 1.

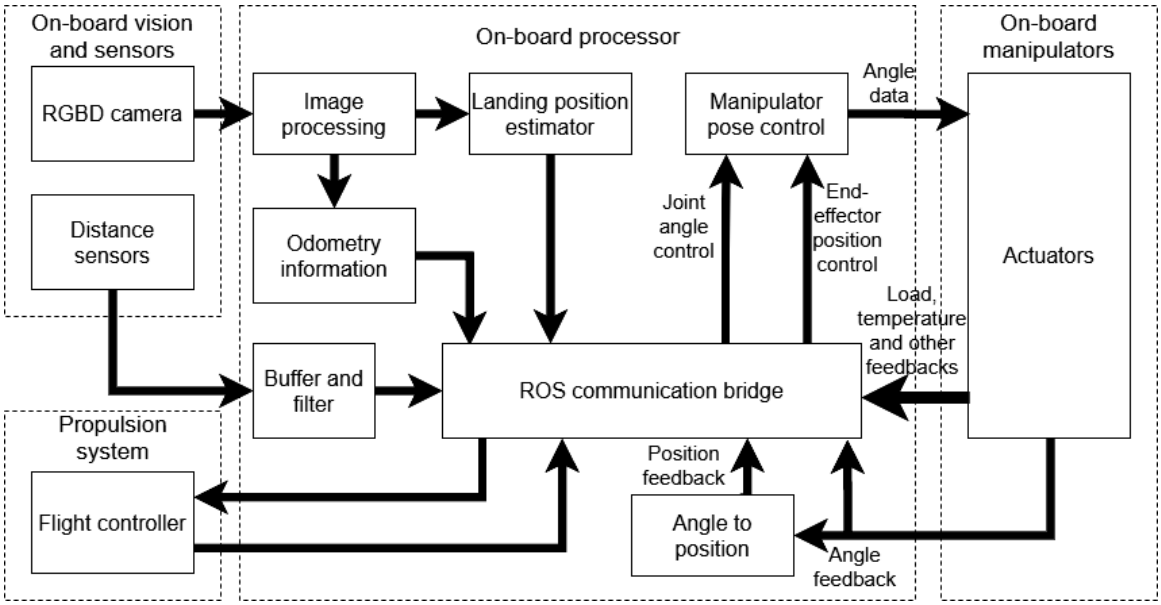

Figure 6.4: Block diagram of the system used in Prototype 2.

6.3 Prototype 2: Autonomous Landing System with Depth Camera

To acquire the information of the terrain under the UAV, a lightweight stereo camera (ZED mini) attached underneath the airframe is used. The depth map of the scene to the on-board processor is obtained in the form of a point cloud. The location of the camera is so that the center of the point cloud precisely corresponds to the UAV frame. The processing is performed in Python, and Open3D [117] is used to achieve the point cloud visualization for validation. The Prototype 2 model is same as that used in our paper [118].

As seen in Figure 6.5, a default position for all manipulators is selected on the $x - y$ plane of the UAV at a local distance of Lz_{mid} from the middle of the UAV. Lz_{mid} is picked so that the manipulators do not block the camera during the landing spot extraction process. However, even if the manipulators partially block the camera during landing, the camera is still able to provide the correct position information.

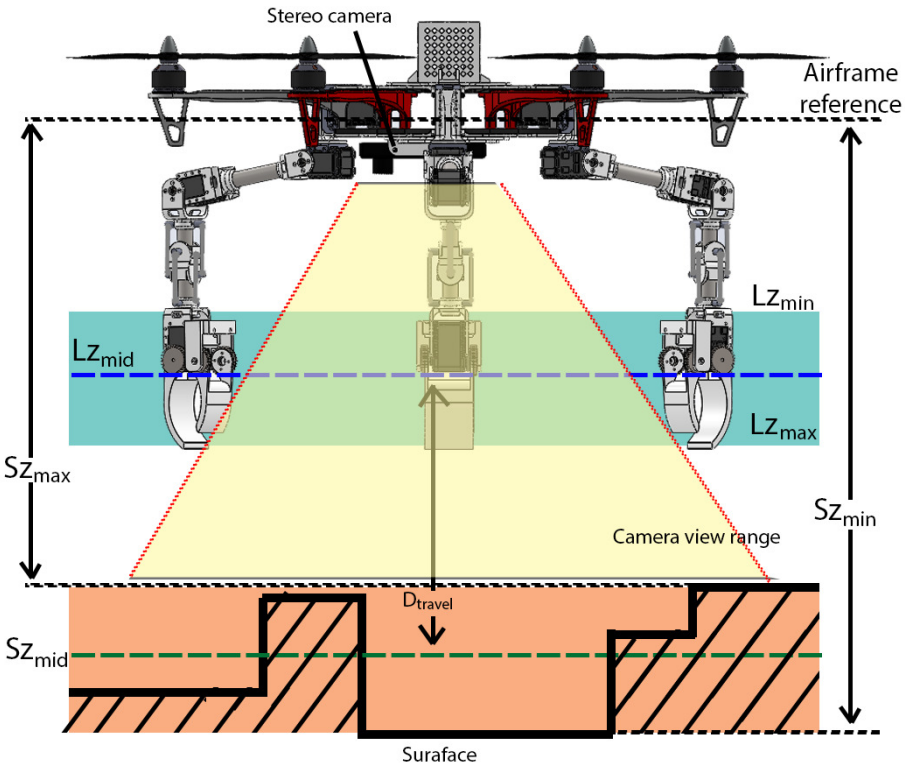

Figure 6.5: Estimating the ground reference and the distance to travel for landing. [97]©2019 IEEE.

6.3.1 Extracting Clearance Region

In order to search for clearance, the first step of depth processing includes segmenting the areas. The clearance area is defined as the shortest distance between the surface of the ground and the lowest part of the body of the vehicle, other than the ground contact region. Let Q be a set of four dimensional vectors denoting points in a point cloud consisting of the x, y, z position and color information. From this set in an $x-y$ plane based on Euclidean distance from the center, two circular regions, one for inner clearance region (Q_{c1}) of 200mm radius and another for outer clearance region (Q_{c2}) of 400mm radius, are obtained. The measurements of 200mm and 400mm are selected according to the size of the UAV used, i.e. the circular area around the protruded underside portion of the UAV frame and the circular region around the

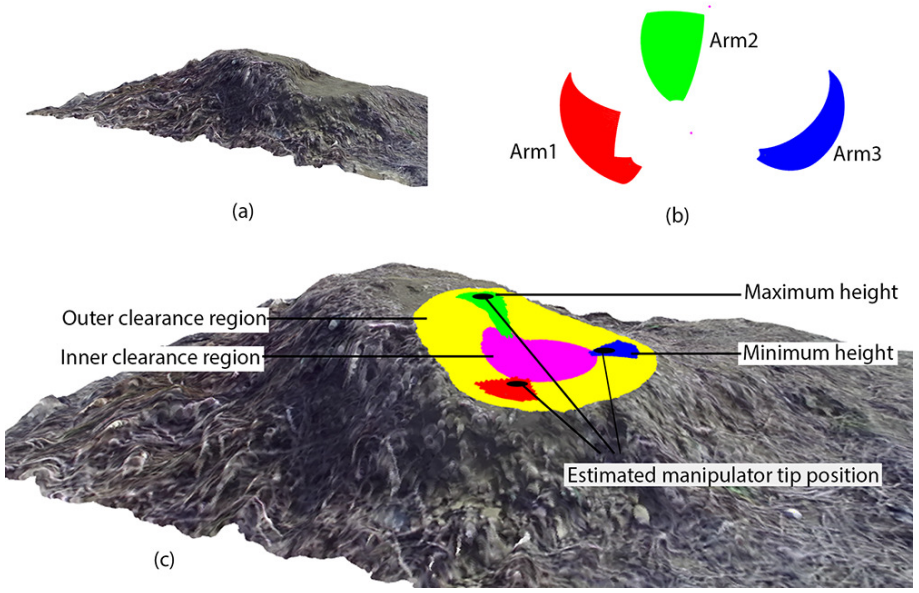

Figure 6.6: Terrain data processing - (a) Depth map of the terrain, (b) Workspace of manipulators used for landing, (c) Processed map with manipulator position on terrain for landing. [97]©2019 IEEE.

UAV, including the propellers respectively.

A distance matrix in $x-y$ plane is calculated using Frobenius norm [119], also called the Euclidean norm and is given by equation 6.5. The term absolute squares in Frobenius norm is used so that it can be applied to complex numbers, However, while in case of point cloud, all the elements are real numbers.

$$\|A\|_F = \sqrt{\sum_{i=1}^{m}\sum_{j=1}^{n}|a_{ij}|^2} \tag{6.5}$$

where, $m \times n$ is the size of the point cloud set Q and a_{ij} is the set of difference elements of size $m \times n$ whose each k^{th} element is calculated by equation 6.6.

$$d_k = \sqrt{(Qcx - Px_k)^2 + (Qcy - Py_k)^2} \tag{6.6}$$

Where Px_k, Py_k and Qcx, Qcy are the X and Y values of k^{th} element in Q and the element with x,y = 0,0 in Q respectively.

Extracting Search-space

The terrain area overlapping with each of these manipulators is extracted to approximate the posture for each of the manipulators depending on the terrain structure. The elbow connection is held perpendicular to the surface during landing, restricting each manipulator's workspace to the angle range as given by the equation 6.7. For the manipulators, the resulting restricted workspace is as shown in Figure 6.6.

$$\begin{aligned} -30 \leq \theta_1 \leq 30 \\ -30 \leq \theta_2 \leq 90 \\ 0 \leq \theta_3 \leq 120 \end{aligned} \tag{6.7}$$

The lowering of the θ_2 angle below 30° increases the height of the L_2 link, striking the propellers while flying, and therefore must be prevented. For each of the three manipulators, a region of the point cloud Q satisfying the condition in equation 6.8 is extracted. This region is the workspace projection (R) of each of the manipulators on the terrain point cloud data in the $x - y$ plane. The resulting matrix hereon will be referenced for each i manipulator as search-space (Si). The search spaces in Figure 6.6(c) are colored in red, green and blue respectively for $Arm1$, $Arm2$ and $Arm3$.

$$\begin{aligned} \text{for every: } Q_{xy} \in R_{xy}, \\ S_i = Q_{xyz} \end{aligned} \tag{6.8}$$

6.3.2 Searching Landing Spots

The purpose of the landing algorithm is to provide for each manipulator (which is at a fixed distance from the UAV base) the reference level Lz_{mid} to horizontally overlap with the ground reference level Sz_{mid}, as shown in Figure 6.5. According to the horizontal ground difference from Sz_{mid}, the manipulator heights are adjusted.

The manipulator reference level Lz_{mid} is selected at the horizontal center of the manipulators workspace, offering equivalent manipulator height displacements in both

the directions. The ground reference level Sz_{mid} is selected at the center of the perceived minimum and maximum ground surface elevations. Using the equation 6.9 and equation 6.10, Lz_{mid} and Sz_{mid} are determined. Where the minimum and maximum reachable height of the manipulator is Lz_{min} and Lz_{max} respectively, in the z axis, from the airframe center. For all three manipulators given by the equation 6.11 and equation 6.12, Sz_{max} and Sz_{min} are the minimum and maximum distance to the terrain in the search-space (S_i) result combined. It is essential to note that only the points for each manipulator in the search-space and Sz_{mid} are used to evaluate the landing pose. For that reason, for the time being the terrain variation outside this region is ignored.

By verifying the z axis value of the points in the area (Q_{c1}) and (Q_{c2}) respectively, clearance under the airframe base and the outer ring clearance under the propeller is guaranteed. For the internal and external areas, the overall elevation height of Sz_{mid} must be less than 200mm and 250mm respectively, for the hardware design used in Prototype 2. If the clearance exceeds these values, before the clearance requirement is fulfilled, Sz_{mid} is relocated upwards.

$$Lz_{mid} = \frac{1}{2}(Lz_{max} - Lz_{min}) + Lz_{min} \tag{6.9}$$

$$Sz_{mid} = \frac{1}{2}(Sz_{min} - Sz_{max}) + Sz_{max} \tag{6.10}$$

$$Sz_{max} = max(Arm1_{min\_z}, Arm2_{min\_z}, Arm3_{min\_z}) \tag{6.11}$$

$$Sz_{min} = max(Arm1_{max\_z}, Arm2_{max\_z}, Arm3_{max\_z}) \tag{6.12}$$

where, $Arm1_{min\_z}$, $Arm2_{min\_z}$ and $Arm3_{min\_z}$ are the minimum Z value in S_i for each of the manipulators respectively and $Arm1_{max\_z}$, $Arm2_{max\_z}$ and $Arm3_{max\_z}$ are the maximum z value in S_i for each of the manipulators respectively.

The difference in the distance between Lz_{mid} and Sz_{mid}, given in the equation 6.13, is the distance to be travelled by the UAV to reach the terrain surface (D_{travel}). The workspace area (R) of the manipulators in equation 6.7 is moved to D_{travel} in the z axis, and approximate intersecting points are obtained in the XYZ region. The potential landing spots for each of the manipulators are these intersecting points.

While all of these spots are ideal for landing, the spot is selected with maximum points having the same z values (wider surface area) from the middle of the search-space region and ii) the angle θ_1 is reduced to provide more stability in the base.

$$D_{travel} = Sz_{mid} - Lz_{mid} \tag{6.13}$$

$$Lz_{max} - Lz_{min} \geq Sz_{min} - Sz_{max} \tag{6.14}$$

For a flat surface, since in the equation 6.10, $Sz_{max} = Sz_{min}$, the Sz_{mid} overlaps with the surface of the terrain. The height of all the manipulators would then be in the mid-way position (at Lz_{mid}). For $Lz_{max} - Lz_{min} = Sz_{min} - Sz_{max}$, at least one of the manipulators extends to its maximum limit and at least one of them moves to the minimum height (Lz_{max} and Lz_{min} respectively).

However there are times where the gap in terrain height is greater than the scope of the manipulators. Therefore before starting the landing process, it is important to check whether the UAV can land or not. The UAV will only land if the condition in the equation 6.14 is satisfied.

However if the UAV rotates within its yaw axis, there might be a range of suitable landing points. This is tested iteratively on the point cloud by rotating 360° of the search space of all three arms together in 10° steps along the yaw axis of the UAV, without altering the position of the UAV physically. The UAV yaw is altered accordingly when detecting the first feasible landing point set. The UAV should be guided to a new position away from the previous landing location, repeating the steps above, if it fails to locate feasible landing points.

6.3.3 Distance Sensor Feedback

As mentioned above by performing an appropriate pose for the manipulators, the imaging system is used to assess if the landing can be accomplished in the given terrain. This method has many limitations. For one with the input video resolution of 1280×720 pixels, it can only have a maximum frame rate of up to 10 frames per second (fps). In addition, once they are in place for landing, the depth camera is

unable to see the surface beneath each manipulator.

For that reason, the information on the point cloud is only used at the beginning to approximate the manipulators' positions. Once the poses are determined, the data from the distance sensors are used to speed up the process and to have an effective landing process during the UAV's touch down. To perceive the distance from the gripper tip to the ground and the distance from the UAV base to the surface, the ultrasonic distance sensors attached to the grippers are used. The former is derived directly from the camera, and the latter is measured using forward kinematics and angle input from the servo motors by incorporating the sensor readings and the gripper's z axis orientation from the UAV frame. To arrange all the manipulator tips to ensure an equal distance to the ground, a corresponding control signal is produced. These sensors also provide the manipulator distance in z axis fine tuning, retaining the same baseline (Sz_{mid}) during the descending process of the UAV.

If when descending, the UAV has a significant displacement in the $x - y$ plane, the manipulators switch to their default location and a new pose for the manipulators is acquired from the camera based on the new terrain heights. The highest surface elevation variation that the robot can overcome and yet securely land on is 220mm in the current configuration (shown in Figure 5.3(a)).

6.4 Autonomous Object Grasping

The object grasping is performed using the same downward-facing depth camera mounted to the UAV frame, equivalent to autonomous landing. The manipulators are raised up when looking for an object, as seen in Figure 6.5, so as not to block the camera.

While there are several studies such as [120] and [121] for object recognition and grasp pose detection from a 3D point cloud, the most difficult challenge is how to describe an object of interest to the robot. The object model in the environment could be entirely new when exploring deployment in an unfamiliar environment and it is not feasible to pre-train these models into the framework. An object maybe

defined based on height, color, form, location, etc. But all the objects in the scene need to be identified and processed by the system in order to achieve so. This method is time-consuming and very complicated for a UAV hovering in air to be done in real time.

The easiest method of identifying the object of interest is considered in this work. We are considering two cases, which are:

1. Find any object immediately below the UAV. Different objects or surfaces are extracted as the UAV moves to a different location. Therefore, before being sensed and grasped, the UAV must be hovering over the object.

2. The user selects the target remotely by specifying the object by mouse-clicking somewhere on the surface of the object, assuming the operator is tracking the stream from a distant location from the camera of the UAV. The UAV hovers over the target to grasp it after recognition. Then following the same method as in the previous example.

In any case, the object is described by a point on the object's upper surface. The object is to be segmented and retrieved from the region after identifying a point on the object. In order to choose an appropriate grasp, it is therefore important to estimate the dimension of the object and to make sure that the object is not too large to be grasped by the system.

6.4.1 Object Segmentation and Extraction from the Point Cloud

Consider the case of an operator specifying an object by selecting a position on the surface of the object (seed point). A human operator monitors the 2D color footage remotely from the stereo camera. If an object of interest is identified by the user, the operator uses a mouse to press on the object from the 2D image stream. The steps of the algorithm follow as defined in the Figure 6.7.

Once the object's seed point is determined, when hovering in the same location, the perception system captures a 3D point data of the scene. This point cloud is an

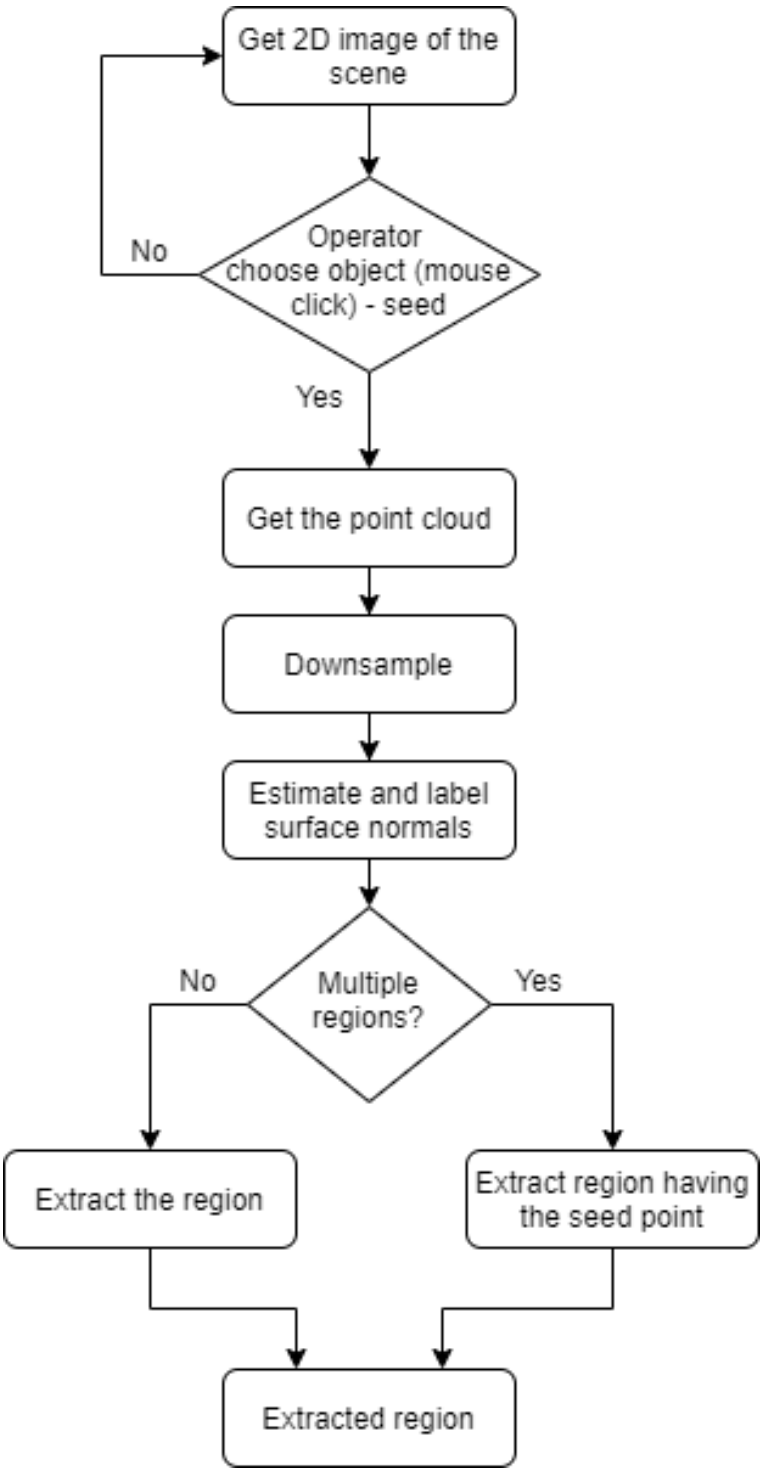

Figure 6.7: Algorithm steps showing the segmentation and extraction of an object of interest from the point cloud.

immense collection of points and the number of points depends on the defined picture resolution. In our case, for improved viewing and speed, we use the 720p video mode with a 2560×720 output resolution. The point cloud is down-sampled to a voxel scale of 10 to conduct quicker sorting, decreasing the number of points by 10 times.

Using the resulting set of points, surface normals are computed. The output of the surface normal consists of the surface normal values for each point in the x, y, z axis. The absolute value of each of the normal is between 0 and 1. If the point's axis value is 1 or -1, it implies that the point's surface is regular to that particular axis. The surface of an object does not necessarily have to be flat. Any anomalies may occur. Therefore, on either side of the z axis, the threshold is assumed to be ± 0.2. A segmentation is then carried out by labeling the connected components. If there is only one region, it is extracted directly. The region consisting of the original seed point is retrieved when there is more than one region. The top surface of the object of interest is the resulting extracted area.

Figure 6.8 shows the object segmentation process without down-sampling (left) and with down-sampling (right) for the point cloud data. Run time without down-sampling is about 7.83s with 238833 points in the point cloud. With down-sampling of voxel size 30 processing is done at 0.05s with only 3947 points in the point cloud. The processing time does not include the image perception delay from the camera.

6.4.2 Estimating the Size of Object

To select a suitable grip, the size of the object is measured. The derived 3D points of the object's top surface are flattened into z, which means that the components of the z axis are omitted since we are interested in the size of the object which is in the $x - y$ plane. A collection of 2D points will be the result of this operation.

The step is followed by convex hull generation and a fitted rectangle approximation around the points. It is possible to measure the dimensions (length and width) of this fitted rectangle, as well as the estimate the object's size. Although the object may not always be a rectangular form, a proper grasp may still be picked using the rectangle fitting as seen in Figure 6.9. As described in Figure 3.2, suitable grasp is

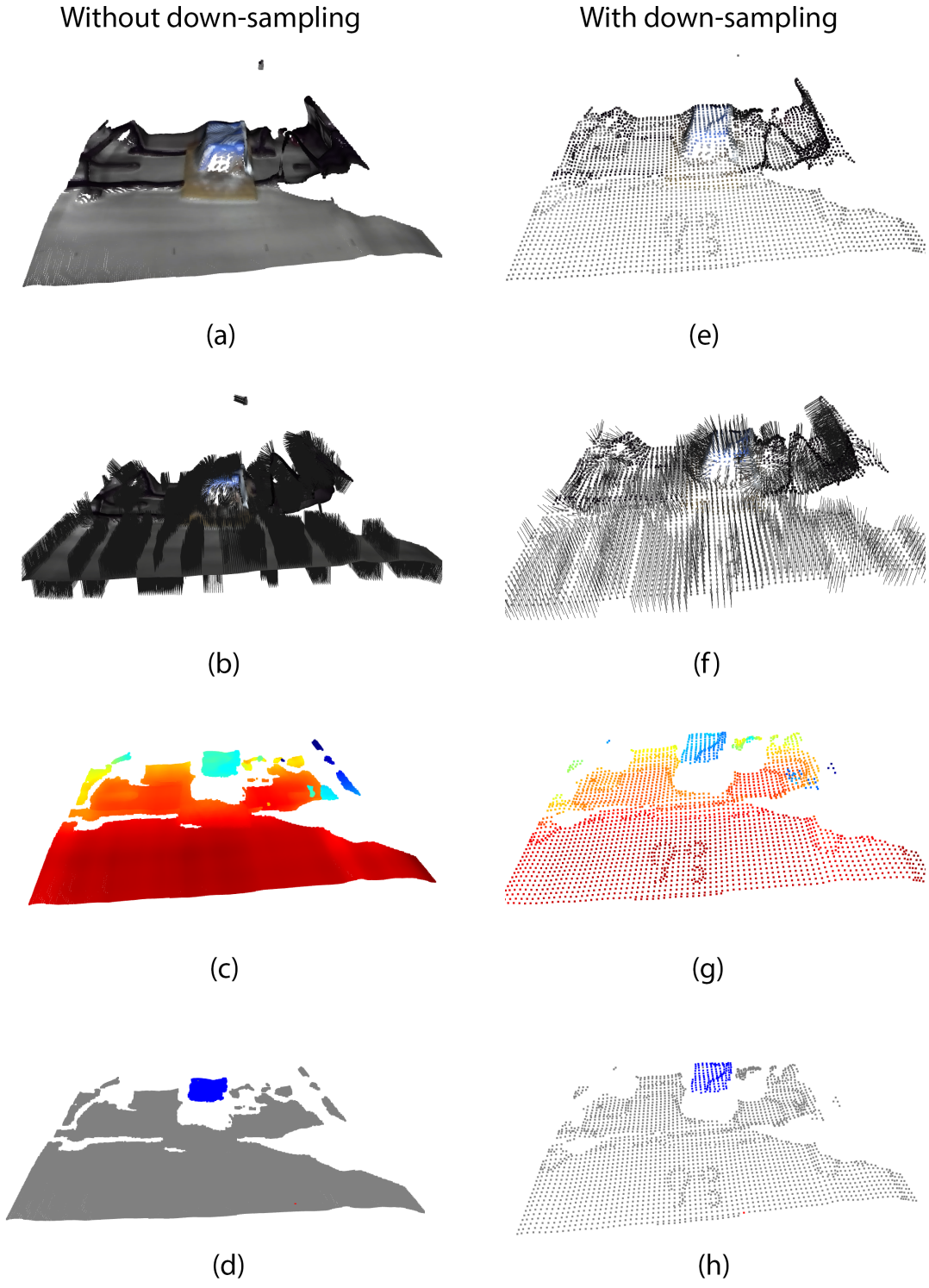

Figure 6.8: Object segmentation from the environment using point cloud. (a,b,c,d) without down-sampling and (e,f,g,h) is with down-sampling.

Real world object	Original dimensions (in mm)	Object in 3D	Estimated dimensions (l x b in mm)	Manipulator configuration
	diameter = 225 h = 130	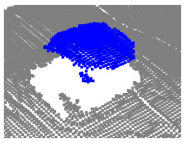	219.8 x 232.6	3 manipulators
	l x b = 215 x 148 h = 115	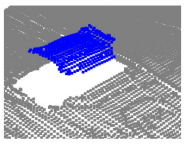	214.5 x 139.5	3 manipulators
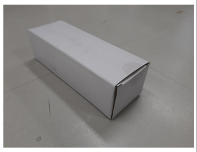	l x b = 188 x 70 h = 57	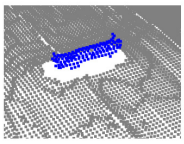	187.9 x 52.2	1 manipulator
	l x b = 610 x 60 h = 60	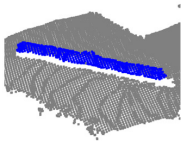	617.7 x 71.9	2 manipulators

Figure 6.9: Some object dimensions and suitable grasp method used in the algorithm.

chosen based on the dimension of the object.

6.5 Obstacle Avoidance around the UAV

The ability to prevent collisions with objects is important for the secure operation of UAVs, as stated in chapter 3. It is important to know the surrounding environment, or at least the distance to the obstacles around the UAV, to do this.

Since the last decade, LIDAR has become popular for mapping with UAV. LIDAR is a form of remote sensing and ranging that operates close to Radio Detection And Ranging (RADAR). Unlike RADAR, LIDAR uses pulses of LASER (light amplification by stimulated radiation emission) light for measuring the time taken by the light to bounce back after reaching a surface, and distance is determined. The benefit of

LIDAR is that it gathers fast, reliable data and is not reliant on sources of ambient light.

Study papers such as [122] have implemented a real-time collision avoidance algorithm based on LIDAR. For remote sensing and navigation, research such as [123] and [124] uses LIDAR mounted on a UAV. The analysis in [123] reveals the applicability of UAV LIDAR for marine environment mapping. Whereas the analysis in [124] highlights the benefits of a UAV-based LIDAR in the estimation of tree height, pole identification, road extraction and digital terrain model refinement .

While LIDAR is usually used to obtain a 3D map of the area in general, in situations such as obstacle detection, a 2D map will often be adequate. Therefore a 2D laser scanner is used for obstacle detection in this work.

On top of the UAV, a low-cost and lightweight 2D laser scanner from Robotis called LDS-01 is equipped. From all 360 degrees around the UAV, it is capable of sensing distance data. It uses a 5V DC IEC60825-1 Category 1 Semiconductor Laser Diode (λ= 785nm). It is suitable f or small robotic applications, like SLAM (Simultaneous Localization and Mapping) and navigation [125], and is designed to consume 400mA or less current. The Table 6.1 includes a complete specification of the sensor. In Figure 6.10 on the left and right, the sensor and measuring angle relationship with UAV and manipulators is shown. The UAV angle and sensor angle are aligned.

The area of the sensor scan is split between the 3 manipulators seen in the Figure 5.9 graph and summarized in the Table 6.2. For obstacle detection and avoidance, a simple algorithm is used. The manipulators are designed to extend beyond the UAV footprint (including the propeller blades) and is outlined in green color, as shown in figure 6.10(b). If an object crosses this point, the propellers will be struck and the UAV may fail. The manipulators in the figure will reach up to a radius marked by a red circle. The manipulator allocated in that area is triggered to travel toward the location of the obstacle when an obstacle is found just about in the red circle. The obstacle is avoided in the region between the green and red circles, therefore avoiding them to reach red circle. It is possible to enable and avoid obstacles in three directions around the UAV simultaneously. If the obstacle to reaching the red circle

Parameters	Specifications
Distance Range	120 ∼3,500mm
Distance Accuracy (120mm ∼499mm)	±15mm
Distance Accuracy(500mm ∼3,500mm)	±5.0%
Distance Precision(120mm ∼499mm)	±10mm
Distance Precision(500mm ∼3,500mm)	±3.5%
Scan Rate	300±10 rpm
Angular Range	360°
Angular Resolution	1°
Dimensions	69.5(W) X 95.5(D) X 39.5(H)mm
Mass	Under 125g

Table 6.1: Performance specifications of LDS-01 laser scanner.

Angle around the UAV (in degrees)	**Respective manipulator angle (in degrees)**		
	Arm1	**Arm2**	**Arm3**
0 to 60	0 to -80	-	-
61 to 180	-	80 to -80	-
181 to 300	-	-	80 to -80
301 to 360	80 to 0	-	-

Table 6.2: Angle division between the manipulators around the UAV.

is broader, the manipulator determines the point which is at a distance closest to the UAV. It can not be ensured that the obstacle will be moved backward by reaching out the manipulator in the direction of the obstacle. In certain situations, based on the weight of the obstacle, the UAV itself may be moved away from the obstacle to prevent a collision.

On top of the UAV frame, the sensor is mounted and the manipulators are actuated from the bottom. As seen in Figure 6.11, there is a certain offset in height between the obstacle sensed and the manipulator level. The height of the manipulator is set under

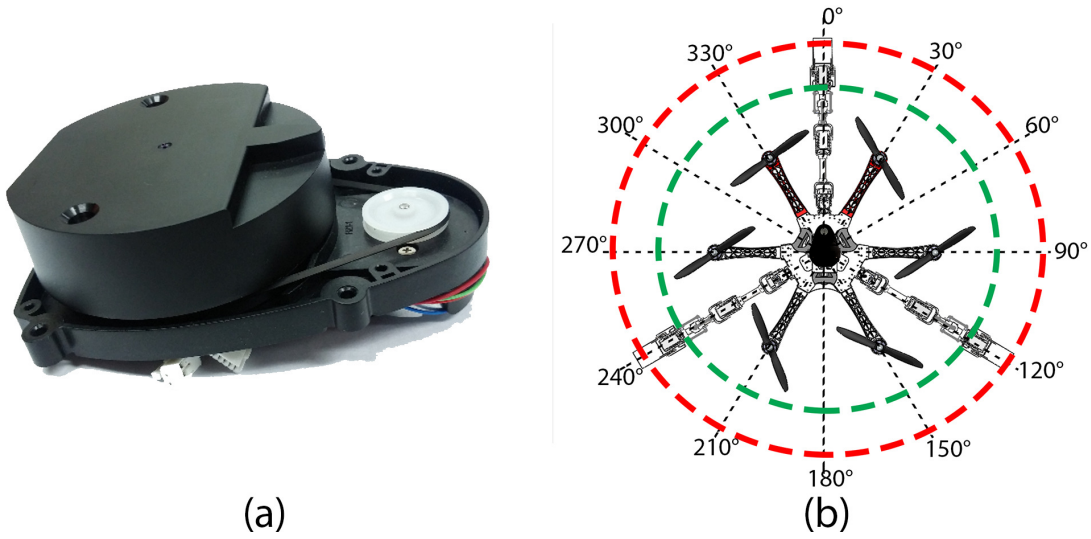

Figure 6.10: (a)LDS-01 2D laser scanner. (b)A scan mapped by the scanner in ROS.

the UAV any time an obstacle needs to be avoided, so as to prevent them touching the propeller blades. Therefore, we assume that the barrier observed is longer than d_{offset} in this algorithm and reaches down to the height of the manipulator. In order to have broader contact with the obstacle board, the manipulator's gripper is left open. Since the gripper is opened vertically, the gripper fingers shield the UAV and the propellers vertically from a wider area.

The distance d_{offset} should be kept small as possible. And the height of the tip of the manipulator should be above the frame height, so that the UAV does not tilt during the impact at high speed. However setting the manipulator tip height slightly below the UAV frame level is acceptable at low speed.

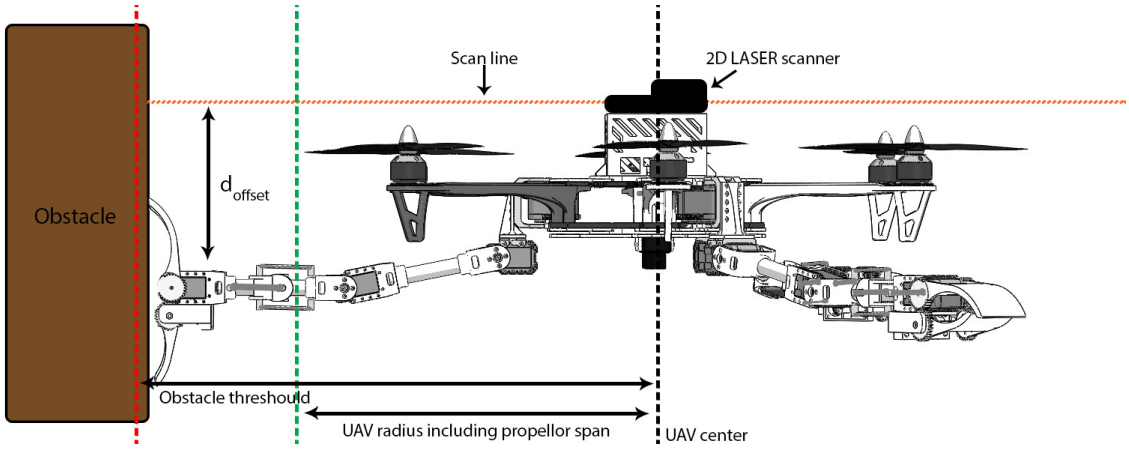

Figure 6.11: Side view of the UAV during obstacle detection and manipulator contact.

Chapter 7

Experiments

In the form of experiments, the performance of the developed system is shown. To execute each of the tasks using the designed algorithms, several experiments were conducted. In some of the situations, though the UAV tests were carried out with rope assistance because of inevitable reasons during indoor experimentation to prevent crashing. While these tests have been performed with rope assistance, the functionality of the device can still be evaluated.

7.1 Autonomous Landing

To test the adaptive capabilities of the developed system in Prototype 1 and Prototype 2, autonomous landing tests were carried out. It specifically addresses the use of distance sensors only and the difference in the integration of depth camera data for surface detection, respectively.

7.1.1 Prototype 1

Description and Setup

Adaptive landing experiments were first carried out using the developed prototype i.e, Prototype 1 using the distance sensor feedback data attached on the grippers. Experiments were conducted to test the performance of the system, simulating a

hover state and changing the surface heights under the UAV. Landing experiments using rope support to control the UAV altitude is used to show the adaptability of the system on the surface in three different scenarios.

Results

The first experiment was conducted to examine the system's reaction against the rise in surface heights. To simulate the hovering situation, we put the UAV in a fixed location at a certain distance above the floor. Then we introduced several objects under the manipulators of varying heights to observe the system's reaction. The corresponding graphs can be seen in Figure 7.1. At the end of instance 1, a box with a height of 110mm is placed on the floor, directly under Arm 3 (see Figure 7.1). It can be observed that the manipulator usually ends up adapting itself to the height difference of the surface within 2s, based on the height of the object introduced. Just before instance 3, the object is withdrawn. The manipulator can be seen returning to its initial location. Similarly, under Arm 1, the same 110mm object is added followed by another 170mm tall object under Arm 3 that can be seen in instances 4 and 5, respectively.

In order to land the UAV on a fully planar surface using the manipulator system, an experiment was carried out. With the assistance of the distance sensors attached near the grippers, the system successfully detected equivalent distance to the surface from all three manipulators. Once the surface was recognized as planar under the UAV airframe, the manipulators automatically extended autonomously, whilst the UAV was still hovering. In order to remain in alignment during the landing process, the manipulator joints are locked. The actuators have adequate torque to maintain their position after landing. In Figure 7.2, the outcomes of these tests can be seen. For each of the arms 1, 2, 3, the distances to the surface and joint angles are labeled in blue, red and yellow respectively. Just the shoulder angles and not the elbow angles of the manipulators are seen for simplicity and better interpretation. Snapshots from the video taken during the trial, from hovering to landing, are added under the graph in the respective instances. And after landing, the arm tip to surface distance does

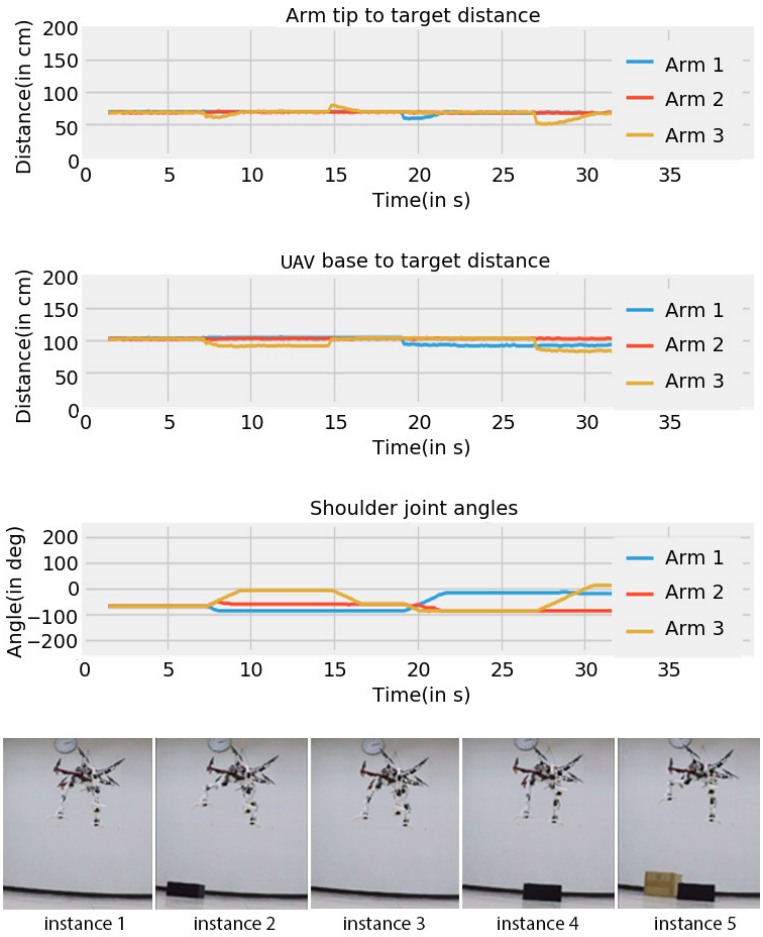

Figure 7.1: Performance of the manipulators against varying surface, when in hovering state (Prototype 1).

not seem to reach 0 mm because the sensor is located significantly away from the tip to prevent errors due to the constraints of the range of the sensor.

The effect of landing on a partly elevated and completely elevated surface is seen in Figure 7.3 and Figure 7.4 respectively. The area under the arm 3 is elevated using a 11mm height box as in the Figure 7.3 experiment, resulting in raise of the manipulator's position against the varying height. Similarly, two objects with different heights (170mm, 110mm) are positioned under arms 1 and 2 respectively in the Figure 7.4 experiment, resulting in the corresponding shift in the positions of the manipulator tip as seen. The manipulators autonomously adapted against the variations of the

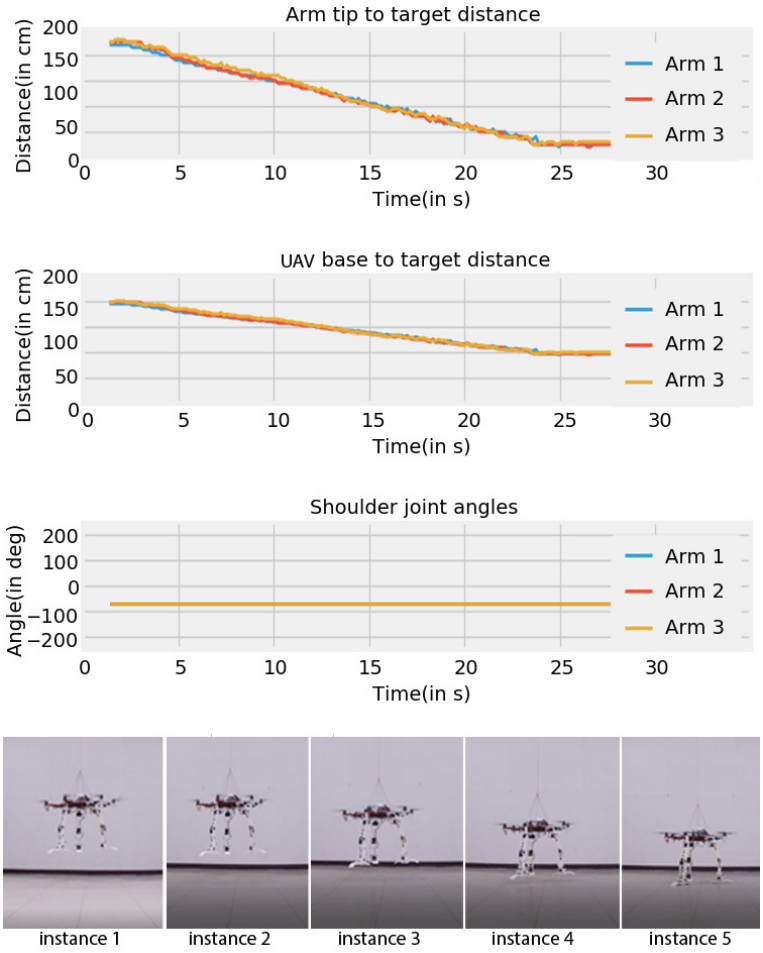

Figure 7.2: Results of landing on a plain surface with the distance sensor readings , the distance between UAV to the surface under each manipulator, and the shoulder angle of each manipulators throughout the landing phase (Prototype 1).

ground surface in both experiments to retain the same end-effector to the surface distance of all the manipulators during the entire landing process. The UAV was able to alter the manipulator positions to allow a safe touch down on a non-planar surface, similar to the first experiment.

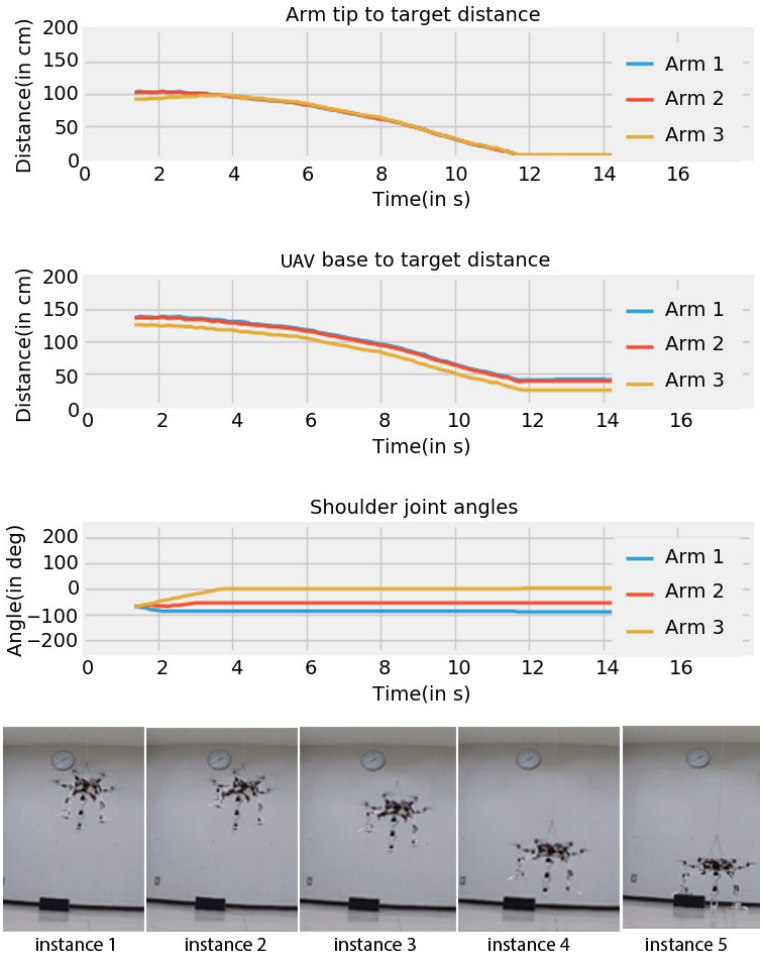

Figure 7.3: Results of landing on slight elevation under one of the manipulators (Prototype 1).

7.1.2 Prototype 2

Description and Setup

In Prototype 1, the key downside that can be observed in the system is the inability to adapt the manipulator tips to an angled surface. Moreover, distance sensors can only measure a distance to a point location. Without shifting the manipulators, it is not so possible to select a suitable landing spot. The concept in Prototype 2, is primarily intended to overcome these problems. After touching down, a passive compliance near the gripper helps it to passively adapt to the surface slope. To clearly perceive

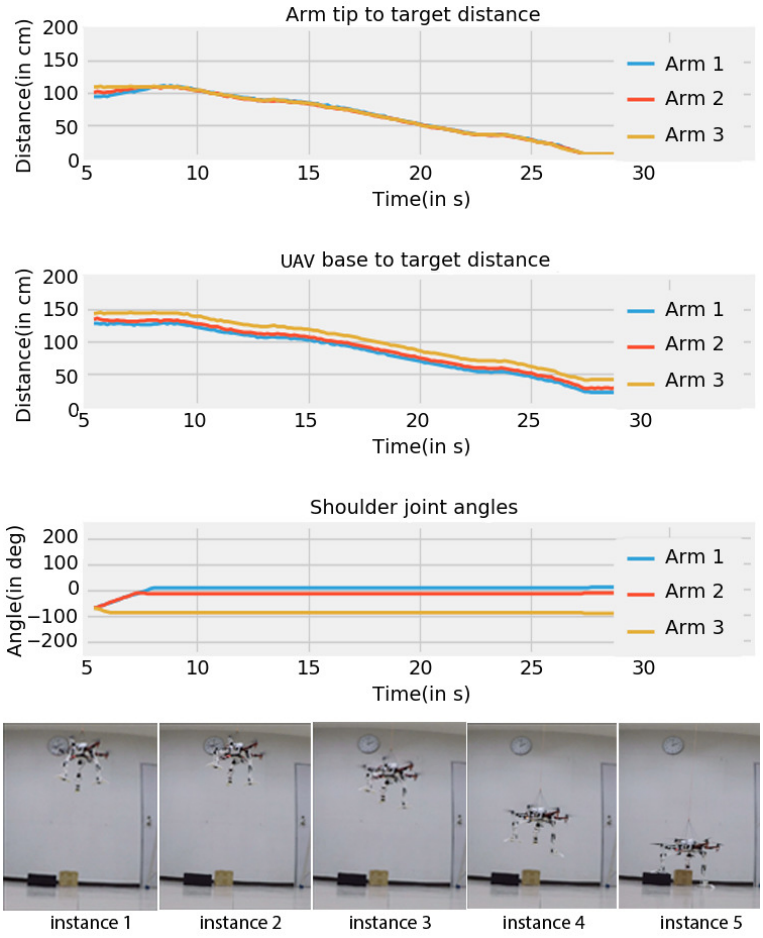

Figure 7.4: Results of landing on varying elevation under all the manipulators (Prototype 1).

the surface of the ground and predict the landing points, a depth camera mounted under the UAV is used.

The trials are carried out to assess the adaptability of the manipulator based on depth camera integrated with the distance sensor data from each tip of the manipulator. Experiments are also carried out by considering the landing on an absolutely plain surface, a partial slope of the surface and a surface with different heights with combined depth camera and distance sensor results. The key aim of the experiment is to assess the manipulator's adaptive capabilities during landing. Therefore most of the tests are carried out indoors in a safe manner. The landing experiments in this

section is published in our work [97]©2019 IEEE.

Results

Similar to the previous experiments, the first experiment was performed to demonstrate the system's reaction to a shift in surface heights based on distance sensor data. To replicate the hovering situation, the location of the UAV is set at a certain distance above the ground. Then under the manipulators, several structures of varying heights are added to observe the system's response. The resulting plots can be seen in Figure 7.5. The UAV height from the ground surface is shown in cyan and the heights are shown in red, green, blue respectively under the $Arm1$, $Arm2$, $Arm3$ manipulators. Under $Arm3$, a box of 110mm height is inserted during the time marked as (2) in the figure. Based on the sensor data and the location of the other manipulators, the manipulator continues to change itself by considering a new z axis position.

At the end of time (2), the object is removed and $Arm3$ returns to its original location. Under the $Arm2$, a new item of 150mm height is added from the time marked as (3) in figure. $Arm2$ adjusts its location to accommodate for the shift in the terrain beneath it. Similarly, under $Arm3$, another object of roughly 240mm height is inserted in the time marked as (4) for which the manipulator moved up accordingly. The manipulators normally finish adapting to the height variation of the surface within 2s, based on the height of the object added.

The system is evaluated to estimate the best position for each of the manipulators using the point cloud data obtained from the depth camera installed under the UAV. The distance sensor information is used to fine-tune the location of the z axis of the manipulators as the UAV approaches and touches the surface.

As seen in Figure 7.6, an experiment is carried out to land the UAV on a surface of varying height. For safety concerns, a tethered experiment is considered. Using the remote joystick, the UAV's yaw is operated manually as it descends. In order to maintain the location of the UAV above the ground during landing, professional piloting is necessary because the navigation is manual, so the ropes were given as

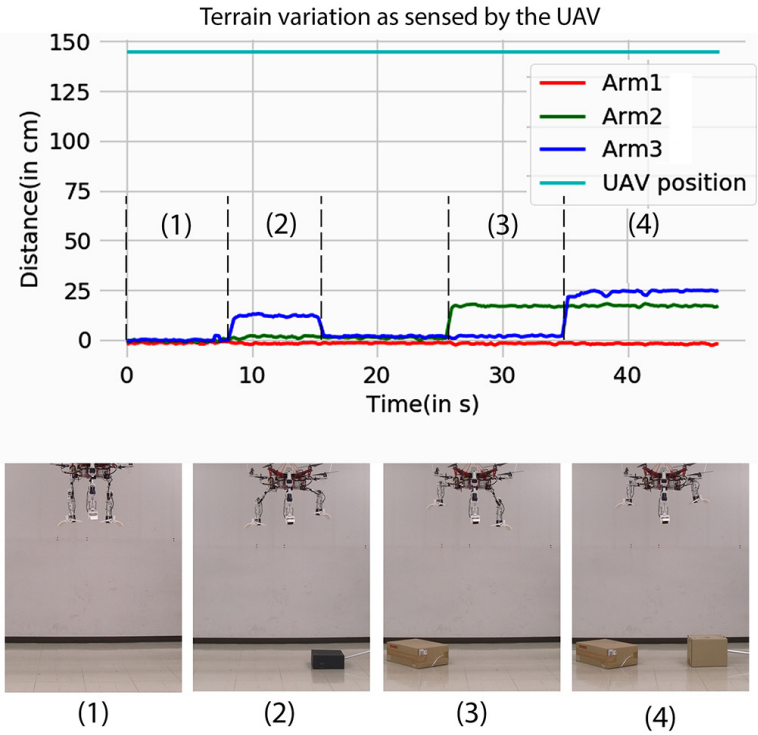

Figure 7.5: Detection and performance of the manipulators against varying surface while holding still position above ground. [97]©2019 IEEE.

support for controlling the height and position of the UAV. The developed system is initialized when the UAV is at a certain height from the ground and is able to sense and adapt the manipulators' locations based on the terrain's processed point cloud information. The UAV is then made to descent towards the ground. Relative distance to the manipulator tips is displayed in Figure 7.6 to make it easier to understand, taking the lowest surface as a reference. Distances from the manipulators tips $Arm1$, $Arm2$, $Arm3$ are displayed in red, green, blue and the UAV frame height from the reference surface is shown in cyan. In the same plot, the relative UAV height from the surface is also seen. From the distance sensor and depth camera data mounted on board, the distances are measured and plotted. After landing and shutting off the propellers of the UAV, the servo motors of the manipulators were observed to provide enough torque to bear the entire weight of the UAV frame without any tethered support. The point cloud information used for processing the positions of the

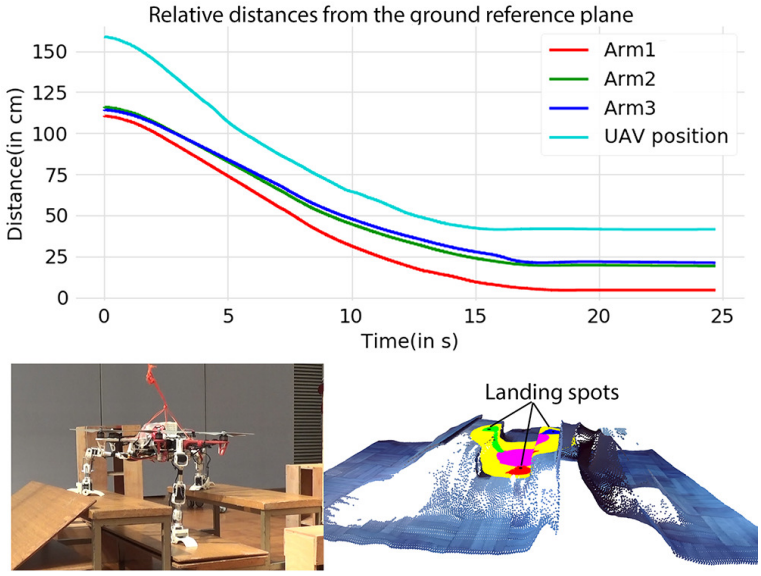

Figure 7.6: Results of landing on surface with different height (top). Final resting position and processed point cloud (bottom). [97]©2019 IEEE.

manipulator and the UAV's final resting location can also be seen in the figure.

Similarly, tests are carried out to land on an almost smooth surface and a sloping surface of around 10°. It is possible to see the final resting pose and the recorded point cloud data used during the landing in Figure 7.7(a) and Figure 7.7(b) using tethered indoor trials, respectively. To keep the UAV frame still horizontal to the earth's horizon, the developed system was capable of adjusting to the terrain. Landing in the event of a sloped surface can be compared to uneven terrain with varying structure heights, where the maximum possible height is selected for manipulators having maximum distance offset to ground.

An experiment without any rope support for the UAV is conducted outdoors. From the ground station, the UAV navigation is operated manually. The system is able to adapt to the ground underneath it when the landing system is triggered and after landing on the surface of the ground and shutting off the propellers, the UAV frame is seen to be maintained statically stable. The processes of landing outdoors from sensing to touch down process are seen in series from left to right

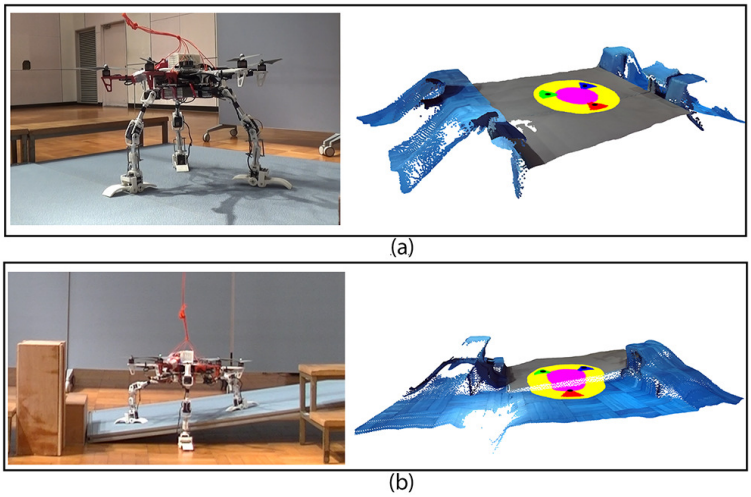

Figure 7.7: Landing position and the processed point cloud for (a) Landing on a flat surface and (b) Landing on a partially sloped surface. [97]©2019 IEEE.

in Figure 7.8(top). Take-off trials are also carried out on an irregular ground. In Figure 7.8(bottom) from left to top, the experiment in chronological order from UAV propeller motor spinning to air hovering can be seen.

7.2 Grasping

Numerous grasping tests are conducted to assess the different grasping capabilities of the developed UAV system. Similar to landing tests with rope support, initial experiments are performed indoors. Followed by tests for object transportation outdoors. Figure 7.9 displays the grasping of some objects using the manipulator grippers. A small cuboid shape with a diameter of 50mm $\times$ 70mm $\times$ 200mm is seen in Figure 7.9(left) picked by one of the grippers. Between the grippers, the shorter side of the object (50mm) is grasped. Two of the grippers of the manipulator are seen in Figure 7.9(center and right) holding a long bar item and a bundle of rope respectively.

An experiment to illustrate the ability to grasp is carried out indoors using all three manipulators in unison. As for the object, a large cylindrical object, about 250mm in diameter and about 100mm in height, was selected. The sequential process

Figure 7.8: Sequential landing process(top) and taking off(bottom) on an uneven surface outdoors. [97]©2019 IEEE.

is seen from left to right in Figure 7.10 during the grasping experiment. For easier positioning control during the experiment phase, the UAV is fixed using rope support (not seen in the figure). The UAV is limited to a height such that the object can be autonomously grasped by the manipulators. The UAV is raised away from the scene after the target is securely grasped.

In addition to the above experiment two further experiments are conducted using the three manipulators to illustrate the transport of objects outdoors by the UAV clutching the objects. A spherical object (200mm diameter) and a cuboid object (210mm $\times$ 210mm $\times$ 80mm) are used to execute the transport operation, as seen in Figure 7.11 and Figure 7.12 respectively. During the experiment, the goal is to move the objects one by one into a blue container (with 800mm $\times$ 600mm opening) that can be seen in the figures and release the object into it. During these trials,

Figure 7.9: Grasping objects using the manipulator's gripper. (From left to right) Grasping a small cuboid object using single gripper, a long pipe using two grippers and a bundle of rope being carried between two grippers.

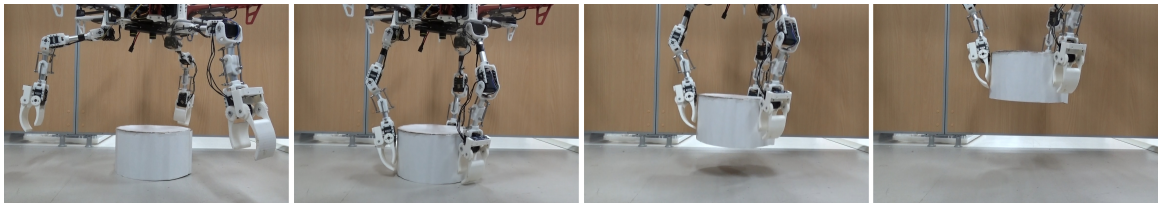

Figure 7.10: Experimental process of grasping a large object of diameter about 250mm.

the control for UAV navigation is manual, but the manipulator control are performed autonomously and triggered by the remote operator.

7.3 Physical Contact with Environment

As explained in chapter 3, we present two outdoor trials in order to illustrate the obstacle avoidance capability using physical contact. In both experiments, we picked

Figure 7.11: Transporting and dropping a spherical object grasped between the manipulators of the UAV into a blue container.

Figure 7.12: Transporting and dropping a cuboid object grasped between the manipulators of the UAV into a blue container.

Figure 7.13: An example task of pushing the UAV away from the obstacle using an on-board manipulator to avoid crashing into an object.

an area close to a wide electric cylindrical pole. The first experiment attempts to force the body of the UAV away from an obstacle as it approaches too close to the pole. This is achieved by extending the manipulator in the direction of the barrier, using the manipulator closer to the target. This helps in moving the UAV body away from the barrier. From left to right, the experiment series can be seen in Figure 7.13.

Another experiment is conducted where the UAV must remain close to the barrier (or a vertical surface). The purpose of this experiment is to conduct a horizontal pushing motion towards an object. One of the manipulators is used to contact the vertical surface, similarly to the preceding experiment. This time, the attitude of the UAV is adjusted so that it travels towards the obstacle after impact with the object while keeping the position of the manipulator steady. The manipulator serves as a spacer between the obstacle and the UAV at this time, so that the UAV body and the propellers do not touch the obstacle. The process for the experiment is seen sequentially from left to right in Figure 7.14.

An experiment was conducted to demonstrate the system's autonomous obstacle avoidance ability. The feedback from the 2D scanner mounter at the top of the UAV

Figure 7.14: Making physical contact with a vertical surface using the manipulator and pushing in the direction of the obstacle using the UAV attitude control.

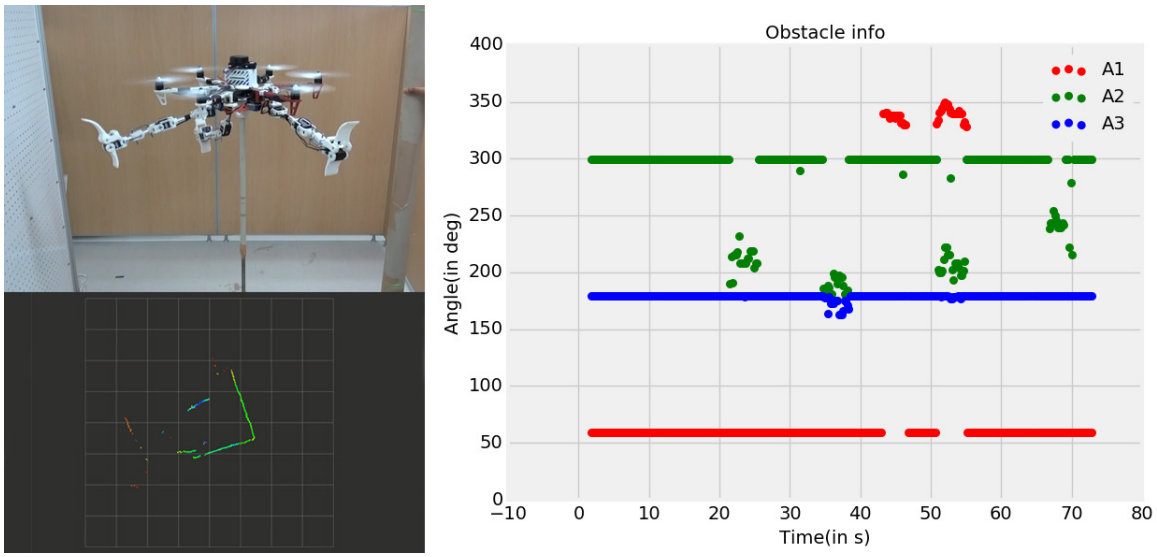

Figure 7.15: Autonomous obstacle detection using 2D laser scanner and avoiding using manipulators.

as discussed in section 6.5 is used to detect the obstructions. The UAV was fixed on a stand during the experiment, as seen in the Figure 7.15(top-left). A board was moved closer to the UAV, and the appropriate manipulator pushes in the direction of the board to stop it as the board reached the threshold perimeter of the UAV. The obstacle detection over time around the UAV is shown in the form of a graph in the Figure 7.15(right). In Figure 7.15(bottom-left), an obstacle map recorded in the on-board processor is shown.

To directly maneuver the UAV through a very narrow tunnel like structure, an experiment was conducted. The tunnel was built by inserting two wide parallel wooden planks with a gap of around 1m. The purpose of the experiment was to measure the

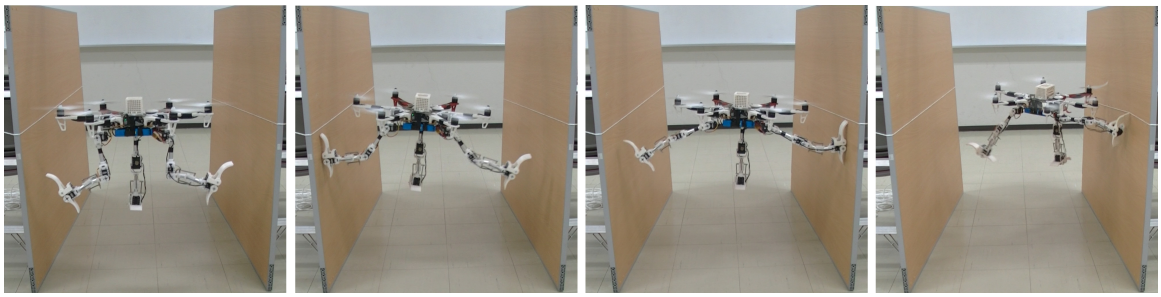

Figure 7.16: Navigating the UAV through a very narrow tunnel resulting in a crash.

motion of the UAV during the manipulator's interaction with an obstacle. The UAV was then manually navigated through the tunnel, with the manipulators extended on either ends. The flight series is as shown in the Figure 7.16. It should be noticed that, directly after entering the tunnel, the UAV moved left, but the left hand manipulator avoided the obstacle. The UAV then went right, and it was again guarded by the right manipulator. But then, while still preserving its position on the right, the UAV shifted forward. During this time, because of friction, the right side manipulator, still being in contact with the wall, acted as an anchor point and swung the drone right, resulting in a crash on the tunnel wall.

7.4 Manipulator Movement Influence on UAV's Attitude

Each of the Prototype 2 manipulators has 4 actuators, distance sensors, compliance mechanism and is made of aluminum pipe and PLA plastic. Fast motions of these manipulators affect the direction of the UAV as it flies. The speed of the actuating motors is then lowered to 50 percent of its maximum RPM in order to limit the speed of motion. But even the smallest aspect of the weight shift would result in the inclination of the UAV pose.

To test its attitude change, we recorded the UAV's IMU data while it was hovering. In the experiment, the position of the manipulator is shifted to see a change of UAV's attitude. The graph obtained during the experiment is shown in the Figure 7.17. It

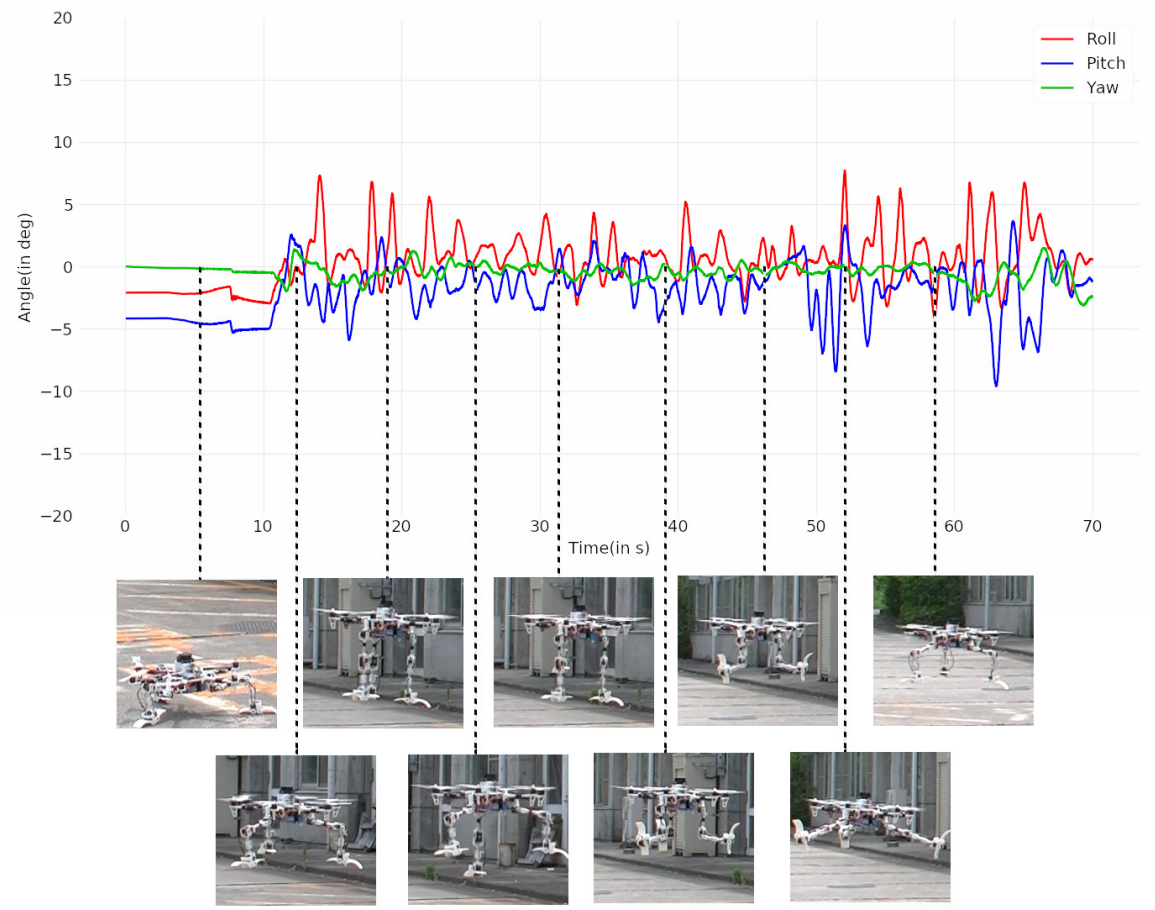

Figure 7.17: IMU data of the UAV showing the orientation change of UAV while moving the manipulators.

can be observerd from the graph that, the maximum change in roll/pitch axis of the UAV during the manipulator shift is less than 10 degrees. Although it affects the attitude, the UAV was still able to hold the position. It is also noted that the yaw in the graph is changing. This is due to the wind and the error from the remote operator. This was observed by multiple experiments performed repeatedly.

7.5 UAV Position Feedback

Various experiments have been carried out as described in the previous sections, to demonstrate the capability of the UAV system designed with three manipulators. However they were all performed by manually controlling the UAV. Other research shows that the UAV can be controlled autonomously. To do this, they use UAV GPS position feedback, on-board sensors, or external setup like a motion capture system. Having an on-board position feedback will be more advantageous as it can be controlled independently in an environment without any pre-setup. Although almost all UAVs are built-in with GPS, it is difficult to receive GPS signals all the time especially indoors.

In our developed system, we use a downward faced stereo camera to get a 3D point cloud for landing and grasping. In addition, this camera can also provide 3D position and orientation feedback, which may be useful for carrying out an autonomous flight. We tested the position feedback provided by the camera in a 6300mm $\times$ 4950mm space during the UAV flight controlled manually by a novice operator. The resulting data is shown in the form of a 3D position graph in the Figure 7.18. The camera's position feedback is based on the texture, color and shape of the objects seen by the camera while moving. The position error with this camera was observed to to less than 100mm when used in a clear textured scene. Having a camera facing down for a UAV is advantageous because they can fly very high and there may be no objects around or above the UAV. But there will still be objects or surfaces under it, which can useful to obtain a precise positioning feedback.

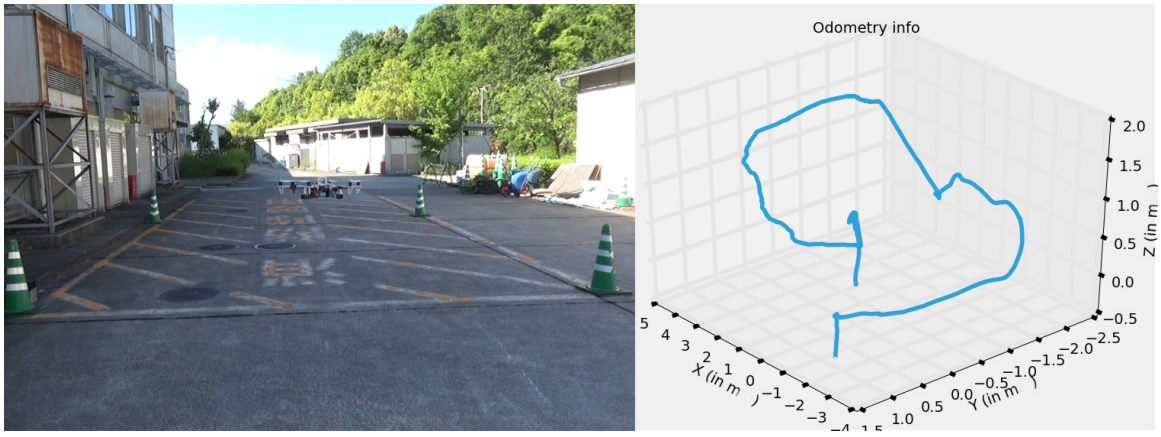

Figure 7.18: UAV position data recorded during UAV flight from the downward facing stereo camera.

Chapter 8

Further Developments

8.1 Summary of the Manipulator System

In the previous chapters, discussions is provided on how a three-arm manipulator system for UAV can be used for various tasks. Strategies on adaptive landing, grasping and obstacle avoidance is provided with experiments. Following summary can be made:

1 When considering landing task, the last link should remain perpendicular to ground and only its height is required to be adjusted.

2 During grasping with three manipulators, the manipulator system can be seen a huge gripper. By setting the last link constant, only the link near the base is actuated to ope and close the huge gripper like structure.

3 Similar to landing case, the manipulators need to stretch to and fro when performing obstacle avoidance sideways.

From the above points a conclusion can be drawn. Instead of using a general purpose manipulator system like in the previous chapters, it is possible to use a special design to realize the same set of tasks with minimum actuation. This can be seen in Figure 8.1, where a parallel link manipulator is shown to perform the same set of tasks efficiently. In each it is required actuate only one joint by fixing the position of other joints. Therefore, the power consumption for motors can be relatively small.

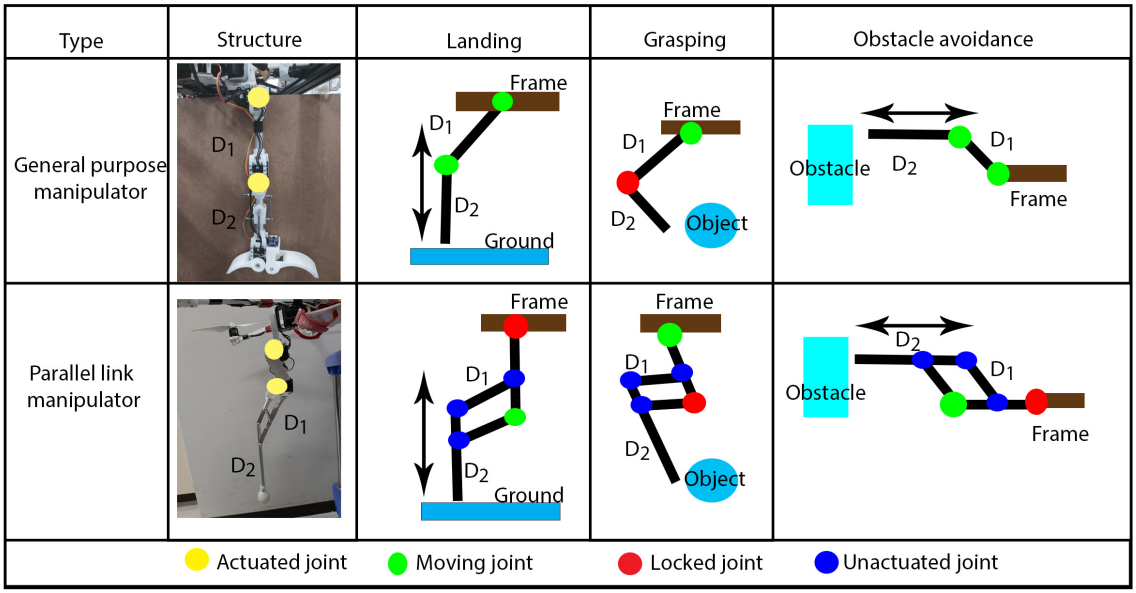

Figure 8.1: Comparison of manipulator posture for different tasks.

8.2 Need for Adapting after Landing

When considering a conventional VTOL type UAV, it is always necessary to make sure that the UAV frame is aligned to the horizon. Failing to meet this condition will result in unexpected movements of the UAV and results in crash. Therefore, some of the modern intelligent flight controllers will not allow the propellers to spin if the UAV frame is not parallel to the horizon, to avoid unexpected movements. In our system we have performed adaptive landing of the UAV using three manipulators for the safe landing. But however after landing, the landed surface may change due to instability. One of the best examples is unstable ship decks. Adaptive landing system will work till landing the UAV on a moving ship deck, but however since the ship deck is not stable, the UAV will not be able to take-off. This may result in failure of operation or taking samples since the UAV cannot return back to its base station. Therefore, a system of UAV frame stabilization is required to keep the frame parallel to the horizon.

As a starting point for the future developments, light weight manipulators using parallel link mechanism are designed as shown in Figure 8.2. The links of the arms

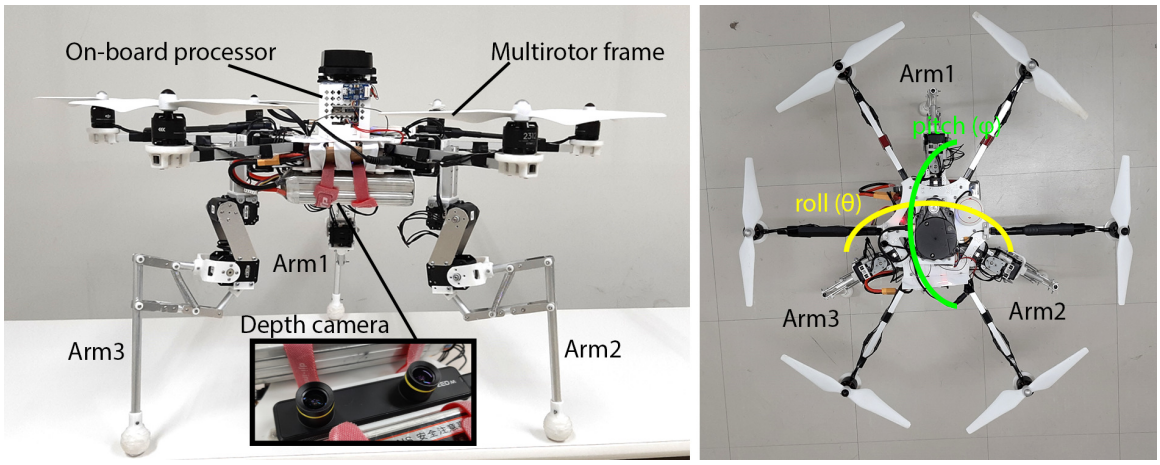

Figure 8.2: Hardware structure of manipulator with parallel link mechanism. (a) Side view showing the manipulators and the camera. (b) Top view showing the manipulator mounting. Roll and pitch axes of the UAV are also marked for understanding.

are made of thin aluminum pipes of 10mm radius. 3D printed PLA parts are used to attach the links together with the actuating motors. For actuation, same set of motors like in previous design (AX12-A) are used. From Figure 8.1, it can be noted that for each tasks only one of the joints are actuated. When considering landing, the whole weight of the robot is resting on the manipulators. Although the motors can hold the weight of the UAV easily, it would require much higher torque to move a manipulator after landed. Therefore for the last link, a motor with a much higher torque is used (MX-28AT). In addition two springs are attached for each manipulators to provide some force to easily stretch the manipulator outwards. For simplicity of the design, the grippers are removed. The manipulators are attached to a custom made UAV frame with thin links for smooth movements of the manipulators to different regions of the UAV. The total weight of the UAV system along with manipulators and batteries is 3kg.

The kinematics of this manipulator can be calculated using the equation 8.1, where s_i and c_i are $\sin\theta_i$ and $\cos\theta_i$ for ith joint respectively and L_1 to L_5 are the link lengths as marked in Figure 8.3.

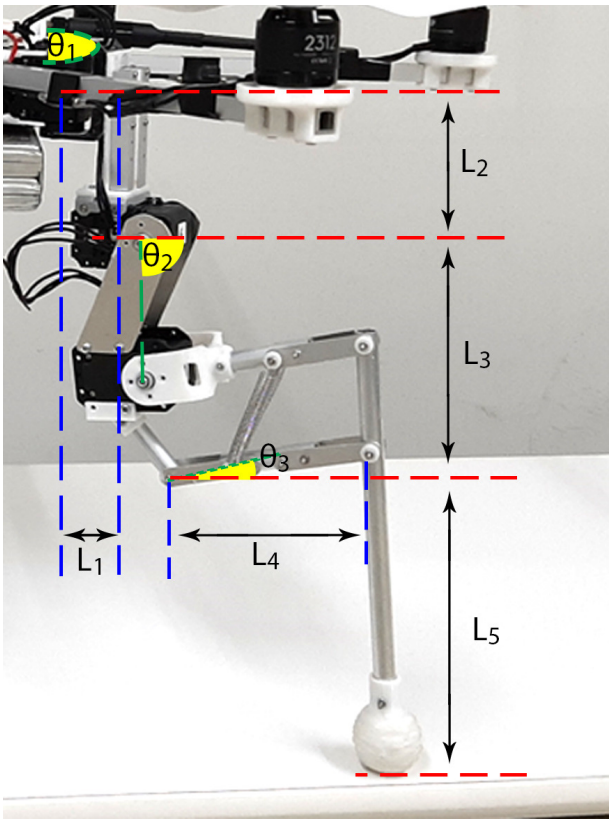

Figure 8.3: Structure of the manipulator with parallel link mechanism with link lengths marked.

$$x = L_1c_1 + L_3c_1c_2 - L_4s_2c_1c_3 - L_4s_3c_1c_2 - L_5(s_2s_3c_1 - c_1c_2c_3)c_3 \\ - L_5(-s_2c_1c_3 - s_3c_1c_2)s_3, \quad (8.1)$$

$$y = L_1s_1 + L_3s_1c_2 - L_4s_1s_2c_3 - L_4s_1s_3c_2 - L_5(s_1s_2s_3 - s_1c_2c_3)c_3 \\ - L_5(-s_1s_2c_3 - s_1s_3c_2)s_3, \quad (8.2)$$

$$z = -L_2 + L_3s_2 - L_4s_2s_3 + L_4c_2c_3 - L_5(-s_2s_3 + c_2c_3)s_3 \\ - L_5(-s_2c_3 - s_3c_2)c_3 \quad (8.3)$$

The inverse kinematics is derived from equation 8.1 using Jacobian and is written as,

$$J_v = \begin{bmatrix} \delta_1 & \delta_2 & \delta_3 \\ \delta_4 & \delta_5 & \delta_6 \\ \delta_7 & \delta_8 & \delta_9 \\ 0 & 0 & 1 \\ 1 & 0 & 0 \\ 1 & 0 & 0 \end{bmatrix} \tag{8.4}$$

where,

$$\begin{aligned} \delta_1 &= (-L_1 - L_3c_2 + L_4s_{23} - L_5c_2)s_1, \\ \delta_2 &= (L_1 + L_3c_2 - L_4s_{23} + L_5c_2)c_1, \\ \delta_3 &= 0, \\ \delta_4 &= -(L_3s_2 + L_4c_{23} + L_5s_2)c_1, \\ \delta_5 &= -(L_3s_2 + L_4c_{23} + L_5s_2)s_1, \\ \delta_6 &= L_3c_2 - L_4s_{23} + L_5c_2, \\ \delta_7 &= -L_4c_1c_{23}, \\ \delta_8 &= -L_4s_1c_{23}, \\ \delta_9 &= -L_4s_{23} \end{aligned} \tag{8.5}$$

8.3 Adapting to a Surface after Landing

In order to adapt a landed UAV to a changing surface on which it is standing, it is necessary to know the attitude of the UAV especially in its roll and pitch axis. Since the UAV flight controllers are already equipped with an IMU, it would be easier to use the data from them directly. A simple controller can be developed to tilt the UAV back to its zero position by using the IMU data and increasing or decreasing the manipulator heights. A simple PD system can be developed as given in equation 8.6.

$$u(t) = K_p e(t) + K_d \frac{\mathrm{d}e(t)}{\mathrm{d}t} \tag{8.6}$$

Where K_p and K_d are the P and D gains respectively. And $e(t)$ is the error between the desired value and the present value.

For a stable parallel pose of the UAV frame, its θ (roll angle) and ϕ (pitch angle) values should be maintained zero. Therefore any non-zero roll and pitch values forms the error $e(t)$. Considering the roll (θ) and pitch (ϕ) axes of the UAV and the manipulator numbering with reference to Figure 8.2(b), the equation 8.6 can be re-written as in equation 8.7 and equation 8.8 for θ and ϕ changes respectively.

$$\begin{aligned} arm2_u(t) &= -K_p\theta(t) + K_d\dot{\theta(t)} \\ arm3_u(t) &= K_p\theta(t) + K_d\dot{\theta(t)} \end{aligned} \tag{8.7}$$

$$\begin{aligned} arm1_u(t) &= -K_p\phi(t) + K_d\dot{\phi(t)} \\ arm2_u(t) = arm3_u(t) &= K_p\phi(t) + K_d\dot{\phi(t)} \end{aligned} \tag{8.8}$$

Where $\theta(t)$ and $\phi(t)$ are the roll and pitch values of the UAV at a given time. And $\dot{\theta(t)}$ and $\dot{\phi(t)}$ are the differences between the current and previous roll and pitch values respectively of the UAV. $arm1_u(t)$, $arm2_u(t)$ and $arm3_u(t)$ are the angle changes applied to the last link of the each manipulators resulting in their height changes.

8.4 Land Adapting Experiment

An experiment was performed to test the adapting capability of the UAV against an unstable surface. The UAV was first made to land on a prepared platform. By checking the direction of the load from torque sensors in the actuators of the last link, it can ensured if that manipulator is touching a surface or not. The adaptive control can be activated automatically if all the manipulators are touching to a surface. After landing on it, the platform was moved manually in both it roll and pitch axes. This result in the unstable pose of the UAV. By using the adaptive control for the UAV, the UAV tried to autonomously stabilize and keep its frame parallel to the horizon

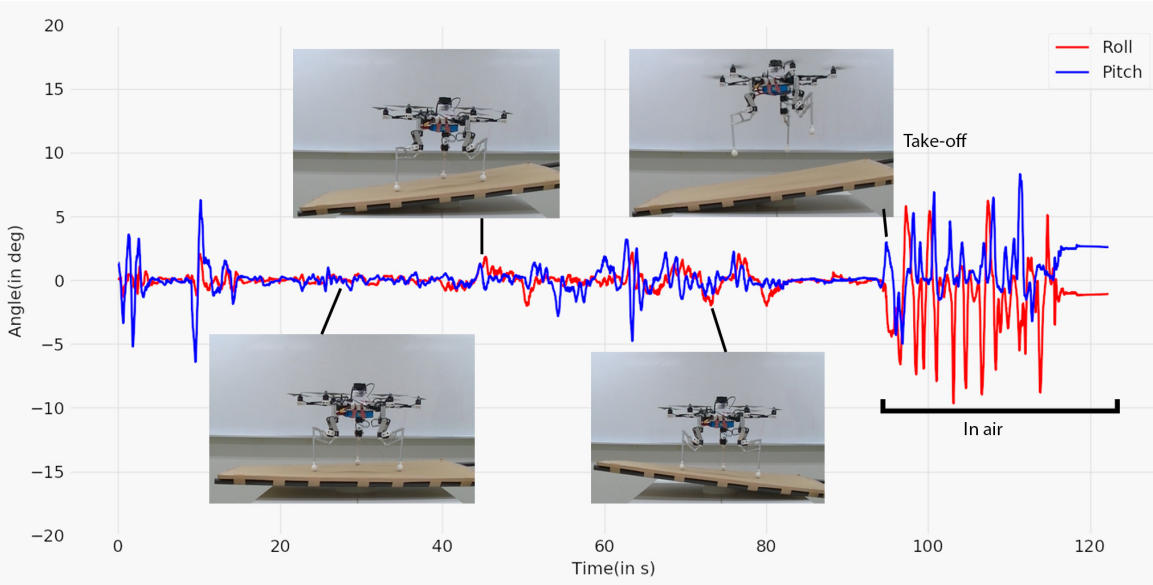

Figure 8.4: Graph showing the roll and pitch angles of the UAV recorded from its IMU during land adapting experiment.

in order to take-off at any instant. This can be observed in the graph of Figure 8.4. Even though the surface shifts to about 10 degrees, the UAV is seen to be able to adjust within 5 degree error. The time required to stabilize for a change is observed to be less than 1s. After take-off the roll and pitch angles seem to change rapidly due to UAV flight.

Chapter 9

Conclusions

9.1 Summary

We present the design and development of an on-board three-manipulator system for UAVs in this study. The robotic platform is intended to be used when multi-task capability is needed in an aerial deployment. This system is designed to not strain a UAV platform's restricted payload capability and make full use of the capabilities of a UAV.

Different tasks are shown in this study, that can be performed using the same set of manipulator system fitted on a UAV. There are three manipulators in the manipulator system that can be conveniently used to execute tasks such as landing, grasping, and making secure physical contact with the environment. The use of on-board sensors and processor, in addition to the mechanical system, provides more space for autonomous tasks to be carried out. Successfully achieving an autonomous adaptive landing using a depth camera and a depth sensor input using the same robotic device has been demonstrated. Furthermore, using different grasps performed by the system, we realized the transport of objects. Experiments have also demonstrated the possibility of making direct contact with vertical objects using the same system.

During the tests, it is found that when a UAV is about to grasp an object, decreasing the UAV altitude too far or too will result in an object not being properly grasped. The UAV altitude should be correctly set and maintained during the grasping process.

In addition, it is difficult to manually operate several systems by a single operator. Typically, according to [126], a UAV conducting a search mission has two functions to play: a pilot operating the UAV and a sensor operator reading the images and other sensors. Usually, these may require more than one operator. It would also be better for a single operator to manage and execute all activities by conducting semi-autonomous or fully autonomous tasks.

While we have shown the multi-task capability of the system, there are a few problems that still require more study when considering the autonomic capability. We found that it is difficult to determine the surface area in a grassy area while conducting an autonomous landing, since the ground beneath the grass is not easily visible. While the force sensors can be integrated into the manipulators to see if they can touch the surface, safe landing cannot be assured in this situation. Having a system combined with vision system as well as force sensors would be more feasible.

9.2 Discussions and Future Works

The experiments carried out demonstrate that the estimation of surface elevations when hovering makes it useful to help locate an appropriate landing spot. Our method of calculating the distance long before landing decides the best possible place to settle on the specified surface in order to prevent landing errors due to design limitations. During both tests, the UAV frame preserves parallel posture to the surface by changing the manipulators autonomously well before reaching the surface.

The actuators of the manipulators have adequate torque to sustain the UAV's stable resting place after landing on any given surface. However it can be seen from the graphs that there is still some sensor noise in the distance sensors due to inadequate filtering, so the manipulator response is slowed (within 2s) against surface variations. Proper filtering and monitoring would help the system respond more rapidly.

In addition, it has been found that the lateral movement of the UAV during steering can result in inaccurate sensor readings as the UAV descends. Therefore the arms are locked just before reaching the floor to prevent a change in arm location

due to incorrect readings. In the future, we will carry out a fully autonomous flight during the landing process in order to prevent significant drifts of the UAV.

After landing, the manipulator tips were able to passively adapt to the surface slope. We attempted to land on a complete slope of around 40°. The system was able to change the manipulators effectively, but the UAV did not maintain a comfortable position after the touchdown due to a lack of friction between the surface and the grippers.

In tests, landings on different surfaces were observed, during which the proposed manipulator system independently adapted and aided the tele-operated landing process. However it was difficult to navigate the UAV manually without lateral displacements, resulting in a very long landing maneuver. A fully autonomous landing system can be realized using position feedback information from the stereo camera attached to the UAV.

In the proposed work, the use of a depth camera on a UAV to record and determine the surface height under the UAV is considered. This can be helpful in analyzing the different potential point sets on the given surface with the best possible pose for the manipulators well before touching the ground. The limitation of the use of distance sensors can only be solved by the use of depth camera to detect distance to inclined surfaces. In addition, the manipulator system is expected to be used in the future as a way of avoiding surrounding obstacles. Due to the high maneuverability and coverage of the workspace of the proposed aerial manipulation system, it is possible to use the manipulators to prevent surrounding obstacles from colliding to them, thereby moving the aerial platform away from them.

References

[1] Jeffrey Delmerico, Stefano Mintchev, Alessandro Giusti, Boris Gromov, Kamilo Melo, Tomislav Horvat, Cesar Cadena, Marco Hutter, Auke Ijspeert, Dario Floreano, et al. The current state and future outlook of rescue robotics. *Journal of Field Robotics*, 36(7):1171–1191, 2019.

[2] Hank Jones and Pamela Hinds. Extreme work teams: using swat teams as a model for coordinating distributed robots. In *Proceedings of the 2002 ACM conference on Computer supported cooperative work*, pages 372–381, 2002.

[3] Robert Bogue. Disaster relief, and search and rescue robots: the way forward. *Industrial Robot: the international journal of robotics research and application*, 2019.

[4] James C Rosser Jr, Vudatha Vignesh, Brent A Terwilliger, and Brett C Parker. Surgical and medical applications of drones: a comprehensive review. *JSLS: Journal of the Society of Laparoendoscopic Surgeons*, 22(3), 2018.

[5] Jonathan W Rosen. Zip. *TECHNOLOGY REVIEW*, 120(4):36–51, 2017.

[6] Mostafa Hassanalian and Abdessattar Abdelkefi. Classifications, applications, and design challenges of drones: A review. *Progress in Aerospace Sciences*, 91:99–131, 2017.

[7] Andreas Birk, Burkhard Wiggerich, Heiko Bülow, Max Pfingsthorn, and Sören Schwertfeger. Safety, security, and rescue missions with an unmanned aerial vehicle (uav). *Journal of Intelligent & Robotic Systems*, 64(1):57–76, 2011.

[8] Michael A Goodrich, Bryan S Morse, Damon Gerhardt, Joseph L Cooper, Morgan Quigley, Julie A Adams, and Curtis Humphrey. Supporting wilderness search and rescue using a camera-equipped mini uav. *Journal of Field Robotics*, 25(1-2):89–110, 2008.

[9] Telmo Adão, Jonáš Hruška, Luís Pádua, José Bessa, Emanuel Peres, Raul Morais, and Joaquim João Sousa. Hyperspectral imaging: A review on uav-based sensors, data processing and applications for agriculture and forestry. *Remote Sensing*, 9(11):1110, 2017.

[10] Takahiro Ikeda, Shogo Yasui, Motoharu Fujihara, Kenichi Ohara, Satoshi Ashizawa, Akihiko Ichikawa, Akihisa Okino, Takeo Oomichi, and Toshio Fukuda. Wall contact by octo-rotor uav with one dof manipulator for bridge inspection. In *2017 IEEE/RSJ International Conference on Intelligent Robots and Systems (IROS)*, pages 5122–5127. IEEE, 2017.

[11] Janosch Nikolic, Michael Burri, Joern Rehder, Stefan Leutenegger, Christoph Huerzeler, and Roland Siegwart. A uav system for inspection of industrial facilities. In *2013 IEEE Aerospace Conference*, pages 1–8. IEEE, 2013.

[12] Hossein Bonyan Khamseh, Farrokh Janabi-Sharifi, and Abdelkader Abdessameud. Aerial manipulation—a literature survey. *Robotics and Autonomous Systems*, 107:221–235, 2018.

[13] Fabio Ruggiero, Vincenzo Lippiello, and Anibal Ollero. Introduction to the special issue on aerial manipulation. *IEEE Robotics and Automation Letters*, 3(3):2734–2737, 2018.

[14] DING Xilun, GUO Pin, XU Kun, and YU Yushu. A review of aerial manipulation of small-scale rotorcraft unmanned robotic systems. *Chinese Journal of Aeronautics*, 32(1):200–214, 2019.

[15] Daniel Mellinger, Quentin Lindsey, Michael Shomin, and Vijay Kumar. Design, modeling, estimation and control for aerial grasping and manipulation. In *2011*

IEEE/RSJ International Conference on Intelligent Robots and Systems, pages 2668–2673. IEEE, 2011.

[16] Syohei Shimahara, Robert Ladig, Suphachart Leewiwatwong, Shinichi Hirai, and Kazuhiro Shimonomura. Aerial manipulation for the workspace above the airframe. In *2015 IEEE/RSJ International Conference on Intelligent Robots and Systems (IROS)*, pages 1453–1458. IEEE, 2015.

[17] Fabio Ruggiero, Miguel Angel Trujillo, R Cano, H Ascorbe, Antidio Viguria, C Peréz, Vincenzo Lippiello, Aníbal Ollero, and Bruno Siciliano. A multilayer control for multirotor uavs equipped with a servo robot arm. In *2015 IEEE international conference on robotics and automation (ICRA)*, pages 4014–4020. IEEE, 2015.

[18] Yoshinori Ohnishi, Takeshi Takaki, Tadayoshi Aoyama, and Idaku Ishii. Development of a 4-joint 3-dof robotic arm with anti-reaction force mechanism for a multicopter. In *2017 IEEE/RSJ International Conference on Intelligent Robots and Systems (IROS)*, pages 985–991. IEEE, 2017.

[19] PRODRONE Unveils the World's First Dual Robot Arm Large-Format Drone [Internet]. 2016 Sept 07 [cited 2020 Mar 11]. Available from: https://www.prodrone.jp/en/archives/1420.

[20] A Suarez, AE Jimenez-Cano, VM Vega, G Heredia, A Rodriguez-Castaño, and A Ollero. Lightweight and human-size dual arm aerial manipulator. In *2017 International Conference on Unmanned Aircraft Systems (ICUAS)*, pages 1778–1784. IEEE, 2017.

[21] Satoshi Suzuki. Recent researches on innovative drone technologies in robotics field. *Advanced Robotics*, 32(19):1008–1022, 2018.

[22] Yuncheng Lu, Zhucun Xue, Gui-Song Xia, and Liangpei Zhang. A survey on vision-based uav navigation. *Geo-spatial information science*, 21(1):21–32, 2018.

[23] Yuri S Sarkisov, Grigoriy A Yashin, Evgeny V Tsykunov, and Dzmitry Tsetserukou. Dronegear: A novel robotic landing gear with embedded optical torque sensors for safe multicopter landing on an uneven surface. *IEEE Robotics and Automation Letters*, 3(3):1912–1917, 2018.

[24] Carl John O Salaan, Yoshito Okada, Shoma Mizutani, Takuma Ishii, Keishi Koura, Kazunori Ohno, and Satoshi Tadokoro. Close visual bridge inspection using a uav with a passive rotating spherical shell. *Journal of Field Robotics*, 35(6):850–867, 2018.

[25] Noriho Koyachi, Hironori Adachi, Makoto Izumi, and Takeshi Hirose. Control of walk and manipulation by a hexapod with integrated limb mechanism: Melmantis-1. In *Proceedings 2002 IEEE International Conference on Robotics and Automation (Cat. No. 02CH37292)*, volume 4, pages 3553–3558. IEEE, 2002.

[26] Geert-Jan M Kruijff, Ivana Kruijff-Korbayová, Shanker Keshavdas, Benoit Larochelle, Miroslav Janíček, Francis Colas, Ming Liu, Francois Pomerleau, Roland Siegwart, Mark A Neerincx, et al. Designing, developing, and deploying systems to support human–robot teams in disaster response. *Advanced Robotics*, 28(23):1547–1570, 2014.

[27] Multi-tasking robots – Doing the dangerous work, so humans don't have to [Internet] [cited 2020 May 22]. Available from: https://stfc.ukri.org/news-events-and-publications/features/multi-tasking-robots/.

[28] AG Korchenko and OS Illyash. The generalized classification of unmanned air vehicles. In *2013 IEEE 2nd International Conference Actual Problems of Unmanned Air Vehicles Developments Proceedings (APUAVD)*, pages 28–34. IEEE, 2013.

[29] Drone technology uses and applications for commercial, industrial and military drones in 2020 and the future [Internet] [cited 2020 May 20]. Available from: https://www.businessinsider.com/drone-technology-uses-applications.

[30] Yash Mulgaonkar, Michael Whitzer, Brian Morgan, Christopher M Kroninger, Aaron M Harrington, and Vijay Kumar. Power and weight considerations in small, agile quadrotors. In *Micro-and Nanotechnology Sensors, Systems, and Applications VI*, volume 9083, page 90831Q. International Society for Optics and Photonics, 2014.

[31] Teppo Luukkonen. Modelling and control of quadcopter. *Independent research project in applied mathematics, Espoo*, 22, 2011.

[32] Robert Mahony, Vijay Kumar, and Peter Corke. Multirotor aerial vehicles: Modeling, estimation, and control of quadrotor. *IEEE Robotics and Automation magazine*, 19(3):20–32, 2012.

[33] Why and When Did Drones Become Popular? [Internet] [cited 2020 May 17]. Available from: http://dronesuavreport.com/2019/02/23/why-and-when-did-drones-become-popular/.

[34] John D Buckley and John J Buckley. *Air power in the age of total war*. Indiana University Press, 1999.

[35] Kettering Bug [Internet] [cited 2020 May 20]. Available from: https://www.daviddarling.info/encyclopedia/K/Kettering_Bug.html.

[36] Warren R Young. *The helicopters*. Time Life Education, 1982.

[37] MEMS market- growth, trends, and forecast (2020 - 2025) [Internet] [cited 2020 May 20]. Available from: https://www.mordorintelligence.com/industry-reports/mems-market.

[38] Benchmarks Of Many ARM Boards From The Raspberry Pi To NVIDIA Jetson TX2 [Internet] [cited 2020 May 20]. Available from: https://www.phoronix.com/scan.php?page=article&item=march-2017-arm&num=1.

[39] Press Release – FAA Registered Nearly 300,000 Unmanned Aircraft Owners [Internet] [cited 2020 May 22]. Available from: https://www.faa.gov/news/press_releases/news_story.cfm?newsId=19914.

[40] Summary of small unmanned aircraft rule (PART 107) [Internet] [cited 2020 May 22]. Available from: https://www.faa.gov/uas/media/Part_107_Summary.pdf.

[41] Commercial Unmanned Aerial Vehicle (UAV) Market Analysis – Industry trends, forecasts and companies [Internet] [cited 2020 May 22]. Available from: https://www.businessinsider.com/commercial-uav-market-analysis.

[42] Drone Use in Civil Engineering and City Planning [Internet] [cited 2020 May 22]. Available from: https://blog.dronebase.com/2018/08/15/drone-use-in-civil-engineering-and-city-planning.

[43] Matúš Tkáč and Peter Mésároš. Utilizing drone technology in the civil engineering. *Selected Scientific Papers-Journal of Civil Engineering*, 14(1):27–37, 2019.

[44] Junwon Seo, Luis Duque, and Jim Wacker. Drone-enabled bridge inspection methodology and application. *Automation in Construction*, 94:112–126, 2018.

[45] AG Entrop and A Vasenev. Infrared drones in the construction industry: designing a protocol for building thermography procedures. *Energy procedia*, 132:63–68, 2017.

[46] Drone-based Plant Count Increases Accountability [Internet] [cited 2020 May 23]. Available from: https://medium.com/aerial-acuity/drone-based-plant-count-increases-accountability-d48ed60033b6#.fjpjbege2.

[47] These tree-planting drones are firing seed missiles to restore the world's forests [Internet] [cited 2020 May 20]. Available from: https://www.fastcompany.com/90329982/these-tree-planting-drones-are-firing-seed-missiles-to-restore-the-worlds-forests.

[48] Amazon.com: Prime Air [Internet] [cited 2020 May 23]. Available from: https://www.amazon.com/b?node=8037720011.

[49] Facebook is reportedly testing solar-powered internet drones again — this time with Airbus [Internet] [cited 2020 May 23]. Available from: https://techcrunch.com/2019/01/21/facebook-airbus-solar-drones-internet-program/.

[50] Drones are revolutionizing the media industry [Internet] [cited 2020 May 22]. Available from: https://www.dronitech.com/drones-are-revolutionizing-the-media-industry/.

[51] Agoston Restas et al. Drone applications for supporting disaster management. *World Journal of Engineering and Technology*, 3(03):316, 2015.

[52] Fabio Ruggiero, Vincenzo Lippiello, and Anibal Ollero. Aerial manipulation: A literature review. *IEEE Robotics and Automation Letters*, 3(3):1957–1964, 2018.

[53] Alejandro Suarez, Victor M Vega, Manuel Fernandez, Guillermo Heredia, and Anibal Ollero. Benchmarks for aerial manipulation. *IEEE Robotics and Automation Letters*, 5(2):2650–2657, 2020.

[54] Julio Mendoza-Mendoza, Victor J Gonzalez-Villela, Carlos Aguilar-Ibañez, Miguel Santiago Suarez-Castañon, and Leonardo Fonseca-Ruiz. Snake aerial manipulators: A review. *IEEE Access*, 8:28222–28241, 2020.

[55] Abdullah Mohiuddin, Tarek Taha, Yahya H Zweiri, and Dongming Gan. A survey of single and multi-uav aerial manipulation. *Unmanned Syst.*, 8(2):119–147, 2020.

[56] Felix Huber, Konstantin Kondak, Kai Krieger, Dominik Sommer, Marc Schwarzbach, Maximilian Laiacker, Ingo Kossyk, Sven Parusel, Sami Haddadin, and Alin Albu-Schäffer. First analysis and experiments in aerial manipulation

using fully actuated redundant robot arm. In *2013 IEEE/RSJ International Conference on Intelligent Robots and Systems*, pages 3452–3457. IEEE, 2013.

[57] Maximilian Laiacker, Felix Huber, and Konstantin Kondak. High accuracy visual servoing for aerial manipulation using a 7 degrees of freedom industrial manipulator. In *2016 IEEE/RSJ International Conference on Intelligent Robots and Systems (IROS)*, pages 1631–1636. IEEE, 2016.

[58] Yuri S Sarkisov, Min Jun Kim, Davide Bicego, Dzmitry Tsetserukou, Christian Ott, Antonio Franchi, and Konstantin Kondak. Development of sam: cable-suspended aerial manipulator. In *2019 International Conference on Robotics and Automation (ICRA)*, pages 5323–5329. IEEE, 2019.

[59] Antonio E Jimenez-Cano, Jesús Martin, Guillermo Heredia, Aníbal Ollero, and Raul Cano. Control of an aerial robot with multi-link arm for assembly tasks. In *2013 IEEE International Conference on Robotics and Automation*, pages 4916–4921. IEEE, 2013.

[60] Alejandro Suarez, Guillermo Heredia, and Anibal Ollero. Lightweight compliant arm for aerial manipulation. In *2015 IEEE/RSJ International Conference on Intelligent Robots and Systems (IROS)*, pages 1627–1632. IEEE, 2015.

[61] AE Jimenez-Cano, G Heredia, and A Ollero. Aerial manipulator with a compliant arm for bridge inspection. In *2017 International Conference on Unmanned Aircraft Systems (ICUAS)*, pages 1217–1222. IEEE, 2017.

[62] Abel Gawel, Mina Kamel, Tonci Novkovic, Jakob Widauer, Dominik Schindler, Benjamin Pfyffer Von Altishofen, Roland Siegwart, and Juan Nieto. Aerial picking and delivery of magnetic objects with mavs. In *2017 IEEE international conference on robotics and automation (ICRA)*, pages 5746–5752. IEEE, 2017.

[63] Han W Wopereis, TD Van Der Molen, TH Post, Stefano Stramigioli, and Matteo Fumagalli. Mechanism for perching on smooth surfaces using aerial impacts.

In *2016 IEEE international symposium on safety, security, and rescue robotics (SSRR)*, pages 154–159. IEEE, 2016.

[64] Kenjiro Tadakuma, Carl John Salaan, Eri Takane, Yoshito Okada, Kazunori Ohno, and Satoshi Tadokoro. Design of aerial manipulator suitable for a uav with two passive rotating hemispherical shells. In *2018 IEEE International Symposium on Safety, Security, and Rescue Robotics (SSRR)*, pages 1–6. IEEE, 2018.

[65] Joe Woong Yeol, Donald Toohey, and Yong-Won Hwang. Design and analysis of a multiple tentacle system for mobile manipulation in micro aerial vehicles. *Procedia Computer Science*, 105:7–13, 2017.

[66] Dongjae Lee, Hoseong Seo, Dabin Kim, and H Jin Kim. Aerial manipulation using model predictive control for opening a hinged door. *arXiv preprint arXiv:2003.08256*, 2020.

[67] Suseong Kim, Hoseong Seo, and H Jin Kim. Operating an unknown drawer using an aerial manipulator. In *2015 IEEE International Conference on Robotics and Automation (ICRA)*, pages 5503–5508. IEEE, 2015.

[68] Dimos Tzoumanikas, Felix Graule, Qingyue Yan, Dhruv Shah, Marija Popovic, and Stefan Leutenegger. Aerial manipulation using hybrid force and position nmpc applied to aerial writing. *arXiv preprint arXiv:2006.02116*, 2020.

[69] James R Kutia, Karl A Stol, and Weiliang Xu. Aerial manipulator interactions with trees for canopy sampling. *IEEE/ASME Transactions on Mechatronics*, 23(4):1740–1749, 2018.

[70] Alejandro Suarez, Alvaro Caballero, Ambar Garofano, Pedro J Sanchez-Cuevas, Guillermo Heredia, and Anibal Ollero. Aerial manipulator with rolling base for inspection of pipe arrays. *IEEE Access*, 8:162516–162532, 2020.

[71] Syohei Shimahara, Suphachart Leewiwatwong, Robert Ladig, and Kazuhiro Shimonomura. Aerial torsional manipulation employing multi-rotor flying robot.

In *2016 IEEE/RSJ International Conference on Intelligent Robots and Systems (IROS)*, pages 1595–1600. IEEE, 2016.

[72] Ryo Miyazaki, Rui Jiang, Hannibal Paul, Koji Ono, and Kazuhiro Shimonomura. Airborne docking for multi-rotor aerial manipulations. In *2018 IEEE/RSJ International Conference on Intelligent Robots and Systems (IROS)*, pages 4708–4714. IEEE, 2018.

[73] Robert Ladig and Kazuhiro Shimonomura. High precision marker based localization and movement on the ceiling employing an aerial robot with top mounted omni wheel drive system. In *2016 IEEE/RSJ International Conference on Intelligent Robots and Systems (IROS)*, pages 3081–3086. IEEE, 2016.

[74] Pengfei Yu, Zihao Wang, and KC Wong. Exploring aerial perching and grasping with dual symmetric manipulators and compliant end-effectors. *International Journal of Micro Air Vehicles*, 11:1756829319877416, 2019.

[75] AE Jimenez-Cano, J Braga, Guillermo Heredia, and Aníbal Ollero. Aerial manipulator for structure inspection by contact from the underside. In *2015 IEEE/RSJ international conference on intelligent robots and systems (IROS)*, pages 1879–1884. IEEE, 2015.

[76] Hannibal Paul, Koji Ono, Robert Ladig, and Kazuhiro Shimonomura. A multirotor platform employing a three-axis vertical articulated robotic arm for aerial manipulation tasks. In *2018 IEEE/ASME International Conference on Advanced Intelligent Mechatronics (AIM)*, pages 478–485. IEEE, 2018.

[77] Jasper LJ Scholten, Matteo Fumagalli, Stefano Stramigioli, and Raffaella Carloni. Interaction control of an uav endowed with a manipulator. In *2013 IEEE International Conference on Robotics and Automation*, pages 4910–4915. IEEE, 2013.

[78] Akihiko Ichikawa, Yuki Abe, Takahiro Ikeda, Kenichi Ohara, Jyunpei Kishikawa, Satoshi Ashizawa, Takeo Oomichi, Akihisa Okino, and Toshio

Fukuda. Uav with manipulator for bridge inspection—hammering system for mounting to uav. In *2017 IEEE/SICE International Symposium on System Integration (SII)*, pages 775–780. IEEE, 2017.

[79] Sujit Rajappa, Markus Ryll, Heinrich H Bülthoff, and Antonio Franchi. Modeling, control and design optimization for a fully-actuated hexarotor aerial vehicle with tilted propellers. In *2015 IEEE international conference on robotics and automation (ICRA)*, pages 4006–4013. IEEE, 2015.

[80] Caiwu Ding and Lu Lu. A tilting-rotor unmanned aerial vehicle for enhanced aerial locomotion and manipulation capabilities: Design, control, and applications. *IEEE/ASME Transactions on Mechatronics*, 2020.

[81] Christos Papachristos, Kostas Alexis, and Anthony Tzes. Efficient force exertion for aerial robotic manipulation: Exploiting the thrust-vectoring authority of a tri-tiltrotor uav. In *2014 IEEE international conference on robotics and automation (ICRA)*, pages 4500–4505. IEEE, 2014.

[82] Karen Bodie, Maximilian Brunner, Michael Pantic, Stefan Walser, Patrick Pfändler, Ueli Angst, Roland Siegwart, and Juan Nieto. An omnidirectional aerial manipulation platform for contact-based inspection. *arXiv preprint arXiv:1905.03502*, 2019.

[83] Sangyul Park, Jongbeom Her, Juhyeok Kim, and Dongjun Lee. Design, modeling and control of omni-directional aerial robot. In *2016 IEEE/RSJ International Conference on Intelligent Robots and Systems (IROS)*, pages 1570–1575. IEEE, 2016.

[84] Moju Zhao, Koji Kawasaki, Xiangyu Chen, Shintaro Noda, Kei Okada, and Masayuki Inaba. Whole-body aerial manipulation by transformable multirotor with two-dimensional multilinks. In *2017 IEEE International Conference on Robotics and Automation (ICRA)*, pages 5175–5182. IEEE, 2017.

[85] Tomoki Anzai, Moju Zhao, Shunichi Nozawa, Fan Shi, Kei Okada, and Masayuki Inaba. Aerial grasping based on shape adaptive transformation by halo: Horizontal plane transformable aerial robot with closed-loop multilinks structure. In *2018 IEEE International Conference on Robotics and Automation (ICRA)*, pages 6990–6996. IEEE, 2018.

[86] Ruben D'Sa and Nikolaos Papanikolopoulos. Design and experiments for multi-section-transformable (mist)-uav. In *2019 International Conference on Robotics and Automation (ICRA)*, pages 1878–1883. IEEE, 2019.

[87] Davide Falanga, Kevin Kleber, Stefano Mintchev, Dario Floreano, and Davide Scaramuzza. The foldable drone: A morphing quadrotor that can squeeze and fly. *IEEE Robotics and Automation Letters*, 4(2):209–216, 2018.

[88] Jonathan Fink, Nathan Michael, Soonkyum Kim, and Vijay Kumar. Planning and control for cooperative manipulation and transportation with aerial robots. *The International Journal of Robotics Research*, 30(3):324–334, 2011.

[89] Hai-Nguyen Nguyen, Sangyul Park, Junyoung Park, and Dongjun Lee. A novel robotic platform for aerial manipulation using quadrotors as rotating thrust generators. *IEEE Transactions on Robotics*, 34(2):353–369, 2018.

[90] Hossein Rastgoftar and Ella M Atkins. Cooperative aerial lift and manipulation (calm). *Aerospace Science and Technology*, 82:105–118, 2018.

[91] Tamara Petrovic, Tomislav Haus, Barbara Arbanas, Matko Orsag, and Stjepan Bogdan. Can uav and ugv be best buddies? towards heterogeneous aerial-ground cooperative robot system for complex aerial manipulation tasks. In *2015 12th international conference on informatics in control, automation and robotics (ICINCO)*, volume 1, pages 238–245. IEEE, 2015.

[92] Nicolas Staub, Mostafa Mohammadi, Davide Bicego, Domenico Prattichizzo, and Antonio Franchi. Towards robotic magmas: Multiple aerial-ground ma-

nipulator systems. In *2017 IEEE International Conference on Robotics and Automation (ICRA)*, pages 1307–1312. IEEE, 2017.

[93] Sven Lange, Niko Sunderhauf, and Peter Protzel. A vision based onboard approach for landing and position control of an autonomous multirotor uav in gps-denied environments. In *2009 International Conference on Advanced Robotics*, pages 1–6. IEEE, 2009.

[94] Phong Ha Nguyen, Muhammad Arsalan, Ja Hyung Koo, Rizwan Ali Naqvi, Noi Quang Truong, and Kang Ryoung Park. Lightdenseyolo: A fast and accurate marker tracker for autonomous uav landing by visible light camera sensor on drone. *Sensors*, 18(6):1703, 2018.

[95] Daewon Lee, Tyler Ryan, and H Jin Kim. Autonomous landing of a vtol uav on a moving platform using image-based visual servoing. In *2012 IEEE international conference on robotics and automation*, pages 971–976. IEEE, 2012.

[96] Robotic Landing Gear Could Enable Future Helicopters to Take Off and Land Almost Anywhere. Defense Advanced Research Projects Agency [Internet]. 2015 Oct 09 [cited 2020 Mar 11]. Available from: https://www.darpa.mil/newsevents/2015-09-10.

[97] Hannibal Paul, Ryo Miyazaki, Robert Ladig, and Kazuhiro Shimonomura. Landing of a multirotor aerial vehicle on an uneven surface using multiple onboard manipulators. In *2019 IEEE/RSJ International Conference on Intelligent Robots and Systems (IROS)*, pages 1926–1933. IEEE, 2019.

[98] Charles A Schue III. Simulation of tripod gaits for a hexapod underwater walking machine. Technical report, NAVAL POSTGRADUATE SCHOOL MONTEREY CA, 1993.

[99] Robert B McGhee and Andrew A Frank. On the stability properties of quadruped creeping gaits. *Mathematical Biosciences*, 3:331–351, 1968.

[100] Ruwen Schnabel, Roland Wahl, and Reinhard Klein. Efficient ransac for point-cloud shape detection. In *Computer graphics forum*, volume 26, pages 214–226. Wiley Online Library, 2007.

[101] Shan Luo, Wenxuan Mou, Kaspar Althoefer, and Hongbin Liu. Novel tactile-sift descriptor for object shape recognition. *IEEE Sensors Journal*, 15(9):5001–5009, 2015.

[102] Andrew T Miller, Steffen Knoop, Henrik I Christensen, and Peter K Allen. Automatic grasp planning using shape primitives. In *2003 IEEE International Conference on Robotics and Automation (Cat. No. 03CH37422)*, volume 2, pages 1824–1829. IEEE, 2003.

[103] Dmitry Berenson, Rosen Diankov, Koichi Nishiwaki, Satoshi Kagami, and James Kuffner. Grasp planning in complex scenes. In *2007 7th IEEE-RAS International Conference on Humanoid Robots*, pages 42–48. IEEE, 2007.

[104] Marius Schnaubelt, Stefan Kohlbrecher, and Oskar von Stryk. Autonomous assistance for versatile grasping with rescue robots. In *2019 IEEE International Symposium on Safety, Security, and Rescue Robotics (SSRR)*, pages 210–215. IEEE, 2019.

[105] Masatoshi Hatano and Toshifumi Fujii. 3-d shape recognitions of target objects for stacked rubble withdrawal works performed by rescue robots. *Artificial Life and Robotics*, 25(1):94–99, 2020.

[106] Van-Duc Nguyen. Constructing force-closure grasps. *The International Journal of Robotics Research*, 7(3):3–16, 1988.

[107] Amirhossein Jabalameli and Aman Behal. From single 2d depth image to gripper 6d pose estimation: A fast and robust algorithm for grabbing objects in cluttered scenes. *Robotics*, 8(3):63, 2019.

[108] Yucong Lin and Srikanth Saripalli. Sampling-based path planning for uav collision avoidance. *IEEE Transactions on Intelligent Transportation Systems*, 18(11):3179–3192, 2017.

[109] Pedro Sanchez-Cuevas, Guillermo Heredia, and Anibal Ollero. Characterization of the aerodynamic ground effect and its influence in multirotor control. *International Journal of Aerospace Engineering*, 2017, 2017.

[110] David Wuthier, Dariusz Kominiak, Emil Fresk, and George Nikolakopoulos. A geometric pulling force controller for aerial robotic workers. *IFAC-PapersOnLine*, 50(1):10287–10292, 2017.

[111] Hideyuki Tsukagoshi, Masahiro Watanabe, Takahiro Hamada, Dameitry Ashlih, and Ryuma Iizuka. Aerial manipulator with perching and door-opening capability. In *2015 IEEE International Conference on Robotics and Automation (ICRA)*, pages 4663–4668. IEEE, 2015.

[112] Amir Shapiro and Elon Rimon. Pcg: A foothold selection algorithm for spider robot locomotion in 2d tunnels. In *2003 IEEE International Conference on Robotics and Automation (Cat. No. 03CH37422)*, volume 3, pages 2966–2972. IEEE, 2003.

[113] NVIDIA Jetson [Internet] [cited 2020 May 22]. Available from: https://developer.nvidia.com/embedded/develop/hardware.

[114] Orbitty Carrier for NVIDIA Jetson TX2/TX2i/TX1 [Internet] [cited 2020 May 22]. Available from: http://connecttech.com/product/orbitty-carrier-for-nvidia-jetson-tx2-tx1/.

[115] AX-12A datasheet [Internet] [cited 2020 May 22]. Available from: http://emanual.robotis.com/docs/en/dxl/ax/ax-12a/.

[116] Derrick Yeo, Elena Shrestha, Derek A Paley, and Ella M Atkins. An empirical model of rotorcrafy uav downwash for disturbance localization and avoidance. In *AIAA Atmospheric Flight Mechanics Conference*, page 1685, 2015.

[117] Qian-Yi Zhou, Jaesik Park, and Vladlen Koltun. Open3d: A modern library for 3d data processing. *arXiv preprint arXiv:1801.09847*, 2018.

[118] Hannibal Paul, Ryo Miyazaki, Robert Ladig, and Kazuhiro Shimonomura. Tams: development of a multipurpose three-arm aerial manipulator system. *Advanced Robotics*, pages 1–17, 2020.

[119] Gene H Golub et al. Cf vanloan, matrix computations. *The Johns Hopkins*, 1996.

[120] Menglong Zhu, Konstantinos G Derpanis, Yinfei Yang, Samarth Brahmbhatt, Mabel Zhang, Cody Phillips, Matthieu Lecce, and Kostas Daniilidis. Single image 3d object detection and pose estimation for grasping. In *2014 IEEE International Conference on Robotics and Automation (ICRA)*, pages 3936–3943. IEEE, 2014.

[121] Marcus Gualtieri, Andreas Ten Pas, Kate Saenko, and Robert Platt. High precision grasp pose detection in dense clutter. In *2016 IEEE/RSJ International Conference on Intelligent Robots and Systems (IROS)*, pages 598–605. IEEE, 2016.

[122] Fábio Azevedo, A Oliveira, André Dias, José Almeida, Miguel Moreira, Tiago Santos, André Ferreira, Alfredo Martins, and Eduardo Silva. Collision avoidance for safe structure inspection with multirotor uav. In *2017 European Conference on Mobile Robots (ECMR)*, pages 1–7. IEEE, 2017.

[123] Yi-Chun Lin, Yi-Ting Cheng, Tian Zhou, Radhika Ravi, Seyyed Meghdad Hasheminasab, John Evan Flatt, Cary Troy, and Ayman Habib. Evaluation of uav lidar for mapping coastal environments. *Remote Sensing*, 11(24):2893, 2019.

[124] Yi Lin, Juha Hyyppa, and Anttoni Jaakkola. Mini-uav-borne lidar for fine-scale mapping. *IEEE Geoscience and Remote Sensing Letters*, 8(3):426–430, 2010.

[125] LDS_01 datasheet [Internet] [cited 2020 May 22]. Available from: http://emanual.robotis.com/docs/en/platform/turtlebot3/appendix_lds_01/.

[126] Kam S Tso, Gregory K Tharp, Wayne Zhang, and Ann T Tai. A multi-agent operator interface for unmanned aerial vehicles. In *Gateway to the New Millennium. 18th Digital Avionics Systems Conference. Proceedings (Cat. No. 99CH37033)*, volume 2, pages 6–A. IEEE, 1999.